

Chapter 11

Thermal Methods

Thermal methods, particularly steamdrive and steam soak, are the most successful enhanced-oil-recovery (EOR) processes. They are certainly the most mature. In [Chapter 1](#), we saw that steam methods currently account for approximately one-half the EOR in the United States. Thermal flooding is commercially successful and has been for almost 50 years. In this chapter, we explore the reasons for this success.

Despite the success—billions of barrels have been recovered by this type of EOR—even more hard-to-recover oil remains. Meyer and Attanasi (2003) report that recoverable heavy oil and bitumen resources are almost 1,000 billion barrels, or approximately twice the amount of recoverable light oil. Much of this target is beyond the limits of current technology; hence, thermal methods are constantly evolving to meet these challenges. This chapter touches on these new technologies.

We can give no more than an overview of these scientifically interesting and complex processes. Several texts (White and Moss 1983; Burger et al. 1985; Boberg 1988; Butler 1997) and a monograph (Prats 1982) are available on thermal flooding alone. There are also extensive treatments in reservoir-engineering texts (Gates 2011). Our intent is to apply the twin bases of this text—phase behavior and fractional-flow theory—to thermal methods in some detail. In addition, we deal with the important ancillary topic of heat loss.

This chapter is organized differently from the others, partly because of the many different processes available. We begin with a discussion of viscosity reduction, followed by an overview of the various processes. The bulk of the chapter focuses on mass and

heat transfer specifically directed to thermal methods. This section could constitute a treatment of heat transfer in general because virtually every form of energy transfer occurs in thermal processes. The chapter concludes by returning to discuss the specific processes.

Thermal methods rely on several displacement mechanisms to recover oil, but the most important is the reduction of crude viscosity with increasing temperature. We can draw several important conclusions from [Fig. 11.1](#), a plot of crude kinematic viscosity ($v_2 = \mu_2/\rho_2$) vs. temperature.

Crude kinematic viscosity decreases dramatically with a rise in temperature. This effect reflects principally the change in dynamic viscosity μ_2 because crude density changes relatively little with temperature. For example, a heavy crude (10–20° API) that undergoes a temperature increase from 300 to 400 K, which is easily obtainable by thermal methods, will produce a viscosity well within the flowing range (less than 10 mPa·s). (The previous sentence begins a practice of using the words *light* and *heavy* for nonviscous and viscous fluids, even though light and heavy, strictly speaking, refer to density. Because there usually exists a correlation between viscosity and density and the usage is thoroughly ingrained, the authors hope that there is no confusion.) [Fig. 11.1](#) greatly compresses the vertical axis simply to plot the observed changes on one scale.

For lighter crudes, the viscosity reduction is less. Therefore, thermal methods are not nearly as advantageous for these crudes, particularly because waterflooding would probably be an attractive alter-native. The viscosity reduction for very heavy crudes (less than 10° API) is substantial, but still not enough to make them flow economically. Therefore, there are practical limits on both viscosity extremes.

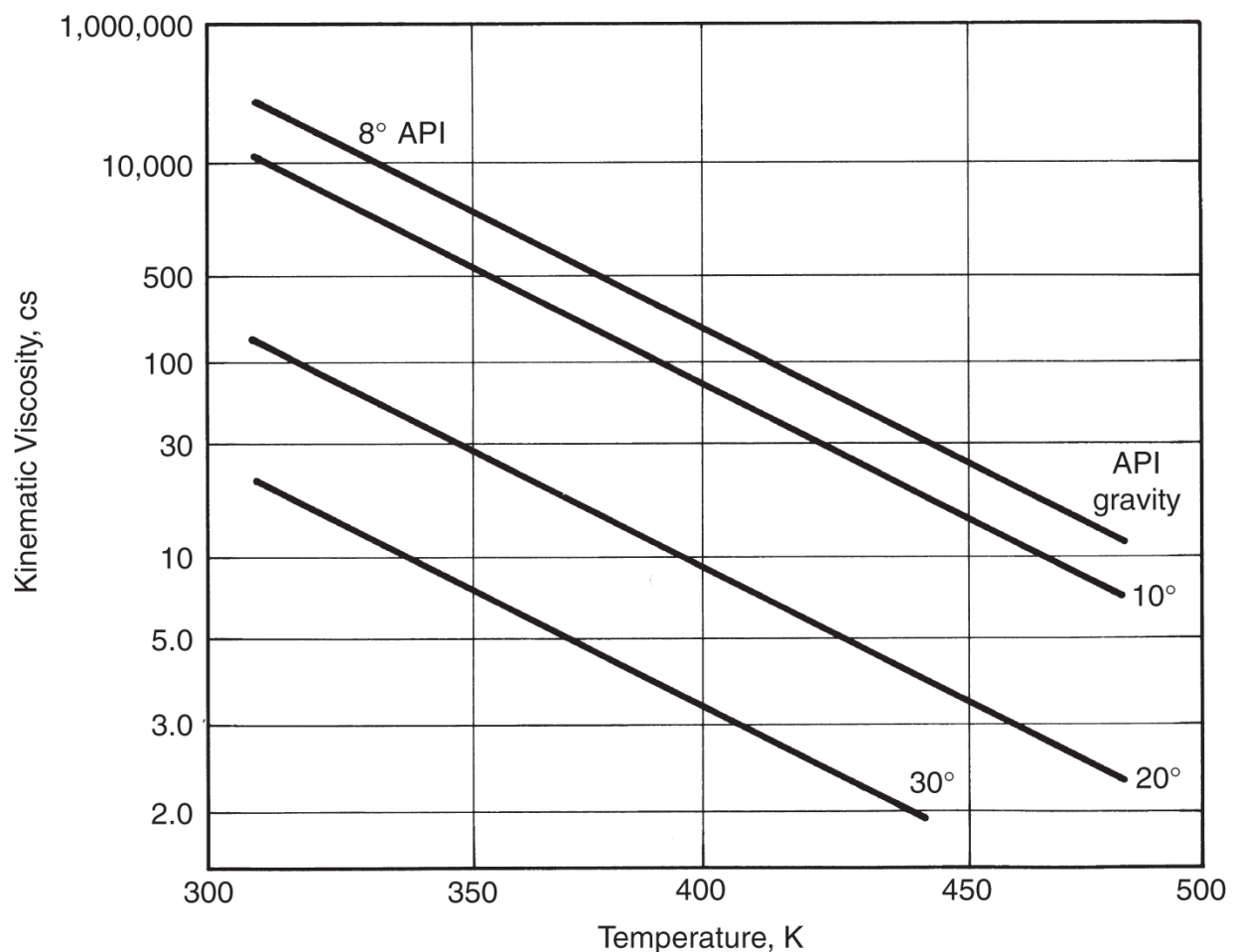


Fig. 11.1—Effect of temperature on crude-oil viscosity [adapted from Farouq Ali (1974)].

11.1 Process Variations

All thermal-recovery processes move or transport energy (usually heat) into or through a reservoir to recover crude. The basic heat-transfer mechanisms are:

Convection. Convection is the transfer of heat by a moving fluid. When the flow is caused by potential (pressure) differences, the convection is said to be *forced*. If it is caused by density differences induced by temperature changes, it is *free* convection. Convection is normally the most important heat-transfer mechanism.

Conduction. Conduction occurs in the absence of fluid movement (e.g., through a tube wall) in the solid portion of a

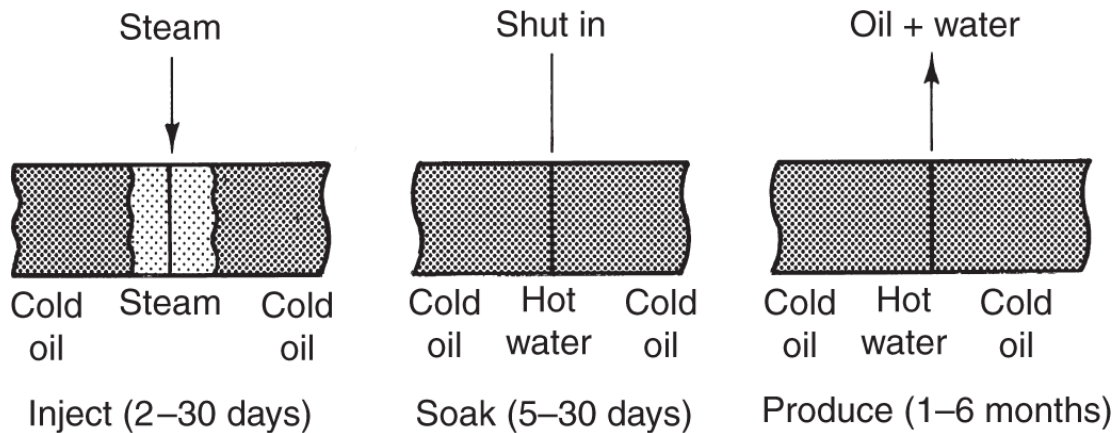
reservoir, or to adjacent strata. It is heat transfer on a molecular level.

Radiation. Radiation is heat transfer that occurs in a nonmaterial or *photon* phase (Bird et al. 2002). Radiation can occur in the absence of a material phase, either solid or liquid, or it can occur with flow of a material phase, in which case some of the radiation is adsorbed into the material phase, raising its temperature

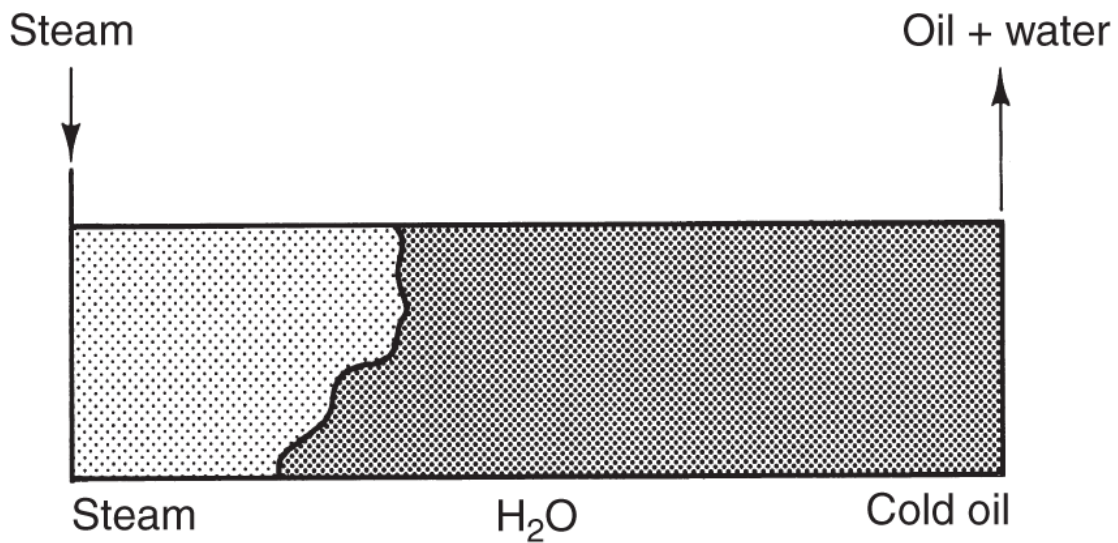
There are many ways to introduce heat into a reservoir. Most of these involve introducing steam.

Steam Soak. In a steam soak (also known as a cyclic stimulation or huff-n-puff), steam is introduced into a well, and then the well is returned to production after a brief shut-in period ([Fig. 11.2a](#)). The steam heats up a zone near the well and also provides some pressure support for subsequent production. The shut-in or soak period enables thermal gradients to equalize, but should not be long enough for the pressure to escape. During shut-in, all the injected steam condenses, and the well produces a mixture of hot water and oil. One great advantage of a steam soak is that all the wells can be producing nearly all the time, the injection and soak periods usually being short.

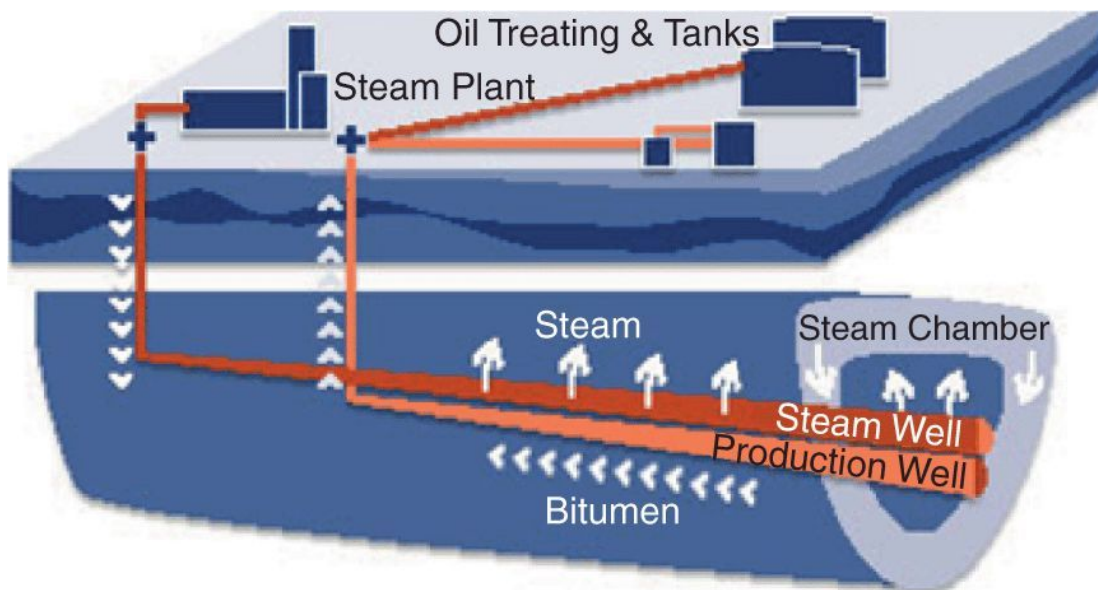
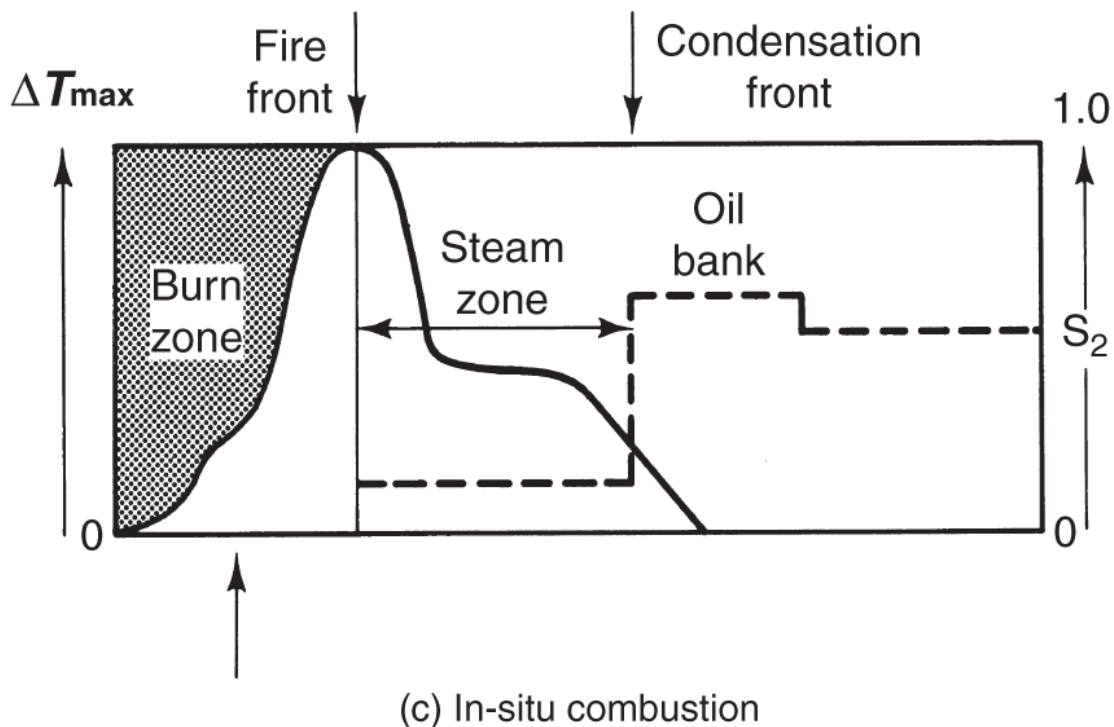
Steamdrive. A steamdrive uses at least two sets of wells, those into which steam is injected and those from which oil is produced ([Fig. 11.2b](#)). A steamdrive usually results in higher ultimate recoveries than a steam soak because it penetrates more deeply into the reservoir than steam soaks. For the same reason, well spacing need not be as close in drives as in soaks for equivalent oil recovery. The close spacing partially offsets the disadvantage of sacrificing some of the wells to injection. Because steamdrive is present to some extent in all thermal processes, we will focus on it in later analyses.



(a) Steam soak or huff-n-puff



(b) Steamdrive



(d) Steam-assisted gravity drainage (SAGD)

Fig. 11.2–Process variations for thermal method: (a) steam soak or huff-n-puff; (b) steamdrive; (c) in-situ combustion [adapted from Prats (1982)]; (d) Steam-assisted gravity drainage (SAGD).

In-Situ Combustion. Fig. 11.2c shows a schematic of a forward in-situ combustion process. The process injects some form of

oxidant (air or pure oxygen) into the formation. The mixture then spontaneously ignites (or ignition is induced), and subsequent injection propagates a fire or burn zone through the reservoir. The fire zone is only a meter or so wide, but it generates very high temperatures. These temperatures vaporize connate water and a portion of the crude, both of which are responsible for some oil displacement. The vaporized connate water forms a steam zone ahead of the burn front, which operates very much like a steamdrive. The vaporized oil consists mainly of light components that form a miscible displacement. The reaction products of high-temperature combustion can also form an in-situ carbon dioxide (CO_2) flood. In-situ combustion processes are sometimes called high-pressure air injection (HPAI).

Steam-Assisted Gravity Drainage (SAGD) (Butler 1982). [Fig. 11.2d](#) shows a schematic of the SAGD process. This process is like both steam soak and steamdrive in that heat, carried through steam, is the recovering fluid. However, SAGD is unlike the previous two in several important respects:

- SAGD uses horizontal rather than vertical wells.
- The horizontal wells are in injector/producer pairs that are closely spaced.

Both items make SAGD different from any other thermal method, and indeed different from any other process covered in this text. SAGD is a singular example of the use of a combination of technologies (in this case, steam injection and horizontal wells) to recover oil.

Closely spaced injectors and producers (they are usually on the order of 10 m apart in SAGD) would be anathema to the other EOR processes discussed here because such close well spacing would result in early breakthrough and extensive bypassing of oil. The key to the success of SAGD is that the main recovery mechanism is buoyancy (because of density differences) rather than viscous driving forces. You will recall from [Chapter 5](#) that in 1D flow, the

competition between buoyancy and viscous forces is expressed through a gravity number as

$$N_g^0 = \frac{k_v k_{r2}^0 \Delta \rho g}{\mu_2 u}.$$

Buoyancy is promoted when this number is large, or when u is small and/or k_v is large. A low velocity is ensured by the length of the wells (often exceeding 10,000 ft), which accumulates the very low velocities, resulting in flow. The process works best when k_v is large.

For most cases, viscosity reduction is by far the most important cause of additional oil recovery by thermal methods, but other mechanisms can also be important [e.g., distillation, miscible displacement, thermal expansion, wettability changes, cracking, and reduced oil/water interfacial tension (IFT)]. The relative importance of each mechanism depends on the oil being displaced and the process. Cracking is relatively unimportant in steam processes with their relatively low temperatures, but it is quite important during in-situ combustion. Thermal expansion and distillation become more important as the API° of the crude decreases.

Another class of thermal processes seeks to introduce heat through a reservoir using electromagnetic energy (Karanikas 2012). [**Fig. 11.3**](#) illustrates one of these processes. Although heat is introduced into the reservoir here, steam plays a minor role, and in fact can be deleterious because boiling water is a source of heat loss.

The in-situ conversion (ISC) process is different in other ways. In ISC, the intent is not so much to decrease viscosity as it is to convert the hydrocarbon chemically from a highly viscous material (tar sands and bitumen are the usual targets here) with a high carbon-to-hydrogen ratio to a much more malleable (and valuable) product with a low carbon-to-hydrogen ratio. The process resembles a subsurface refinery in which high-quality product (e.g., kerosene) is produced instead of crude. Viscous crudes form as a result of several

degradation mechanisms occurring over a long time. ISC intends to reverse this process over a short time period through heating.

In Fig. 11.3, energy is injected into a reservoir through a series of closely spaced resistive-heater wells. The combined effect of these closely spaced vertical wells is to accumulate energy over large volumes of a reservoir so that thermal cracking can occur. Other ways to introduce energy into a reservoir include resistive heating between subsurface anodes and cathodes, inductive heating, use of a heat-transfer fluid, and antennas (Carrazales 2010; Callarotti 2002).

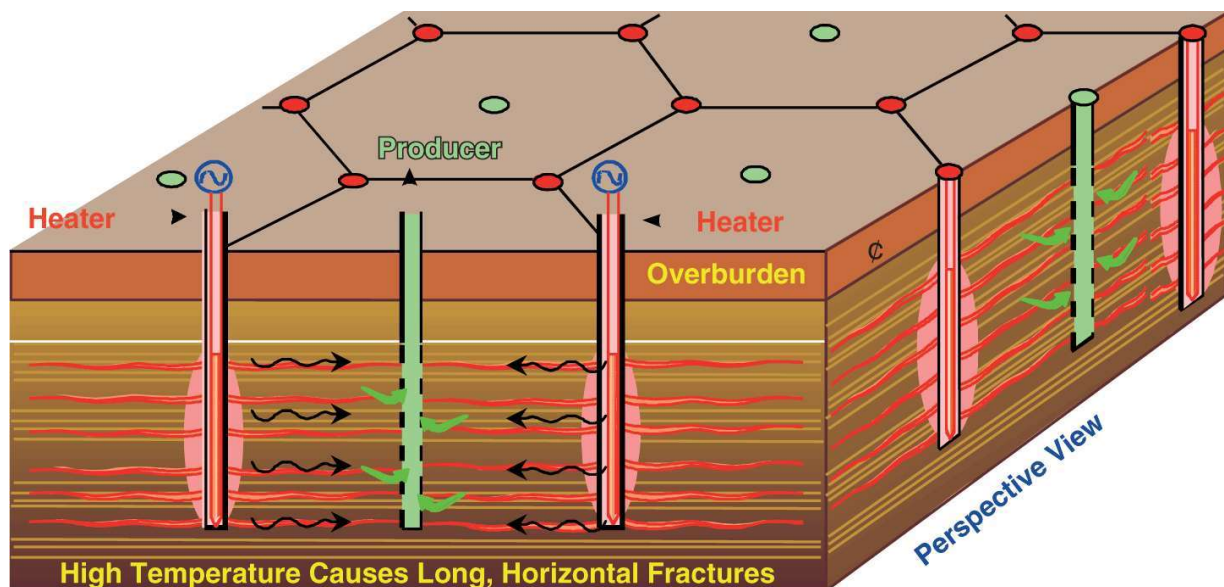


Fig. 11.3—Schematic of the in-situ conversion (ISC) process (Karanikas 2012).

11.2 Physical Properties

Elucidating the mechanisms of thermal methods begins with understanding the thermodynamic and transport properties of water and crude. We review these properties and their temperature dependence in this section. The most important water properties for this treatment are the steam/water phase envelope, steam quality, and latent heat of vaporization. For crudes, the most important property is the temperature dependence of viscosity.

11.2.1 Water Properties. The temperature rises in a thermal flood because additional energy is introduced or generated in the

reservoir. In both cases, water plays a central role. The following paragraphs review water properties; you will notice parallels to the generic treatment of phase behavior in [Chapter 4](#).

[Fig. 11.4](#) shows the vapor pressure of water from subatmospheric pressure to its critical point. Remember that the vapor pressure is the value of pressure (or temperature) at which a pure component (here water) changes phase (here, liquid to vapor) at a fixed value of temperature (pressure). The figure also shows the operating range for several successful steamdrives; operating pressures tend to be lower than for chemical methods and much lower than for solvent methods. Thermal methods are intrinsically low-pressure processes. As we will see in the following, the properties of saturated water are important to the efficiency of steam methods, and, therefore, the diagram also shows the range of temperatures—320–660°F (433–622 K)—for these methods.

[Fig. 11.5](#) shows the pressure-specific volume diagram for water. The saturated vapor curve on the right of the envelope shows that steam density is much lower than saturated liquid density except very near the critical point. This figure contains lines indicating steam quality, a property discussed later.

This energy content of water is well approximated by the enthalpy. [Fig. 11.6](#) shows a pressure/enthalpy diagram for water. This diagram is analogous to the pressure/composition diagrams discussed in Section 4.1, with enthalpy being the composition variable. [Fig. 11.6](#) illustrates several important landmarks.

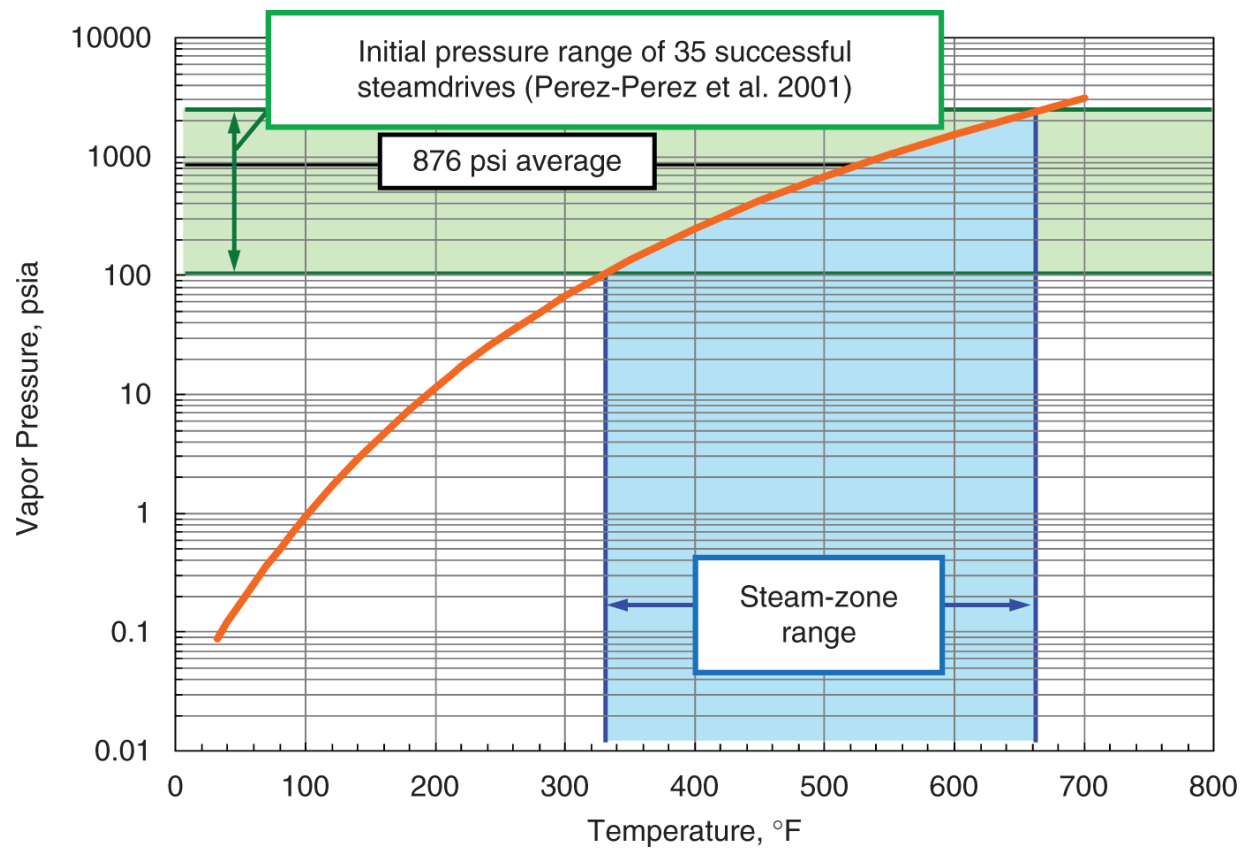


Fig. 11.4—Vapor-pressure diagram of water.

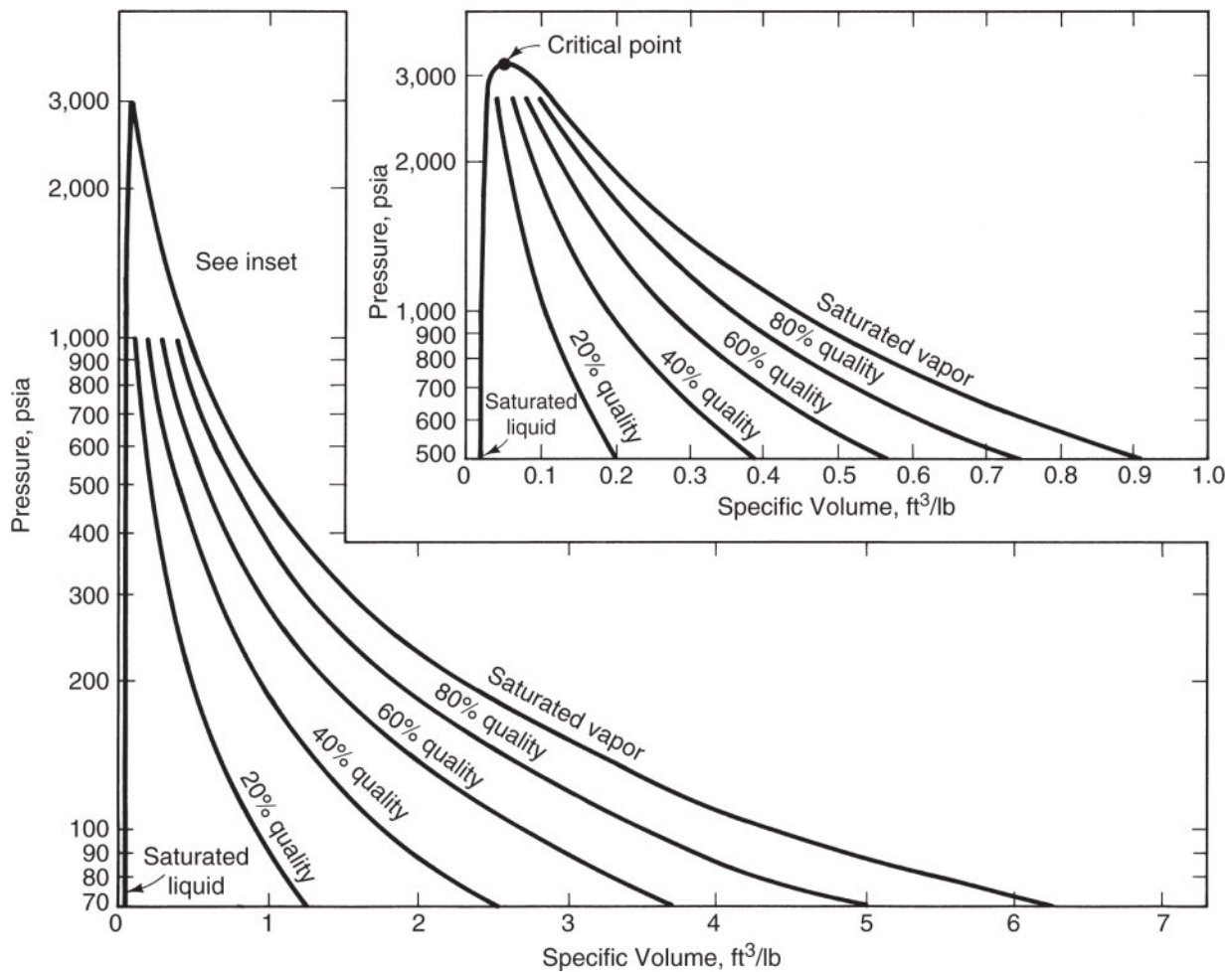


Fig. 11.5—Pressure vs. specific-volume diagram for water (Bleakley 1965).

1. Two-phase envelope. The envelope defines the region of two-phase behavior, as does the envelope on the pressure/molar volume diagram in [Fig. 4.2](#). The left boundary is the bubblepoint curve, and the right boundary is the dewpoint curve. To the left and right of the envelope are the supercooled liquid and superheated vapor (steam) regions, respectively. Within the two-phase region, temperature depends on pressure according to [Fig. 11.4](#). These are *saturated* temperature and pressure, respectively.
2. Steam quality. Steam quality y is the amount of the total vapor, by weight, expressed as a fraction (or a percentage) of the mass of liquid plus vapor,

Quality is normally reported as a percentage, but, like fluid saturation (the S in Eq. 11.1), is always used in calculations as a fraction. The quality lines within the two-phase envelope represent the relative amount of the total mass that is steam. Lines of constant temperature (only one is illustrated) in [Fig. 11.6](#) fall steeply in the liquid region, are constant across the two-phase envelope, and then fall steeply again in the steam region.

3. Saturated liquid. A liquid is *saturated* if it exists at the temperature and pressure at which steam can be generated. The saturated-liquid curve represents 0% steam quality.
 4. Saturated vapor. Saturated vapor is water at the temperature and pressure at which exactly 100% of the water present has been converted to a vapor.

Both phases in the two-phase region are saturated.
 5. Latent heat. Latent heat of vaporization L_V is the quantity of heat added to a given mass of saturated water (0% quality steam) to convert it to saturated vapor (100% quality steam) at constant temperature. The heat is *latent* because the temperature of the system does not change as the liquid is converted to vapor. On an enthalpy/pressure diagram, latent heat is the difference in the x -coordinates between the dewpoint and bubblepoint curves in [Fig. 11.5](#) at a particular pressure. The latent heat vanishes at the critical point of water, 3206.2 psia and 705.4°F (21.8 MPa and 647 K). The location of the critical pressure is important in steam processes. We will show in Example 11.3 that the velocity of a steam front slows at high pressure because latent heat vanishes.
 6. Sensible heat. Sensible heat is the quantity of heat that must be added to a given mass of water to raise its temperature without changing its phase. This quantity is *sensible* because a thermometer in the water will sense a temperature increase as heat is added (at a constant pressure) until steam

generation begins. Sensible heat is a product of a heat capacity and a temperature difference.

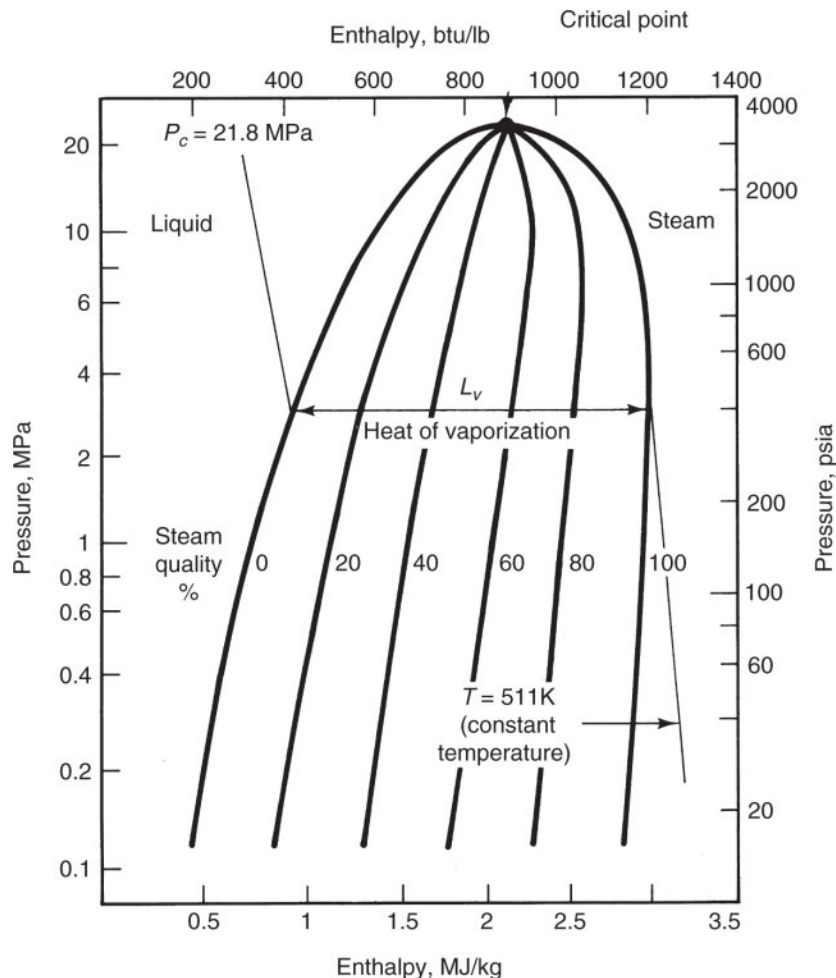


Fig. 11.6—Enthalpy vs. pressure diagram for water [adapted from Bleakley (1965)].

Thermodynamic properties, types of which are the two previous diagrams, are usually taught with temperature changing rather than pressure, as illustrated in [Fig. 11.7](#). In this figure, superheated vapor is above the two-phase envelope and the supercooled region below. Constant- T lines within the two-phase region are vertical. As the figure illustrates, the change in enthalpy with temperature is the heat capacity,

$$C_p = \left(\frac{\partial H}{\partial T} \right)_P .$$

This can be either per mole or per mass depending on the units of H . If it is the latter, C_p is often called the *specific heat*. You can see from the plot that the heat capacity is nearly independent of both T and P (the slopes are constant) in the liquid. This is essentially the case in the vapor regions, except in the region near the critical point. We will assume constant heat capacities in much of what we do below.

The physical properties in [Figs. 11.4](#) through [11.7](#) appear in steam tables (Keenan et al. 1969 and online). You should use these for precise work. Often reading information from these figures is sufficient.

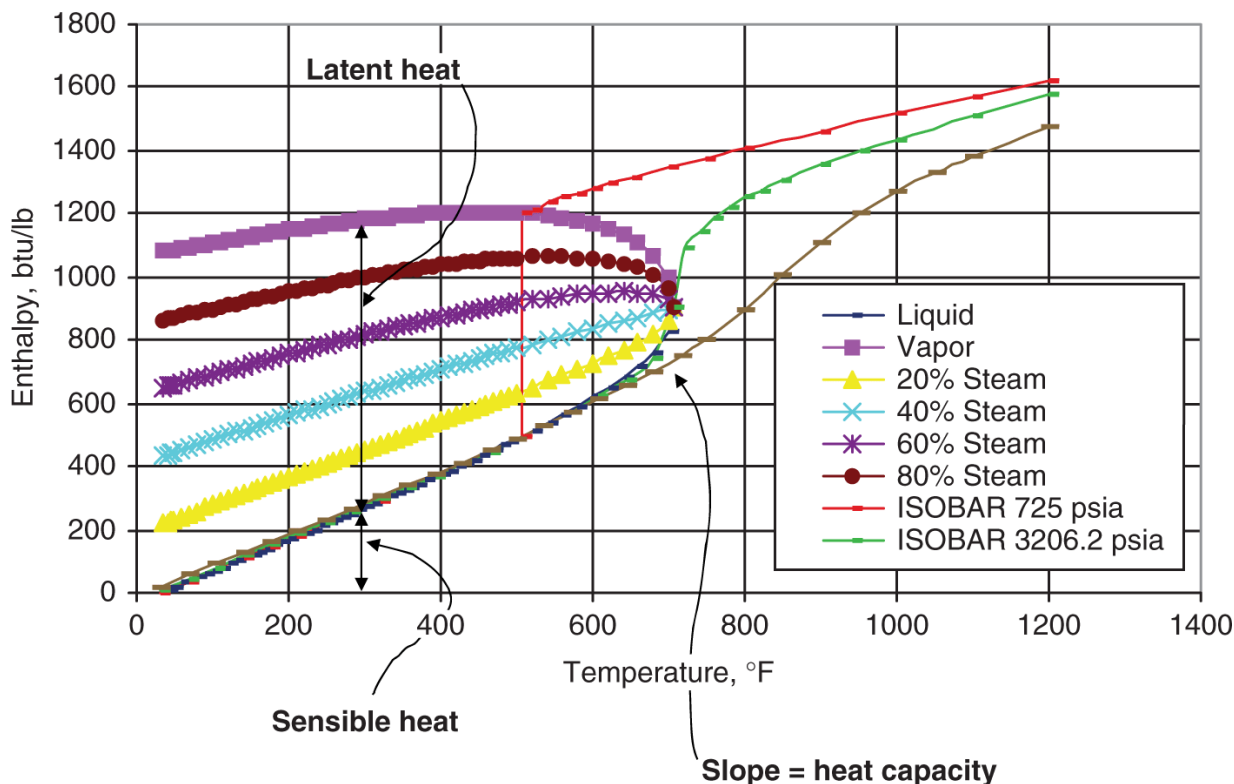


Fig. 11.7—Enthalpy-temperature diagram for water.

Example 11.1. Enthalpy Changes. Use [Fig. 11.7](#) in the following:

- Estimate the enthalpy content in 1 lbm of water at $T = 600^\circ\text{F}$ and $P = 725 \text{ psia}$. What is the state of the fluid at this point?

The fluid is superheated vapor or steam. Directly from the graph, we have $H_{13} = 1,300$ Btu. Like all thermodynamic quantities, this number is relative to an arbitrary zero. Recall that the subscript 3 means vapor phase here.

- b. Relative to the enthalpy of saturated water at the same T , how much of this heat is sensible and how much is latent?

Also from the graph, the enthalpies of saturated liquid (sl) and saturated vapor (sv) are \dots , so that the enthalpy change from the conditions of Part (a) is \dots , of which \dots is latent heat and the remainder, \dots , is sensible heat. Note that the pressure had to be increased substantially to condense the fluid.

- c. If the enthalpy of the fluid is $H_1 = 900$ Btu, what is the steam quality? From [Fig. 11.6](#), $y = 55\%$ quality steam. Remember that all the quantities discussed here are at equilibrium.

One of the disadvantages of these graphical representations is that it is difficult to show enthalpy variations with both T and P . Farouq Ali (1974) has fitted approximate analytical expressions to water properties ([Table 11.1](#)).

TABLE 11.1—THERMAL PROPERTIES OF WATER [ADAPTED FROM FAROUQ ALI (1974)]

Quantity x	English, $P [=]$ psia			Limit psia	Quantity x	SI, $P [=]$ MPa			Percent error
	a	b	aP^b			a	b	Limit MPa	
Saturation temperature ($^{\circ}$ F)	115.1	0.225	300		Saturation temperature -256 (K)	197	0.225	2.04	1
Sensible heat (Btu/lbm)	91	0.257	1,000		Sensible heat (MJ/kg)	0.796	0.257	6.80	0.3
Latent heat (Btu/lbm)	1,318	-0.0877	1,000		Latent heat (MJ/kg)	1.874	-0.0877	6.80	1.9
Saturated steam enthalpy (Btu/lbm)	1,119	0.0127	100		Saturated steam enthalpy (MJ/kg)	2.626	0.0127	2.04	0.3
Saturated steam specific volume (ft ³ /lbm)	363.9	-0.959	1,000		Saturated steam specific volume (m ³ /kg)	0.19	-0.959	6.80	1.2

Note: $x = aP^b$.

Example 11.2. Table Comparisons. The expressions in [Table 11.1](#) are very handy, and, therefore, it is of interest to see how well these

equations predict the actual properties. We will use the same conditions as in Example 11.1. The pressure $P = 725$ psi is well outside the limit of the saturation temperature and steam enthalpy in [Table 11.1](#).

- Estimate the saturation temperature. From the table (using English units), $T_s = aP^b = 115.1(725 \text{ psi})^{0.225} = 507^\circ\text{F}$ compared to $T = 510^\circ\text{F}$ from [Fig. 11.7](#).
- Estimate the latent heat of vaporization. From [Table 11.1](#), $L_v = aP^b = 1,318(725 \text{ psi})^{-0.0877} = 740 \frac{\text{Btu}}{\text{lb}_m}$, compared to $690 \frac{\text{Btu}}{\text{lb}_m}$.
- Estimate the saturated steam enthalpy. Again, $H_{11}^s = aP^b = 1,119(725 \text{ psi})^{0.012} = 1,211 \frac{\text{Btu}}{\text{lb}_m}$, compared to $1,190 \frac{\text{Btu}}{\text{lb}_m}$.
- Estimate the saturated-steam specific volume. $v_1^{sv} = aP^b = 363.9(725 \text{ psi})^{-0.959} = 0.657 \frac{\text{ft}^3}{\text{lb}_m}$, compared to $0.69 \frac{\text{ft}^3}{\text{lb}_m}$ from Fig. 11.4.

Even when outside the recommended ranges, the accuracy of [Table 11.1](#) is sufficient for most engineering purposes.

11.2.2 Crude-Oil Properties. Curiously, there seems to be no universal definition for what constitutes a heavy oil. The United States Geological Survey (USGS) definitions are given below:

- *Light or conventional oil*: Crude with an API gravity $>22^\circ$ and a viscosity of $\mu_2 < 100 \text{ mPa}\cdot\text{s}$.
- *Heavy oil*: Crude with an API gravity $<22^\circ$ and $\mu_2 > 100 \text{ mPa}\cdot\text{s}$.
- *Extra-heavy crude*: The portion of heavy crude with API gravity $<10^\circ$ and $\mu_2 > 10,000 \text{ mPa}\cdot\text{s}$.

All the quoted viscosities are at reservoir conditions. The USGS also adds criteria on the basis of asphaltene and sulfur content (Meyer and Attanasi 2003).

- *Natural bitumen*: Also called tar or oil sands; these are extra-heavy crudes with $\mu_2 > 1,000,000 \text{ mPa}\cdot\text{s}$.

Easily the most important crude-oil property for thermal flooding is the viscosity dependence on temperature. As for most liquids, the Andrade (1930) equation captures this dependence:

$$\mu_2 = A e^{B/T}, \dots \quad (11.2a)$$

where T is in absolute degrees. A and B are empirical parameters for which the values are determined from two viscosity measurements at different temperatures. For extrapolation or interpolation, Eq. 11.2a indicates that a semi-log plot of viscosity vs. T^{-1} should be a straight line.

If only one measurement is available, a coarse estimate of viscosity can be obtained from [Fig. 11.8](#). This single-parameter correlation assumes that viscosity change is a universal function of temperature change. To use the plot, enter the vertical axis with the known viscosity (4.38 mPa·s in this case), find the x-axis coordinate, move to the right by the temperature increase (101.6°C), and then return to the curve. The y-axis reading is the desired viscosity.

Another representation that is useful in derivation work was given by Butler (1997) as

$$\frac{v_1}{v} = \left(\frac{T - T_2}{T_1 - T_2} \right)^m, \dots \quad (11.2b)$$

where 1 and 2 are the reference conditions, usually the saturated-steam and reservoir conditions, respectively, and v is the kinematic viscosity.

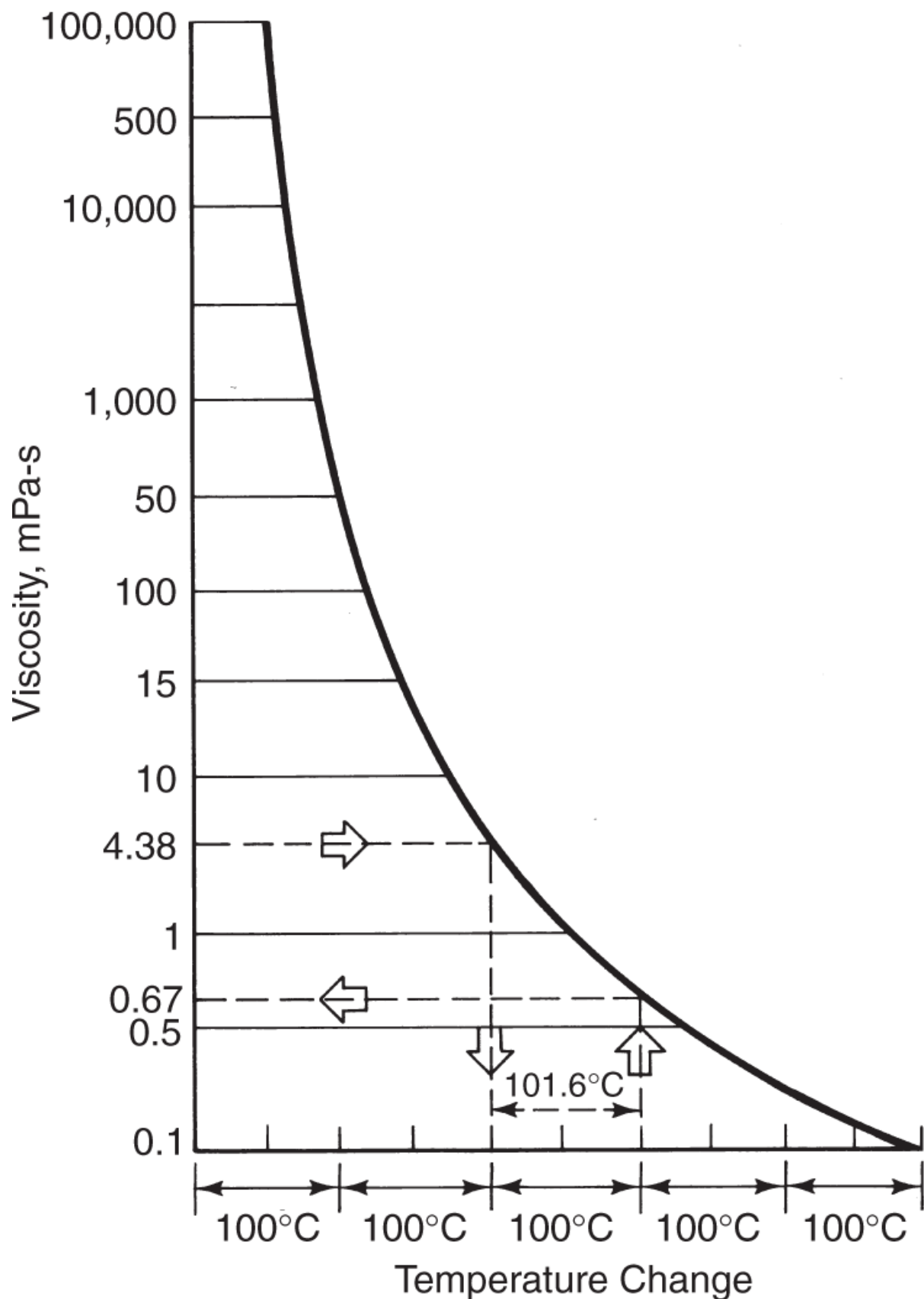


Fig. 11.8—Single-parameter viscosity correlation (Lewis and Squires 1934).

Several other crude-oil properties, such as specific heat, volumetric heat capacity, and thermal conductivity, are functions of temperature. Empirical equations to predict these properties include the Gambill (1957) equation for specific heat,

$$C_{p2} = \frac{0.7 + 0.0032T}{\rho_2^{0.5}}, \dots \dots \dots \quad (11.2c)$$

where C_{p2} is in $\text{kJ/kg}\cdot\text{K}$, T in K, and ρ_2 in g/cm^3 , and the thermal conductivity (Maxwell 1950) is

$$k_{T2} = 0.135 - 2.5 \times 10^{-5}T. \dots \dots \dots \quad (11.3)$$

k_{T2} in this equation has units of $\text{kJ/m}\cdot\text{h}\cdot\text{K}$. Eq. 11.3 is based on correlations for heavy crude fractions. These estimates are generally accurate to within 5%. For more details on these correlations, see the original references.

Eqs. 11.2 and 11.3 make it possible to estimate the *thermal diffusion coefficient*,

$$K_{T2} = \frac{k_{T2}}{\rho_2 C_{p2}}, \dots \dots \dots \quad (11.4)$$

for crudes. This quantity has units of m^2/s , as do the dispersion coefficients in Eq. 2.57.

11.2.3 Solid Properties. The total thermal conductivity of an unconsolidated sand-filled medium with a single phase j is

$$k_T = 0.0149 - 0.0216\phi + 8.33 \times 10^{-7}k - 10^{-4} \left(\frac{D_{90}}{D_{10}} \right) + 7.77D_{50} + 4.188k_T + 0.0507k_{Ts}. \dots \dots \quad (11.5)$$

The parameters in this equation have their usual meanings, except that D_{10} and D_{90} are particle diameters smaller than 10 and 90% of the total sample by weight. The units on the total, fluid j , and solid

(k_{Tt}, k_{Tj}, k_{Ts}) thermal conductivities are J/m-s-K, the permeability k is in μm^2 , and the median grain size D_{50} is in mm.

For fluid-filled consolidated sandstones, the analogous relation is

$$\frac{k_n}{k_{Td}} = 1 + 0.299 \left[\left(\frac{k_{Tj}}{k_{Ta}} \right)^{0.33} - 1 \right] + 4.57 \left(\frac{\phi}{1-\phi} \frac{k_{Tj}}{k_{Td}} \right)^{0.482} \left(\frac{\rho}{\rho_s} \right)^{-4.30}, \dots \quad (11.6)$$

where the subscripts a and d refer to air and dry rock. ρ is the density of the liquid-saturated rock. The thermal conductivities in Eqs. 11.5 and 11.6 are determined at a reference temperature of 293 K; they are rather weak functions of temperature, but corrections are given in Somerton (1973).

The volumetric heat capacity appears in the energy balances for thermal processes. It is defined for all phases, including the solid, as

$$M_{Tj} = \rho_j C_{pj}, \quad j = 1, \dots, N_p, s. \dots \quad (11.7)$$

We have encountered this quantity before in Eq. 2.83, which defined a total volumetric heat capacity.

Table 11.2 gives representative values of density, specific heat, thermal conductivity, and thermal diffusion coefficient for selected media. These values are appropriate for rough estimates of the rock-fluid thermal properties or for comparison to more refined estimates from Eqs. 11.5 through 11.7. The heat capacity of the solid phase varies relatively little with the type of solid, but the thermal conductivity can vary by a factor of two (compare the values for limestone and siltstone). The origin of the phrase, “heat can go where fluids cannot”, derives from the latter statement. The spatial variability of most nonthermal properties, permeability in particular, is far greater than this.

TABLE 11.2—DENSITY, SPECIFIC HEAT, THERMAL CONDUCTIVITY, AND THERMAL DIFFUSION COEFFICIENT OF SELECTED ROCKS [ADAPTED FROM FAROUQ ALI (1974)]

<u>Rock</u>	<u>Bulk Density (g/cm³)</u>	<u>Specific heat (kJ/kg-K)</u>	<u>Thermal conductivity (J/s-m-K)</u>	<u>Thermal diffusion coefficient (mm²/s)</u>
Dry				
Sandstone	2.08	0.729	0.831	0.55
Silty sand	1.90	0.801	(0.66)	(0.43)
Siltstone	1.92	0.809	0.649	0.42
Shale	2.32	0.761	0.989	0.56
Limestone	2.19	0.801	1.611	0.92
Fine sand	1.63	0.726	0.593	0.50
Coarse sand	1.74	0.726	0.528	0.42
Water-saturated				
Sandstone	2.27	0.999	2.610	1.15
Silty sand	2.11	1.142	(2.50)	(1.04)
Siltstone	2.11	1.094	(2.50)	(1.08)
Shale	2.38	0.844	1.600	0.79
Limestone	2.38	1.055	3.360	1.34
Fine sand	2.02	1.344	2.607	0.96
Coarse sand	2.08	1.249	2.910	1.12

Note: Values in parentheses are estimated.

Example 11.3. Heat Losses to Rock and Water. Later sections deal with various forms of heat losses, but we can introduce the largest source of heat loss now.

The total internal energy term in Eq. 2.3-1 is

$$\rho \hat{U} = \phi \sum_{j=1}^{N_p} \rho_j S_j \hat{U}_j + (1 - \phi) \rho_s \hat{U}_s.$$

Away from the critical point of water, internal energies and enthalpies are nearly equal, and therefore the preceding equation becomes

$$\rho \hat{H} = \phi (\rho_1 S_1 \hat{H}_1 + \rho_2 S_2 \hat{H}_2) + (1 - \phi) \rho_s \hat{H}_s.$$

We will work the hot-water case here in which the medium (the solid, subscript *s*) of porosity ϕ contains only water ($i = 1$) and oil ($i = 2$). You can tackle the steam case in Exercise 11.2.

Now, the fraction of heat that resides in the crude is

$$F_{\text{Heat}} = \frac{\phi \rho_2 S_2 \hat{H}_2}{\phi (\rho_1 S_1 \hat{H}_1 + \rho_2 S_2 \hat{H}_2) + (1 - \phi) \rho_s \hat{H}_s}.$$

Because there is no steam, the preceding equation can be written as

$$F_{\text{Heat}} = \frac{\phi \rho_2 S_2 C_{p2} (T - T_{\text{ref}})}{\phi [\rho_1 S_1 C_{p1} (T - T_{\text{ref}}) + \rho_2 S_2 C_{p2} (T - T_{\text{ref}})] + (1 - \phi) \rho_s C_{ps} (T - T_{\text{ref}})},$$

where we have used the heat capacities discussed previously (assumed independent of T) and T_{ref} is a reference temperature. Using the volumetric heat capacities from Eq. 2.83, this becomes

$$F_{\text{Heat}} = \frac{\phi S_2 M_{T2}}{\phi (S_1 M_{T1} + S_2 M_{T2}) + (1 - \phi) M_{Ts}}.$$

This ratio is mainly a function of the oil saturation S_2 and the porosity ϕ . Using typical values for the heat capacities ($M_{T1} = 3.97 \text{ MJ/m}^3 \cdot \text{K}$, $M_{T2} = 1.78 \text{ MJ/m}^3 \cdot \text{K}$, and $M_{Ts} = 2.17 \text{ MJ/m}^3 \cdot \text{K}$) yields the following values.

F_{Heat}	$\phi = 0.2$	$\phi = 0.3$
$S_1 = 0.2$	0.16	0.23
$S_1 = 0.5$	0.09	0.14

For a high-porosity, high- S_2 media, more than 20% of the heat resides in the oil. This value falls to less than 10% for tertiary floods in a low-porosity reservoir. These percentages also suggest guidelines for the best use of thermal methods: they are most

efficient in high-porosity reservoirs (where there is less rock to heat up) undergoing secondary flooding.

Considering the success of thermal methods, such small percentages of heat going into the crude are remarkable. The success of thermal methods, where so little of the heat actually resides in the oil (recall that we have not yet accounted for losses to the wellbore and adjacent strata), must be the result of the effectiveness of this method in reducing oil viscosity ([Fig. 11.1](#)).

11.3 Fractional Flow in Thermal Displacements

11.3.1 Propagation of Thermal Fronts. Noncombustion heat fronts can propagate in three ways: as hot water, as saturated steam, or as a noncondensable gas. Each has a characteristic velocity of propagation.

Let Fluid 3 displace Fluid 1 in a 1D medium with constant cross-sectional area. There are no other fluids in the medium. As always, Fluid 1 is cold water, but Fluid 3 can be hot water, noncondensable gas, or saturated steam. Fluid 3 has a higher temperature (T^+) than Fluid 1 (T^-), and in all cases, the displacement takes place without mixing. This means that neither the miscibility (or lack thereof) of the displacement nor its stability is at issue. We further assume that conduction is negligible (this eliminates heat losses to adjacent media), that displacement takes place at constant pressure, that the reference temperature for all enthalpies is T^- (that is, $H_{ii}^- = 0$), and finally, that all thermal properties are independent of temperature. These assumptions are the extension of the fractional-flow assumptions presented originally in [Chapter 5](#) for thermal floods.

The equations describing this displacement are the 1D versions of the mass and energy balances, Eqs. 2.11 and 2.36. These equations are hyperbolic and reducible with the above assumptions, and, therefore, we expect the methods introduced in several previous chapters to apply here also (see Section 5.6). Under these restrictions, energy and mass waves move at the same velocity. We

can express the front velocity as a multiple of the cold-water velocity u_1/ϕ .

On the basis of Eq. 5.41b, the front velocity is

$$v = \frac{1}{\phi} \left(\frac{\rho_3 u_3 - \rho_1 u_1}{\rho_3 - \rho_1} \right), \quad \dots \dots \dots \quad (11.8)$$

and on the basis of a shock velocity derived from the conservation of energy, the same velocity is

$$v = \frac{1}{\phi} \frac{\rho_3 u_3 H_3}{\rho_3 H_3 + \left(\frac{1-\phi}{\phi} \right) \rho_s H_s}. \quad \dots \dots \dots \quad (11.9)$$

The velocities in both equations are dimensional. Eq. 11.9 neglects all forms of energy other than thermal and assumes that enthalpy is equal to internal energy. $H_s = C_{ps}(T^+ - T^-) = C_{ps}\Delta T$ is the specific enthalpy of the solid. Three special cases follow from Eqs. 11.8 and 11.9.

Fluid 3 is Hot Water. In this case, $\rho_3 = \rho_1$, $H_3 = C_p \Delta T$, and Eq. 11.9 becomes

$$v_{HW} = \frac{1}{1 + \frac{1-\phi}{\phi} \frac{M_{Ts}}{M_{T3}}}, \quad \dots \dots \dots \quad (11.10)$$

where v_{HW} is the specific velocity of the front, normalized by $\frac{u_3}{\phi}$, the water flux. Eq. 11.10 has used the definition (Eq. 11.83) of volumetric heat capacity and Eq. 11.39, which for this case, gives $u_3 = u_1$, so that

$$v_{HW} = \frac{1}{1 + D_{HW}}, \quad \dots \dots \dots \quad (11.11)$$

where

is the retardation factor for the thermal front. Eq. 11.11 is a combination of the mass and energy balances. The velocity in Eq. 11.11 is independent of the temperature difference. For this case of incompressible flow, the heat fronts propagate more slowly than the tracer fronts, $v_{HW} = 1$. This slower propagation occurs because the thermal mass of the solid forces D_{HW} tends to be positive in much the same way as do the retardation factors for polymer and surfactant/polymer flooding in Eqs. 8.28a and 9.14.

Fluid 3 is Steam of Quality y . Here, we have $H_3 = C_{p1}\Delta T + yL_V$, where L_V is the latent heat of vaporization. Substituted into Eq. 11.9, this gives

Eliminating u_3/ϕ using Eq. 11.8 gives

where D_{SF} is the retardation factor for the steam front,

and h_D is a dimensionless latent heat,

h_D is the ratio of latent to sensible heat. Because $h_D \geq 0$, steam fronts ($\Delta T > 0$) move faster than hot-water fronts under equivalent conditions. In other words, L_V causes the front to propagate faster because it

stores heat better. Faster-moving heat fronts are more thermally efficient because the reservoir is contacted sooner and there is less time for heat losses to the under- and overburden. D_{SF} now depends on the temperature difference (through the $C_{p1}\Delta T$ term) and on pressure (through L_V). High-pressure steamfloods approach the hot-water limit because $L_V \rightarrow 0$ as the pressure approaches the critical point of water.

Example 11.4. Propagation of Thermal Fronts. Steam fronts have a larger velocity (are more efficient) than hot-water fronts for equivalent injected enthalpy, a fact that emphasizes the effect of pressure on thermal methods. Use the saturation temperature of [Fig. 11.4](#) and the enthalpy/pressure diagram of [Fig. 11.6](#) in this example.

We will consider two injections: saturated steam at a pressure of 2000 psia, and 50% quality steam at $P = 200$ psia. Both conditions have an injected enthalpy of approximately $\hat{H}_j = 620 \frac{\text{Btu}}{\text{lb}_m}$. The initial reservoir temperature is 85°F. We will use the volumetric heat capacities from the previous example and assume that the values for saturated water are the same at both pressures. From Eq. 11.12,

$$D_{HW} = \left(\frac{1-\phi}{\phi} \right) \frac{M_{Ts}}{M_{T1}} = \left(\frac{1-0.3}{0.3} \right) \left(\frac{2.17 \frac{\text{MJ}}{\text{m}^3\text{-K}}}{3.97 \frac{\text{MJ}}{\text{m}^3\text{-K}}} \right) = 1.28,$$

from which we can obtain $v_{HW} = \frac{1}{1+1.28} = 0.439$. This means that the hot-water front moves at less than one-half the velocity of a tracer front.

For the saturated-steam case, we must look up some values. [Fig. 11.5](#) gives $yL_v = (0.4)(3-0.9)\frac{\text{MJ}}{\text{kg}}$. We will need the saturated-steam temperature, which from [Fig. 11.4](#) is $T_s = 38^\circ\text{F}$, for which $\Delta T_s = (380-82)^\circ\text{F} = 166 \text{ K}$. Then

$$h_D = \frac{yL_v}{C_{p1}\Delta T} = \frac{(0.4)(2.1)\frac{MJ}{kg}}{\left(1\frac{Btu}{lb_m \cdot ^\circ F}\right)(298^\circ F)} \left\{ \frac{0.454 \text{ kg}}{1 \text{ lb}_m} \frac{1 \text{ Btu}}{10^{-3} \text{ MJ}} \right\} = 3.2$$

and $D_{SF} = \frac{D_{HW}}{1 + h_D} = \frac{1.28}{1 + 3.2} = 0.3$, which gives the final result of $v_{SF} = \frac{1}{1 + D_{SF}} = \frac{1}{1 + 0.3} = 0.77$.

The value is twice that of a hot-water velocity, but still slower than a tracer velocity. This ordering persists over the entire pressure range up to the critical point; even the magnitude of the velocities is relatively insensitive to pressure.

In both cases, the input enthalpy was the same; it is the presence of the latent heat that causes steam to be more efficient. All steam-based processes operate more efficiently at low pressure because latent heat is larger.

The preceding equations give a way to confirm what was implicitly assumed earlier: that a steam front is self-sharpening. Let us start by combining Eqs. 11.14 through 11.16:

$$v_{SF} = \frac{1}{1 + D_{SF}} = \frac{1}{1 + \frac{D_{HW}}{1 + h_D}} = \frac{1}{1 + \frac{D_{HW}}{1 + \frac{yL_v}{C_{p1}\Delta T}}}.$$

For a displacement of saturated water ($y = 0$) by 100% quality steam ($y = 1$), the range of velocities is

$$v_{SF} \Big|_{y=0} = \frac{1}{1 + D_{HW}}$$

for saturated water and

$$v_{SF} \Big|_{y=1} = \frac{1}{1 + \frac{D_{HW}}{1 + \frac{L_v}{C_{p1}\Delta T}}}$$

for saturated steam. Therefore, $v_{SF} \Big|_{y=0} < v_{SF} \Big|_{y=1}$, and the front is a shock because the larger steam qualities move faster than the smaller qualities. The converse would, of course, be true for saturated water displacing saturated steam. That the steam front is a shock accounts for much of the success of steam drives.

Fluid 3 is a Noncondensable Gas. This case is similar to the hot-water case except that $H_3 = C_{p3} \Delta T$. A similar procedure to the above yields

$$v_G = \frac{1}{1 + D_G}, \dots \quad (11.17)$$

where the retardation factor is now

$$D_G = \left(\frac{1-\phi}{\phi} \right) \frac{M_{T_3}}{M_{T_3}}. \dots \quad (11.18)$$

Because $\rho_3 C_{p3} \ll \rho_1 C_{p1}$, D_G is much greater than D_{HW} . Hence, heated gasfloods propagate the most slowly of the three cases.

11.3.2 Flow With Oil. In the next few sections, we will analyze some simple thermal displacements using fractional-flow theory. The basic governing equations are the strong forms of conservation of water,

$$\frac{\partial(\rho_1 S_1 + \rho_3 S_3)}{\partial t_D} + \frac{\partial(\rho_1 f_1 + \rho_3 f_3)}{\partial x_D} = 0, \dots \quad (11.19a)$$

conservation of oil,

and conservation of energy,

$$\frac{\partial \left[\rho_1 S_1 H_1 + \rho_2 S_2 H_2 + \rho_3 S_3 H_3 + \frac{(1-\phi)}{\phi} \rho_s S_s H_s \right]}{\partial t_D} + \frac{\partial (\rho_1 f_1 H_1 + \rho_2 f_2 H_2 + \rho_3 f_3 H_3)}{\partial x_D} = 0. \dots \dots \quad (11.19c)$$

The mass balances are from the basic 1D fractional-flow equation (Eq. 2.53)—with water in a second phase 3—and the energy balance equation (Eq. 2.64). Of course, to write these, we have made some fairly restrictive assumptions that deserve special discussion when applied to thermal flooding.

Writing the equations in terms of fractional flow rather than flux (with f_j instead of u_j) means that we have invoked the fractional-flow assumptions. The portion of the fractional-flow assumptions least likely to apply in general is that of incompressible fluids and rock. Oil and water (hot or cold) can generally be assumed to be incompressible without great error, but steam is highly compressible. Aside from consistency with the other parts of this book and the attendant simplifications, there is no compelling reason for assuming steam to be incompressible. [For a treatment that does not assume incompressible fluids and solids, see Shutler and Boberg (1972); Aydelotte and Pope (1983).]

However, pressure gradients in steam zones are usually low, so that the densities therein can be considered approximately constant. Of course, assuming an incompressible solid means that there can be no oil production because of pore compression. The no-dissipation part of the fractional-flow assumptions now includes thermal conductivity, which is absent from Eq. 11.19c.

The equations further assume that there is no solubility of oil in water and no oil vaporization. We neglect all forms of energy except thermal energy, and we assume that internal energies are equal to enthalpies. Finally, we solve Eq. 11.19c by assuming no lateral heat loss. These assumptions mean that we can use the conventional

definitions of dimensionless time and position (Eq. 5.9) and the fractional-flow methods to solve for $S_1(x_D, t_D)$ and $T(x_D, t_D)$.

11.3.3 Hot Waterfloods. For this case, $S_3 = 0$, and the assumption of incompressible fluids and solids is good. With this, Eq. 11.19a is the only independent material balance; its strong form becomes

which has the saturation velocity

Similarly, writing the energy Eq. 2.80 in a fractional-flow form yields

$$\left(M_{T_1}S_1 + M_{T_2}S_2 + \frac{1-\phi}{\phi} M_{T_s} \right) \frac{\partial T}{\partial t_p} + \left(M_{T_1}f_1 + M_{T_2}f_2 \right) \frac{\partial T}{\partial x_p} = 0. \quad \dots \quad (11.21a)$$

We have also used the mass-balance equations for water and oil to eliminate saturation derivatives. Eq. 11.20b implies a velocity for the temperature change,

$$v_T = \frac{M_{T1}f_1 + M_{T2}f_2}{M_{T1}S_1 + M_{T2}S_2 + \frac{(1-\phi)}{\phi}M_{Ts}} \dots \dots \dots \quad (11.21b)$$

v_T is a function of T only through the temperature dependence of f_j . This temperature dependence is much weaker than the dependence of μ_2 on T . Therefore, the temperature wave is a shock in hot-water displacements.

The velocities in Eqs. 11.20b and 11.21b are set equal, which yields

$$\frac{df_1}{dS_1} = \frac{f_1 + \frac{M_{T_2}}{M_{T_1} - M_{T_2}}}{S_1 + \frac{M_{T_2} + \frac{(1-\phi)}{\phi} M_{Ts}}{M_{T_1} - M_{T_2}}} \dots \dots \dots \quad (11.22)$$

on eliminating $S_2 = 1 - S_1$ and $f_2 = 1 - f_1$. Eq. 11.22 determines the water saturation S_1^* just behind the hot-water front using the construction suggested in [Fig. 11.9](#). The construction is analogous to that in [Fig. 8.15](#) for polymer flooding except that the straight material-balance line does not begin from a point on the x -axis. This feature, which is caused by the difference between water and oil volumetric heat capacities in Eq. 11.22, arises because water is convecting heat to the thermal front, while oil is convecting heat away from it. By our assumptions, convection is the only form of heat transfer occurring in this displacement.

The rear of the oil bank must propagate at the same velocity; hence, the extension of the material-balance line to the cold-oil fractional-flow curve gives the oil-bank saturation. The leading edge of the cold oil bank follows from the by now usual secant construction shown in [Fig. 11.9](#).

11.3.4 Steam Displacements. We anticipate that in the absence of lateral heat loss, a steam front will propagate faster than a hot-water front (Example 11.3) and that there can be no condensation. With heat losses, some condensation can occur, but we save this discussion for the later treatment of heat losses. Behind the steam front, temperature must be constant because, by assumption, pressure is constant (pressure gradients being negligible). Hence, the entire left side of the energy balance becomes

$$\frac{\partial(\rho_3 S_3)}{\partial t_D} + \frac{\partial(\rho_3 f_3)}{\partial x_D} = 0. \dots \dots \dots \quad (11.23)$$

in one dimension. From Eqs. 11.19a, 11.19b, and 11.23, we see that the mass of each phase is conserved in the steam zone. However,

this is exactly the same problem that was solved in Section 5.7, where we considered the flow of water, gas, and oil as immiscible phases. There we constructed the composition-path diagram ([Fig. 5.21](#)), which illustrated the transition from an initial condition *I* to an injected condition *J* in two waves.

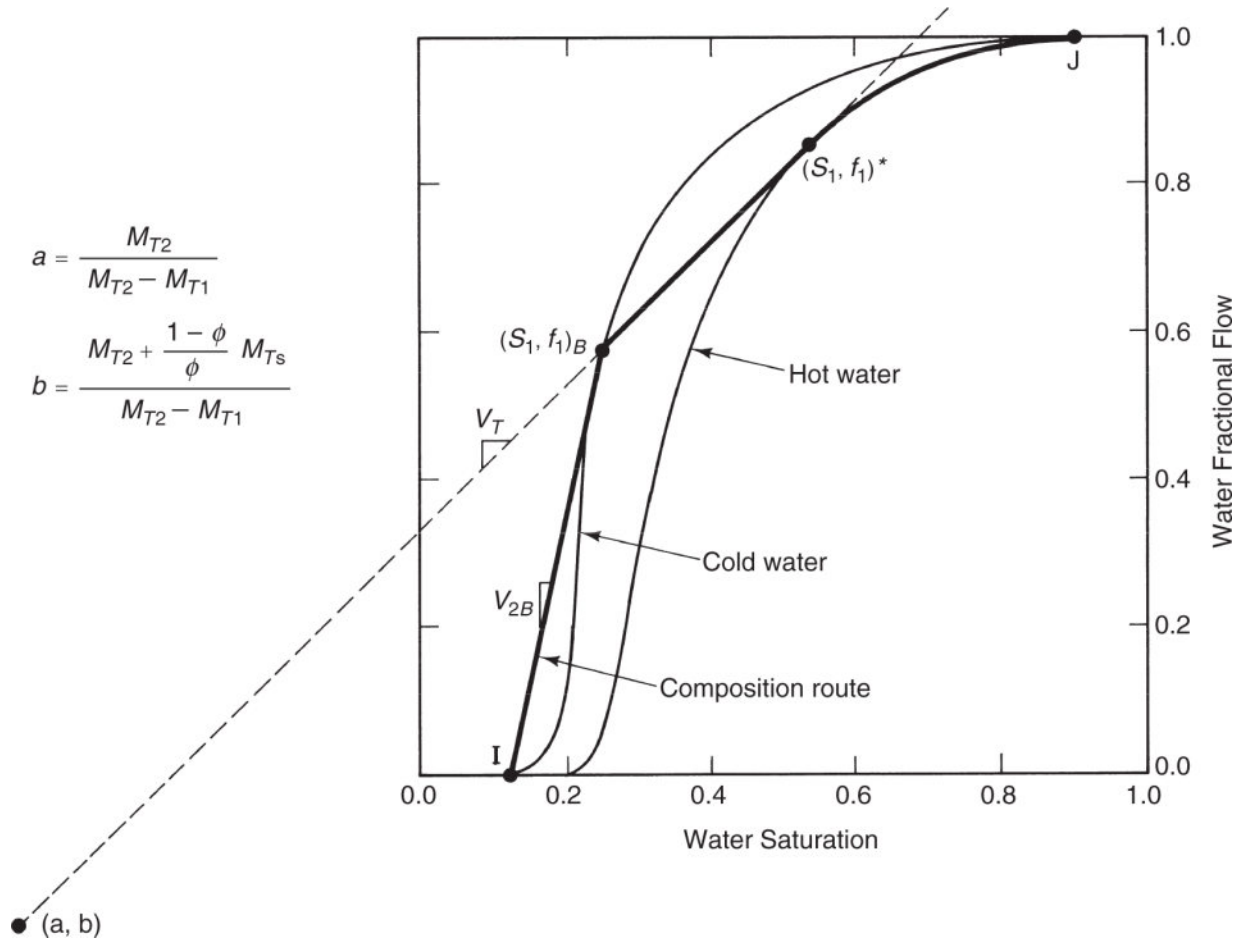


Fig. 11.9—Graphical construction of hot waterflood solution.

Although the solution presented in [Fig. 5.21](#) is the same as the solution to a propagating steam front, they differ in one important respect: the initial condition *I* in the current problem is no longer given because this is the condition immediately behind (upstream of) the steam front. To find condition *I*, we must resort to applying the coherence condition across the steam front.

The integral coherence condition for the steam front, written in terms of oil and water amounts, is

$$\frac{\rho_1 (f_1 H_1)^+ + \rho_2 (f_2 H_2)^+ + \rho_3 (f_3 H_3)^+}{\rho_1 (S_1 H_1)^+ + \rho_2 (S_2 H_2)^+ + \rho_3 (S_3 H_3)^+ + \frac{(1-\phi)}{\phi} \rho_s H_s^+} = \frac{\rho_1 f_1^+ + \rho_3 f_3^+ - \rho_1 f_1^-}{\rho_1 S_1^+ + \rho_3 S_3^+ - \rho_1 S_1^-} = \frac{f_2^+ - f_2^-}{S_2^+ - S_2^-}, \quad \dots \quad (11.24)$$

(energy) (water) \quad (oil)

where the + and – represent conditions immediately upstream (the “injected” condition) and downstream of the front. No negative term appears in the energy equation because the reference temperature for enthalpy is T^- by assumption. We can simplify Eq. 11.24 by letting $H_3 = H_1 + L_V$ and $H_j = C_{pj}T$ (for $j = 1$ and 2). This yields

Normally, the steam-zone temperature T^+ is known, leaving ten unknowns (f_j^+ and S_j^+ for $j = 1, 2, 3$, and C and \bar{C}) in the two equations (Eq. 11.25). There are five independent relations between fractional flow and saturation—three for the upstream side and two for the downstream side—and, of course, the S_j and f_j on both sides must sum to unity, adding another two equations. We are left with an indeterminate system because there are nine total equations in ten unknowns.

One way around this problem is to invoke additional assumptions regarding the upstream conditions (Shutler and Boberg 1972). An example of this would be to let $f_j^+ = 0$. The most rigorous method would be to derive additional jump conditions by restoring the dissipative terms and solving the profile in a moving coordinate system, the so-called traveling wave problem (Bryant et al. 1986; Lake et al. 2002). Once the upstream conditions (+) have been determined, the solution proceeds, as in Section 5.7.

11.4 Heat Losses From Equipment and Wellbores

Example 11.2 showed that heat losses to rock and water easily represent the most significant source of heat loss in thermal

methods. Although preventing this is beyond our reach (except for judicious selection of thermal candidates), minimizing heat losses from equipment and wellbores and to adjacent strata *is* within our power.

11.4.1 Equipment Losses. Heat is lost from surface equipment such as pipes, fittings, valves, and boilers. Such equipment is routinely insulated, so that losses are small, except under extreme circumstances. Most heat-transfer books give procedures for detailed calculation from surface lines. [Table 11.3](#) gives approximate heat losses that are adequate for most designs.

11.4.2 Wellbore Losses. Heat losses from the wellbore, on the other hand, can cause a sizable energy debit if the reservoir is deep. We devote the remainder of this section to estimating wellbore-fluid temperature and quality and the rate of heat lost at a given depth. Versions of this calculation occur in production of hot fluid below aquifers and permafrost. The treatment here is for injectors, where estimates of heat loss are important to the efficiency of thermal methods.

TABLE 11.3—TYPICAL VALUES OF HEAT LOSSES FROM SURFACE PIPING

Insulation	Conditions	Heat Loss, Btu/h·ft ² Surface Area for Inside Temperatures of:			
		200°F	400°F	600°F	800°F
Bare metal pipe	Still air, 0°F	540*	1560	3,120	—
	Still air, 100°F	210	990	2,250	—
	10-mph wind, 0°F	1,010	2,540	4,680	—
	10-mph wind, 100°F	440	1,710	3,500	—
	40-mph wind, 0°F	1,620	4,120	7,440	—
	40-mph wind, 100°F	700	2,760	5,650	—
Heat Loss, Btu/h·ft of Linear Length of Pipe at Temperatures of:					
Magnesium pipe insulation, air temperature 80°F	Standard on 3-in. pipe	50**	150	270	440
	Standard on 6-in. pipe	77	232	417	620
	1½ in. on 3-in. pipe	40	115	207	330
	1½ in. on 6-in. pipe	64	186	335	497
	3 in. on 3-in. pipe	24	75	135	200
	3 in. on 6-in. pipe	40	116	207	322

*1 Btu/h·ft² \cong 3.0 J/m²·s.

**1 Btu/h·ft = 0.91 J/m·s.

Estimating heat losses from a wellbore provides an excellent extended example of the application of heat-transfer theory and approximate solutions. The approach consists of three segments: steady-state heat transfer through the drillhole region, transient heat conduction in the earth adjacent to the well, and an overall heat balance on the fluid in the wellbore itself. With appropriate assumptions, each problem can be solved separately and then merged to give the final result. Combining steady-state, transient, and overall balances, as we are about to do, is a *quasisteady-state* approximation. The basic equations for strong- and weak-form energy conservation are Eqs. 2.36 and 2.92, respectively. Steady state exists when the time derivatives are zero.

11.4.3 Estimating the Overall Heat-Transfer Coefficient.

Estimates of heat-transfer rate through an element of height Δz in the drillhole region can be obtained from the following equation:

where $\Delta\dot{Q}$ is the heat-transfer rate (energy units divided by time) through a section of a vertical wellbore Δz in height having an outer tubing radius of R_{to} . U_T is the overall heat-transfer coefficient based on the outer surface of the tubing. Using Eq. 11.26 requires an estimate of U_T .

Heat transfer through the drillhole region involves several different resistances between the fluid flowing in the tubing and the formation. Starting with the formation and moving inward, these are a cement zone, casing, annulus, tubing insulation, the tubing itself, and the flowing fluid. [Fig. 11.10](#) shows a schematic of the temperature profile and definitions of symbols. Eq. 11.26 is expressed in terms of the temperature difference between the fluid T_f and the temperature at the drillhole radius T_d .

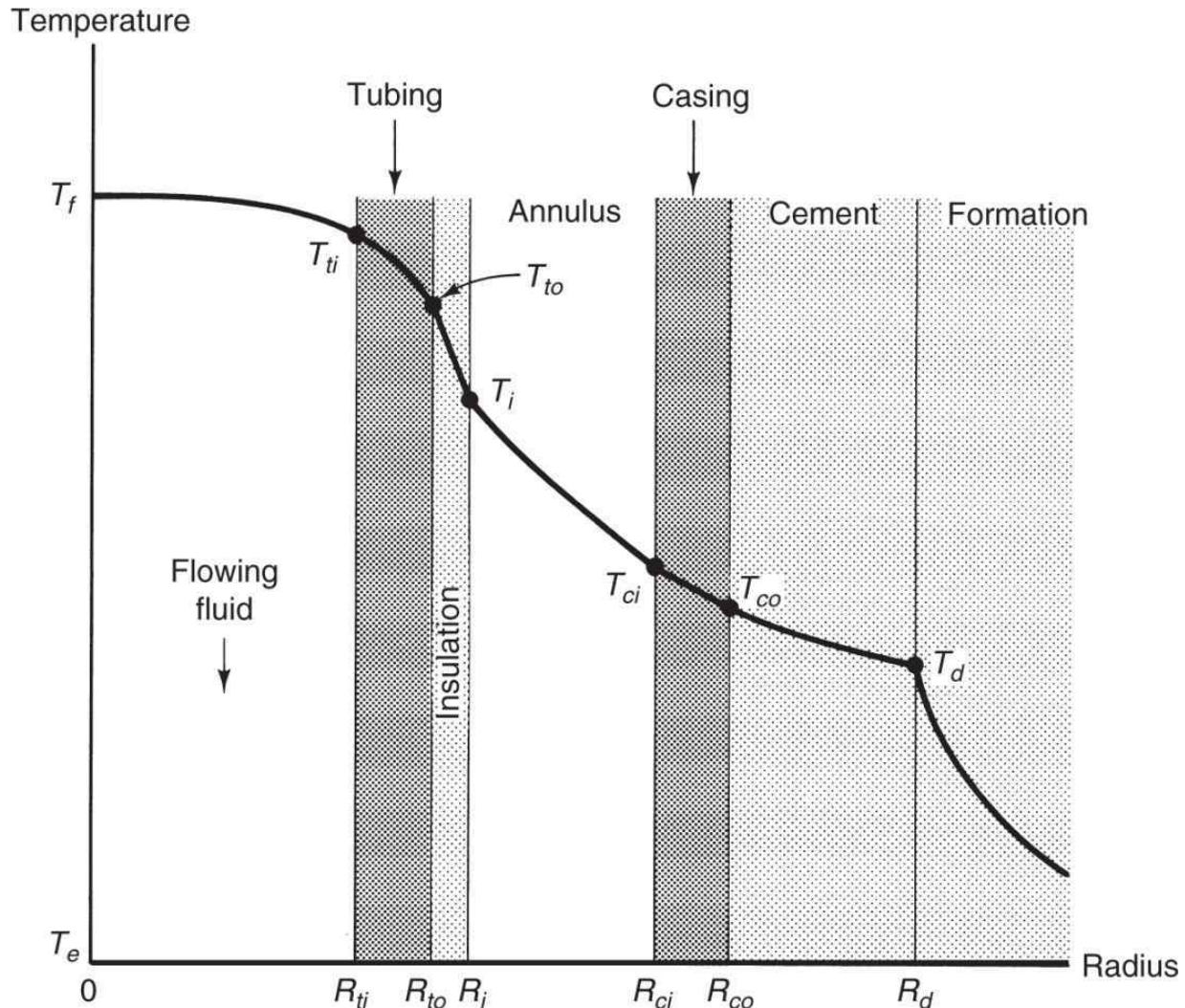


Fig. 11.10—Schematic-temperature profile in a drillhole [adapted from Willhite (1967)].

Following Willhite (1967), we assume radial symmetry in the drillhole, no heat transfer in the z-direction, and temperature-independent thermal conductivities. Because the drillhole region occupies a much smaller volume than the formation, it is reasonable to assume that temperature transients here decay much faster than in the formation. Therefore, we can assume that a steady-state energy balance applies in the tubing, insulation, casing, and cement:

$$\frac{d}{dr}(rq_c) = 0, \dots \quad (11.27)$$

where q_c is the radial component of the conductive heat flux \vec{q}_c in Eq. 2.33, heat transfer here being solely by conduction. Because the radius-heat flux product is a constant, the heat-transfer rate over height z is also a constant:

Eq. 11.28 can be integrated for the temperature differences between the inside and outside of each region:

k_{Tt} , k_{Ti} , k_{Tc} and k_{Tcem} in Eq. 11.29a are the thermal conductivities of the tubing, insulation, casing, and cement, respectively.

Neither the fluid in the tubing nor the fluid in the annulus transfers heat strictly by conduction; hence, they must be treated separately. Let the heat-transfer rates through these regions be expressed as

by analogy to Eqs. 11.26. h_{Tf} and h_{Ta} are the heat-transfer coefficients of the fluids in the tubing and annulus, respectively. They can be estimated mainly through correlations, as discussed in the following.

We can sum Eqs. 11.29 and 11.30 to give the overall temperature drop,

$$T_f - T_d = \frac{\Delta\dot{Q}}{2\pi\Delta z} \left[\frac{1}{R_{ti}h_{Tf}} + \frac{\ln\left(\frac{R_{to}}{R_{ti}}\right)}{k_{Ti}} + \frac{\ln\left(\frac{R_i}{R_{to}}\right)}{k_{Ti}} + \frac{1}{R_i h_{Ta}} + \frac{\ln\left(\frac{R_{co}}{R_{ci}}\right)}{k_{Tc}} + \frac{\ln\left(\frac{R_d}{R_{co}}\right)}{k_{Tcem}} \right], \dots \quad (11.31)$$

which, inserted into Eq. 11.26, gives the overall heat-transfer coefficient,

$$U_T^{-1} = R_{to} \left[\frac{1}{R_{ti}h_{Tf}} + \frac{\ln\left(\frac{R_{to}}{R_{ti}}\right)}{k_{Ti}} + \frac{\ln\left(\frac{R_i}{R_{to}}\right)}{k_{Ti}} + \frac{1}{R_i h_{Ta}} + \frac{\ln\left(\frac{R_{co}}{R_{ci}}\right)}{k_{Tc}} + \frac{\ln\left(\frac{R_d}{R_{co}}\right)}{k_{Tcem}} \right]. \dots \quad (11.32)$$

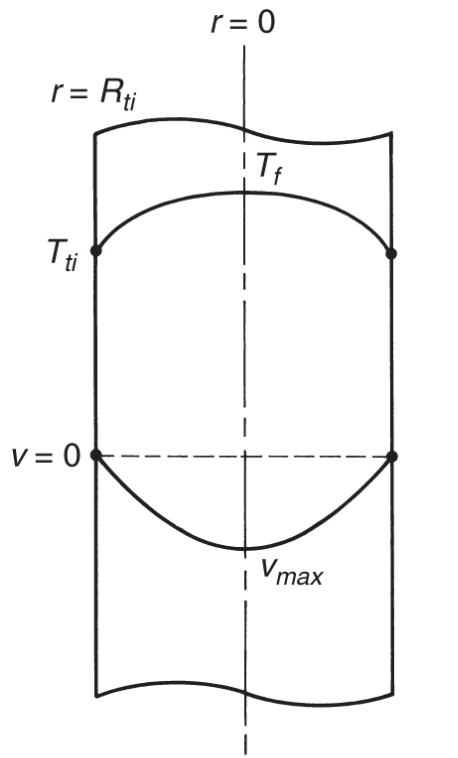
This equation expresses the total conductance between the fluid and the formation as a sum of series resistances each weighted by geometrical factors. If any one of the zones in Fig. 11.8 is absent (inner and outer radii equal), that term will be absent in Eq. 11.32. Moreover, if the thermal conductivity of a component is high, as is usually true with the tubing and casing, the corresponding term in Eq. 11.32 will be small. Many times, in fact, a single term will dominate the overall heat-transfer coefficient (as might occur in insulated tubing where k_{Ti} is small). Using Eq. 11.32 requires estimates of h_{Tf} and h_{Ta} .

11.4.4 Heat-Transfer Coefficient in Tubing and Annulus. The major difficulty in using Eq. 11.32 is estimating h_{Tf} and h_{Ta} because the other terms are constant. Heat transfer from a flowing fluid is by conduction and convection, and if the flow rate is large, heat is dissipated by viscous heating. Fig. 11.11a shows schematic velocity

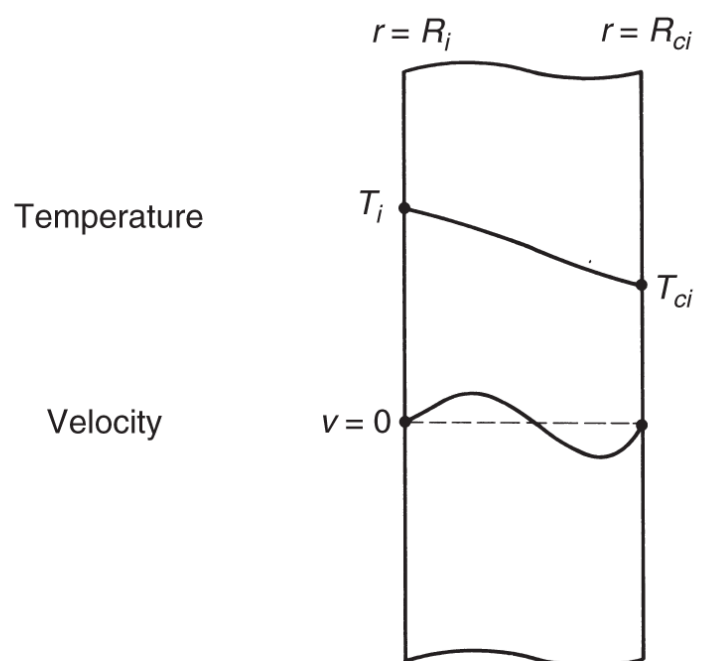
and temperature profiles. Theoretical arguments (Bird et al. 2002) suggest that h_{Tf} correlates as the following dimensionless equation:

for tubes with large length-to-diameter ratios. The dimensionless groups in Eq. 11.33 are

where the overbar in Eq. 11.34c indicates a volume average.



(a) Tubing – forced convection



(b) Annulus – free convection

Fig. 11.11—Schematic velocity and temperature profiles in tubing and annulus [adapted from Willhite (1967)].

As their naming after persons suggests, these are familiar groups in the heat-transfer literature. Each group has a physical interpretation: N_{Nu} is the ratio of total to conductive heat transfer; N_{Pr} is the ratio of convective to conductive heat transfer; N_{Re} is the ratio of inertial to viscous forces in the fluid flow; and N_{Br} is the ratio of viscous heat dissipation to conduction. Of these four, N_{Br} is the only one containing a temperature difference; however, if it is small, as it often is for liquid flows, this dependence is weak. For simple geometry, the specific form of Eq. 11.33 can be derived theoretically; in practical cases, the relationship is empirical (Bird et al. 2002). See Exercise 11.6.

Heat transfer through an annulus is even more complicated. If the annulus is sealed at both ends, there can be no bulk flow; however, the temperature difference between T_i and T_{ci} causes local density differences in the annulus fluid that cause flow. We call such flow

free convection to distinguish it from the *forced* convection in the tubing. [Fig. 11.11b](#) shows schematic velocity and temperature profiles for the annulus. Another dimensional argument suggests a relation among dimensionless groups, a particular form of which is (Willhite 1967)

$$N_{Nu} = 0.0499 \left(N_{Gr} N_{Pr} \right)^{1/3} N_{Pr}^{0.074} \dots \dots \dots \quad (11.35)$$

for flat plates with large length-to-diameter ratios. The additional group in Eq. 11.35 is the Grashof number,

$$N_{Gr} = \frac{\left(R_{ci} - R_i \right)^3 g \rho_a \beta_T (T_i - T_{ci})}{\mu_a}, \dots \dots \dots \quad (11.36)$$

which is the ratio of free convection transport to viscous forces. The parameter β_T is a thermal expansion coefficient defined as $-1/\rho_a(\partial_a/\partial T)_P$, and the subscript *a* refers to the annulus fluid. The fluid properties in N_{Nu} , N_{Pr} , and N_{Gr} are now based on the annulus fluid. The Grashof number contains a temperature difference that is usually unknown *a priori*; therefore, in applications, it may be necessary to solve for heat loss by trial and error.

Usually an annulus is air-filled, but on occasion, it has been evacuated. When this occurs, heat transfer is almost exclusively through radiation. Radiation is a form of heat flux independent of convection or conduction. Under some circumstances, radiation can account for a substantial fraction of heat transfer.

11.4.5 Heat Conduction in the Formation. The immense thermal mass of the earth surrounding the wellbore, only a small fraction of which is in contact with the reservoir, suggests that heat transfer here is transient. In this segment, we repeat a procedure first described by Ramey (1959) for calculating temperatures beyond the drillhole, $r > R_d$.

Let heat transfer in the formation be strictly by radial conduction. In the absence of any velocities, Eq. 2.36 becomes

$$\frac{\partial T}{\partial t} = \left(\frac{k_T}{\rho C_p} \right)_s \frac{1}{r} \frac{\partial}{\partial r} \left(r \frac{\partial T}{\partial r} \right) = \frac{K_{Ts}}{r} \frac{\partial}{\partial r} \left(r \frac{\partial T}{\partial r} \right), \dots \quad (11.37)$$

where Eq. 2.34 has been inserted for conductive heat flux and Eq. 11.4 has been used for the thermal diffusion coefficient. Eq. 11.37 also assumes an incompressible, single-phase formation so that a change in internal energy is manifest only as a change in temperature (there is no latent heat). Once this equation has been solved for $T(t, r)$ for $r > R_d$, the heat-transfer rate follows from the spatial gradient at $r = R_d$. The following boundary and initial conditions apply to Eq. 11.37:

$$T(0, r) = T(t, \infty) = T_e. \dots \quad (11.38a)$$

$$-k_{Ts} \left(\frac{\partial T}{\partial r} \right)_{r=R_d} = \frac{\Delta \dot{Q}}{2\pi R_d \Delta z}, \dots \quad (11.38b)$$

where Δz is the overall height difference. The undisturbed external temperature T_e is a function of z because of the geothermal gradient

$$T_e = a_T z + T_0, \dots \quad (11.39)$$

where a_T is usually approximately 0.18 K/km, and T_0 is the mean surface temperature. The existence of this gradient implies a constant rate of heat transfer from the Earth's core; it also suggests a z -dependency in the problem that is not explicit in the equations. The solution, therefore, will be for a particular z , but the variation with z arises only when solving the energy balance for the flowing fluid. Eq. 11.38b expresses the continuity of heat flux at $r = R_d$. Combining it with Eq. 11.26 gives the "conduction" condition,

$$-k_{Ts} \left(\frac{\partial T}{\partial r} \right)_{r=R_d} = \frac{U_T R_{to} (T_f - T_d)}{R_d}. \dots \quad (11.40)$$

As discussed earlier, all temperatures are functions of z .

For nonzero R_d , the solution to Eqs. 11.37, 11.38, and 11.40 must be numerical (using Laplace inversion), but once it is known, the heat-transfer rate follows from Eq. 11.38b to give

$$\Delta\dot{Q} = \frac{2\pi k_{Ts} (T_d - T_e) \Delta z}{f_T(t_D)}, \dots \quad (11.41)$$

where f_T is a function of dimensionless time t_D and formation Nusselt number,

$$t_D = \frac{K_{Ts} t}{R_d^2} \dots \quad (11.42a)$$

$$N_{Nu} = \frac{R_{to} U_T}{k_{Ts}} \dots \quad (11.42b)$$

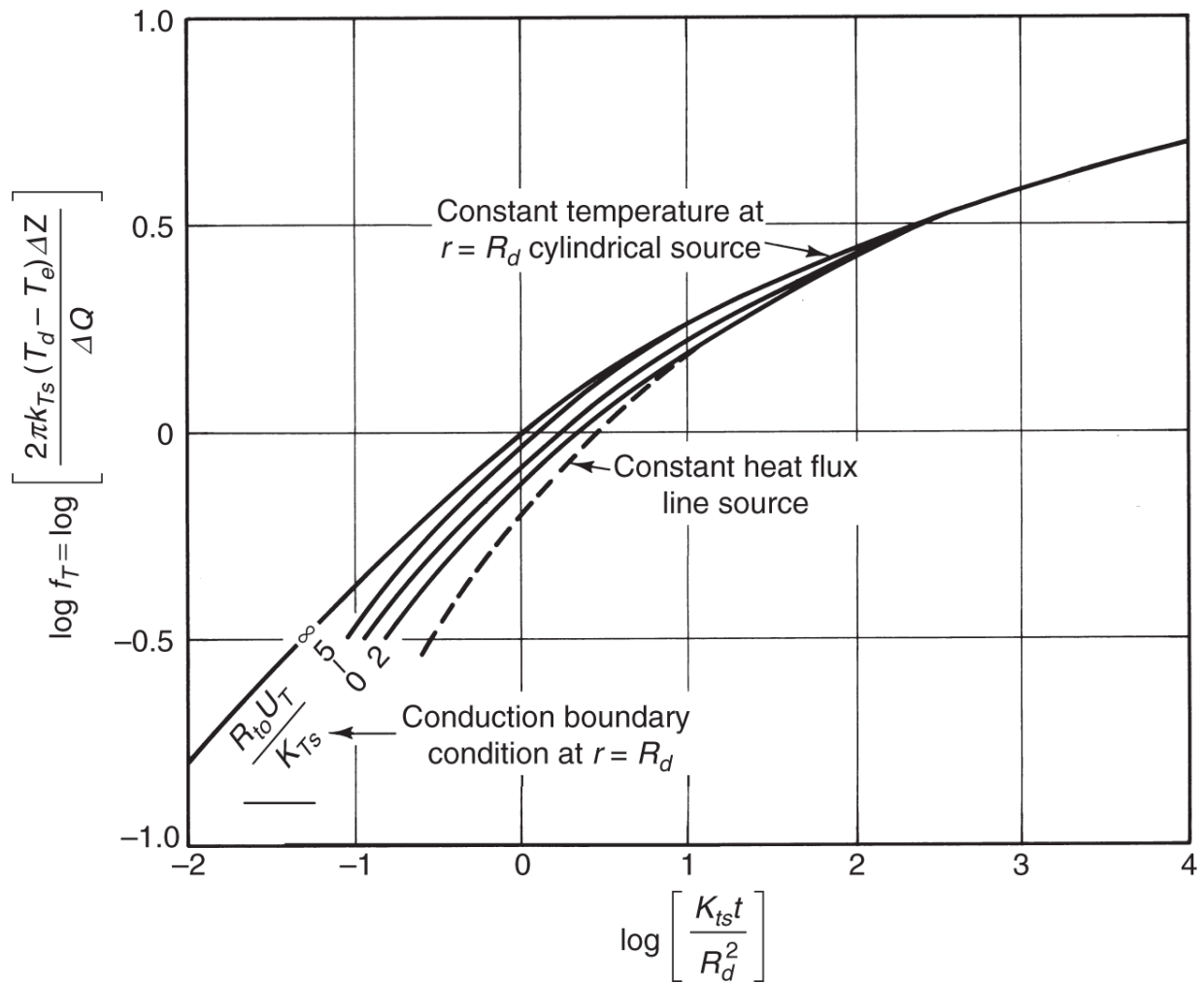


Fig. 11.12—Transient heat-transfer function (Ramey 1962).

[Fig. 11.11](#) shows the logarithm of f_T plotted vs. the logarithm of t_D with N_{Nu} as a parameter.

Ramey (1959) gives the procedure for using these equations. Let us solve for the inner casing temperature T_{ci} and heat loss rate $\Delta\dot{Q}$ at a given depth and time. We know the radii in [Fig. 11.12](#); the thermal conductivities of the tubing, insulation, casing, and cement zone; the thermal properties of the flowing fluid, the annulus fluid, and the formation; the viscosity and average velocity of the flowing fluid; and the depth z and the bulk fluid temperature T_f . The procedure is as follows:

1. Calculate T_e from Eq. 11.39 and calculate N_{Pr} and N_{Re} for the flowing fluid and N_{Pr} for the annulus fluid from Eqs. 11.34. Calculate t_D from Eq. 11.42a.
2. Assume a value for h_{Ta} and calculate U_T from Eq. 11.32, all other quantities being independent of temperature. If N_{Br} is not small, a value for h_{Tf} must be assumed also.
3. Calculate the formation Nusselt number from Eq. 11.42b and, using this and t_D , estimate f_T from Fig. 11.12. Calculate T_d from

$$T_d = \frac{T_f f_T(t_D) + \left(\frac{k_{Ts}}{R_{to} U_T} \right) T_e}{f_T(t_D) + \left(\frac{k_{Ts}}{R_{to} U_T} \right)}. \quad \dots \quad (11.43)$$

T_f in this equation follows from eliminating $\Delta\dot{Q}$ between Eqs. 11.26 and 11.41. We can now calculate $\Delta\dot{Q}$ from either equation.

4. With $\Delta\dot{Q}$ and T_d known, the casing temperature T_{ci} and all the others follow from successive application of Eqs. 11.29 and 11.30.

The solution would now be complete, but the assumed value of h_{Ta} in Step 2 may be incorrect. Proceeding further requires a trial-and-error process.

5. Calculate N_{Gr} from Eq. 11.36 and use Eq. 11.35 to estimate h_{Ta} . If radiation is important, we would correct for it here.
6. Recalculate U_T from its definition (Eq. 11.32). Compare this value to that used in Step 2; repeat Steps 2 through 6 with the new value of U_T if agreement is not satisfactory. The convergence test is on U_T , a much weaker function of temperature than h_{Ta} . Convergence should be obtained in three or fewer steps.

11.4.6 Heat Loss From the Wellbore. We now focus attention on the element Δz , through which heat is passing at rate $\Delta \dot{Q}$. First, we eliminate T_d between Eqs. 11.26 and 11.41 to give

$$\Delta \dot{Q} = \frac{2\pi k_{Ts} R_{to} U_T}{k_{Ts} + R_{to} K_{Ts} f_T(t_D)} (T_f - T_e) \Delta z. \quad (11.44)$$

In what follows, we assume U_T to be constant.

If we apply the overall energy balance (Eq. 2.56) to the element Δz , we have

$$A \Delta z \frac{d}{dt} (\overline{\rho_f U}) + \Delta \dot{H} - \bar{v} \rho_f A g \Delta z = -\Delta \dot{Q}, \quad (11.45a)$$

where we have neglected kinetic energy and mechanical work terms. Furthermore, by writing the enthalpy rate entering and leaving Δz as the product of a specific enthalpy and a constant mass flow rate $\dot{m} = \bar{v} r_{\rho_f} A$, we can obtain

$$\dot{m} (\Delta \bar{H} - g \Delta z) = -\Delta \dot{Q}. \quad (11.46b)$$

Eq. 11.46b has also dropped the time derivatives using the same quasisteady-state argument used previously for the drillhole.

The simplest heat-loss model follows from Eq. 11.41 by assuming that T_f is constant at the surface inlet temperature (this makes $\Delta \bar{H} = 0$) and integrating the resulting ordinary differential equation for dQ/dz (in the limit $\Delta z \rightarrow 0$) (Ramey 1964):

$$\dot{Q}(z) = \frac{2\pi k_{Ts} R_{to} U_T}{k_{Ts} + R_{to} U_T f_T(t_D)} \left[(T_f - T_0) z - \frac{a_T z^2}{2} \right], \quad (11.46)$$

where we have replaced T_e by Eq. 11.39 and T_d by Eq. 11.26 before integrating. This equation yields the maximum heat-loss rate up to depth z because the temperature difference between T_f and T_e is the maximum possible value. $(T_f - T_0)$ is the difference between inlet and surface temperatures.

For more general cases, let us eliminate $\Delta\dot{Q}$ between Eqs. 11.44 and 11.45b, which yields, after again taking the limit as $\Delta z \rightarrow 0$,

$$\frac{d\bar{H}}{dz} - g = -\frac{2\pi k_{Ts} R_{to} U_T (T_f - T_e)}{\dot{m} [k_{Ts} + R_{to} U_T f_T(t_D)]}. \quad (11.47)$$

Eq. 11.47 is a working equation. The sign convention is that z increases downward and \dot{Q} is positive when heat is lost from the wellbore. We can invoke Eq. 11.47 for several special cases by taking different forms for the specific enthalpy.

If the fluid flowing in the tubing is an ideal gas, because single-phase steam would be at low pressure, the enthalpy is independent of pressure:

$$d\bar{H} = C_{p3} dT_f. \quad (11.48a)$$

Substituting this into Eq. 11.47,

$$\frac{dT_f}{dz} = \frac{g}{C_{p3}} - \frac{2\pi k_{Ts} R_{to} U_T (T_f - T_e)}{C_{p3} \dot{m} [k_{Ts} + R_{to} U_T f_T(t_D)]}. \quad (11.48b)$$

Eq. 11.48b will integrate to

$$T_f = a_T z + T_0 - A_T \left(a_T + \frac{g}{C_{p3}} \right) + \left[(T_f - T)_0 + A_T \left(a_T + \frac{g}{C_{p3}} \right) \right] e^{-z/A_T}. \quad (11.48c)$$

for constant heat capacity, where

$$A_T(t_D) = \frac{\dot{m} C_{p3} [k_{Ts} + R_{to} U_T f_T(t_D)]}{2\pi k_{Ts} R_{to} U_T}. \quad (11.48d)$$

and T_{f0} in Eq. 11.48c is the inlet surface temperature at $z = 0$. With T_f now determined as a function of depth, we can integrate Eq. 11.45b for the heat loss down to z . These two equations state that the fluid temperature and heat loss vary with depth as an exponential function

plus a linear term, the rate of change being determined by A_T , which is proportional to the mass flow rate.

If the flowing fluid is a superheated vapor at the inlet surface temperature, Eq. 11.48c will describe its temperature down to the saturation temperature. Below this point, the fluid will be a saturated two-phase mixture for some distance down in the tubing, where the fluid will condense gradually to saturated water as more heat is lost. In this case, the specific enthalpy relates to the steam quality as

If pressure is constant, this leads to a relatively simple differential equation in quality (Satter 1965),

where

$$A_T(t_D) = \frac{\dot{m}L_v [k_{Ts} + R_{to}U_T f(t_D)]}{2\pi R_{to} k_{Ts}}. \quad \dots \quad (11.49c)$$

Because a change in steam quality at constant pressure must take place at constant temperature, we can integrate Eq. 11.49b with T_f constant at the saturation temperature for the fluid quality in the tubing,

$$y = 1 + \left[\frac{\left(\frac{gA_T}{L_v} \right) + T_0 - T_f}{A_T} \right] z + \frac{a_r z^2}{2A_T}, \dots \dots \dots \quad (11.49d)$$

where $y = 1$ at $z = 0$. The heat loss follows from Eq. 11.49a; note that a constant flowing temperature does not imply the absence of heat loss if the fluid is condensing.

Eq. 11.49d is deceiving in its simplicity. It has neglected the hydrodynamics of two-phase flow in a vertical pipe and the

significant effect that U_T (through h_{Tf}) can bring about with condensation. Still, the equation is quite instructive, particularly when merged with a heat-loss calculation for flowing gas.

Heat is lost from the wellbore because a temperature difference exists between the heated wellbore and the geothermal temperature in the surrounding formation. [Fig. 11.13](#) shows the state of fluids in a wellbore, into which superheated steam is being injected, as a function of depth and injection time. This calculated result assumes that pressure is constant in the wellbore.

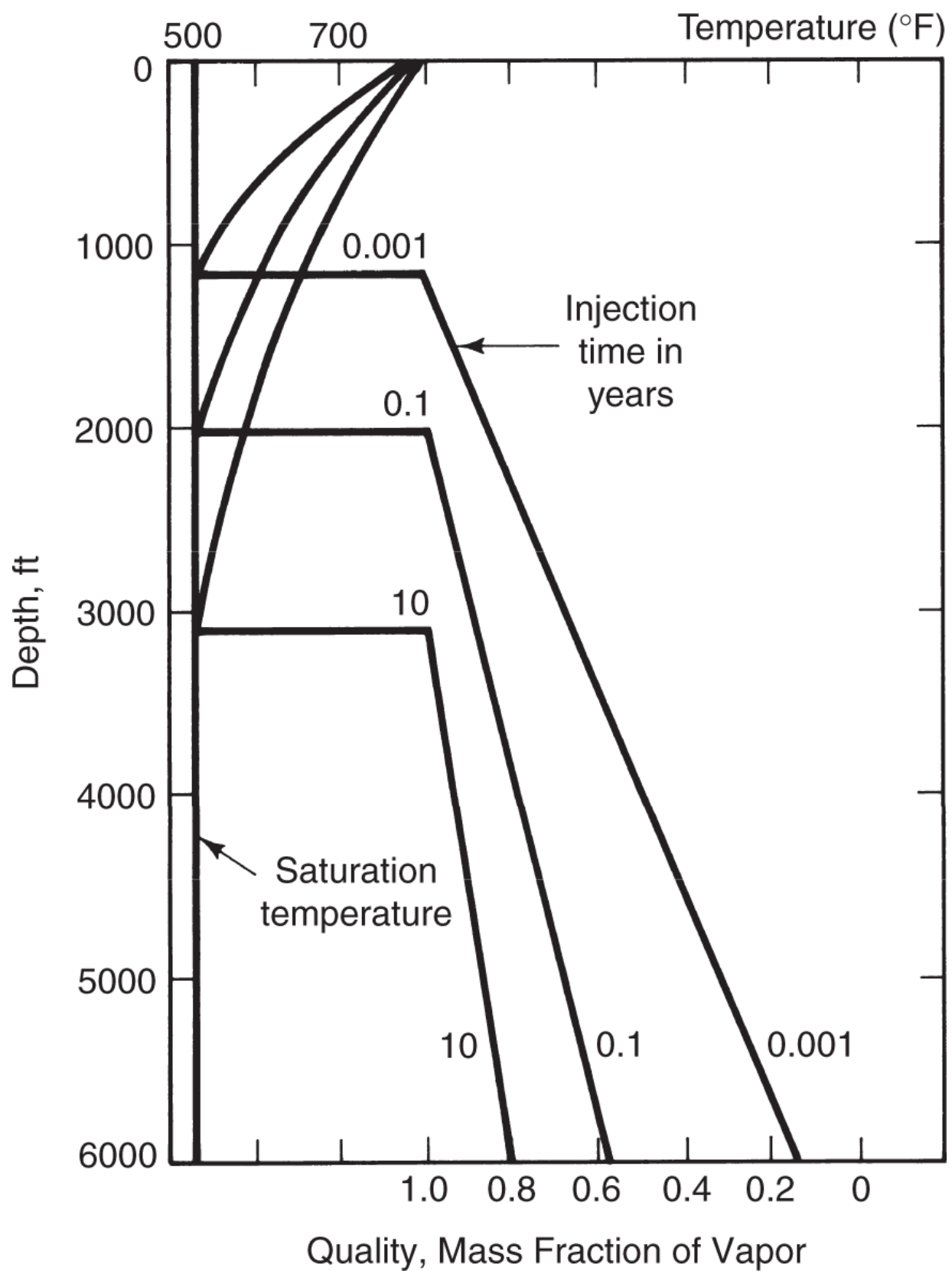


Fig. 11.13—Change in temperature or steam quality with depth (Satter 1965).

The progression in [Fig. 11.13](#) can be seen on the enthalpy-pressure diagram in [Fig. 11.4](#). Suppose that the wellbore pressure is 3.1 MPa and the surface temperature is 800 K. The temperature falls to the dewpoint temperature at the wellbore pressure. Eq. 11.48c approximates the temperature change, which is represented by a horizontal line in the superheated steam region in [Fig. 11.4](#). From this point down, the wellbore temperature becomes constant, and steam quality declines as predicted by Eq. 11.49d. The change becomes apparent in [Fig. 11.4](#), where the extension of the horizontal line from the superheated-steam region coincides with lines of constant temperature but decreasing quality. At a fixed time, the heat lost per unit mass of steam is given by the difference in the x-coordinates on the enthalpy/pressure diagram. The entire progression moves down the wellbore with increasing time.

11.4.7 Controlling Heat Loss. Heat losses from the wellbore to the surrounding formation can be controlled in three ways.

1. Restrict application. [Fig. 11.13](#) and [Fig. 11.14](#) indicate that deep wells and long producing lives are to be avoided. Steam processes, in particular, are generally not practical at depths of more than 1000 m. If the reservoir depth is not too large, pattern spacing can be relatively close, which will cause short producing lives. Close spacing will also reduce the amount of heat lost to the adjacent strata.
2. Insulate the tubing. The mechanisms for wellbore heat loss are conduction from the casing, radiation between the tubing and the casing, and free convection in the annulus. We can suppress all these mechanisms by insulating the casing or tubing from the formation.

[Fig. 11.14](#) shows the dramatic effect of insulation. The insulation causes a tenfold reduction in heat losses in hot-water injection. The reduction would not be quite as large in steam injection because the vapor heat-transfer coefficient is already approximately one-half that of hot water.

Whether or not insulation is appropriate depends on the benefit in heat saved weighed against the cost of insulation. This, in turn, depends on the type of insulation and the depth of the well. By now, it has become common practice to leave an air space between the annulus and tubing to provide partial insulation.

3. Inject at high rate or high surface pressure. As the injection rate increases, so does the heat transfer from the hot fluid. Several of the equations given previously attest to this; examine the fluid temperature change in Eq. 11.48b and the quality change in Eq. 11.49d. Heat-loss rate increases with \dot{m} , but the heat-loss rate does not increase as fast as the rate that heat is delivered to the formation, so the *relative* loss rate goes down. [**Fig. 11.15**](#) shows the advantages of this strategy; tripling the injection rate reduces the relative heat losses by approximately a factor of three. A secondary benefit to be gained from a high injection rate is a short project life.

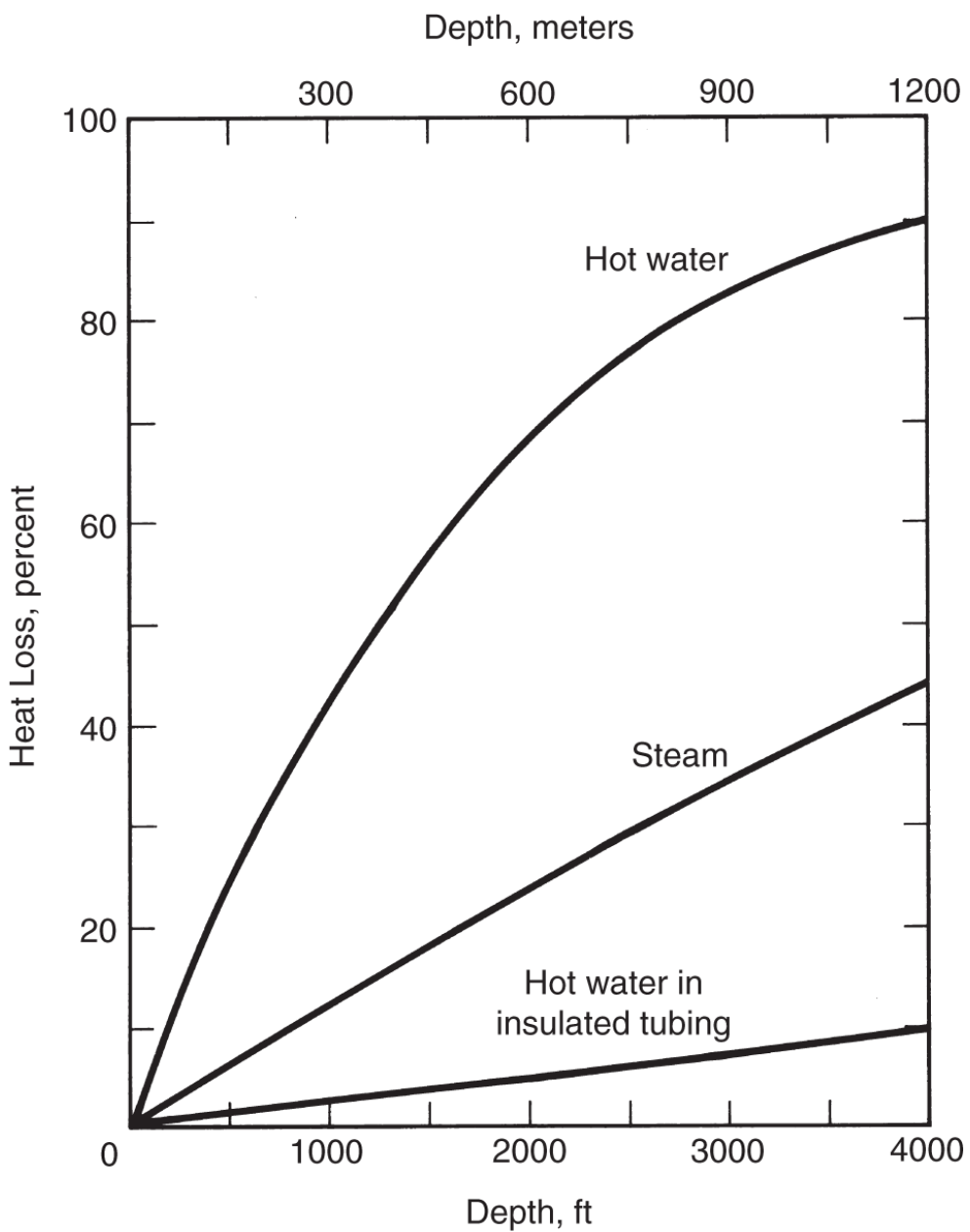


Fig. 11.14—Effect of insulation on heat loss (Ramey 1962).

There are two further cautions. The injection pressure must not be so high that it exceeds the formation parting pressure. Just as in waterflooding, such parting can introduce high-permeability channels into the formation, with resulting loss of volumetric sweep efficiency (although this problem is not as severe in thermal methods as in other EOR methods). The second concern is that high injection rate in a steamdrive will lead to excessive heat losses through the

producers if continued after steam breakthrough. The rate of loss from the wellbore must be balanced with the rate of loss through the producers when this happens, but usually the injection rate is reduced once steam breaks through.

An obvious way to avoid wellbore heat losses is to generate the heat in situ or at the bottom of the wellbore. The first technique is the basis for in-situ combustion (see Section 11.8), which extends the practical depth of thermal floods to approximately 2000 m. Below this depth, compression costs tend to be prohibitive. The second technique implies downhole steam generation.

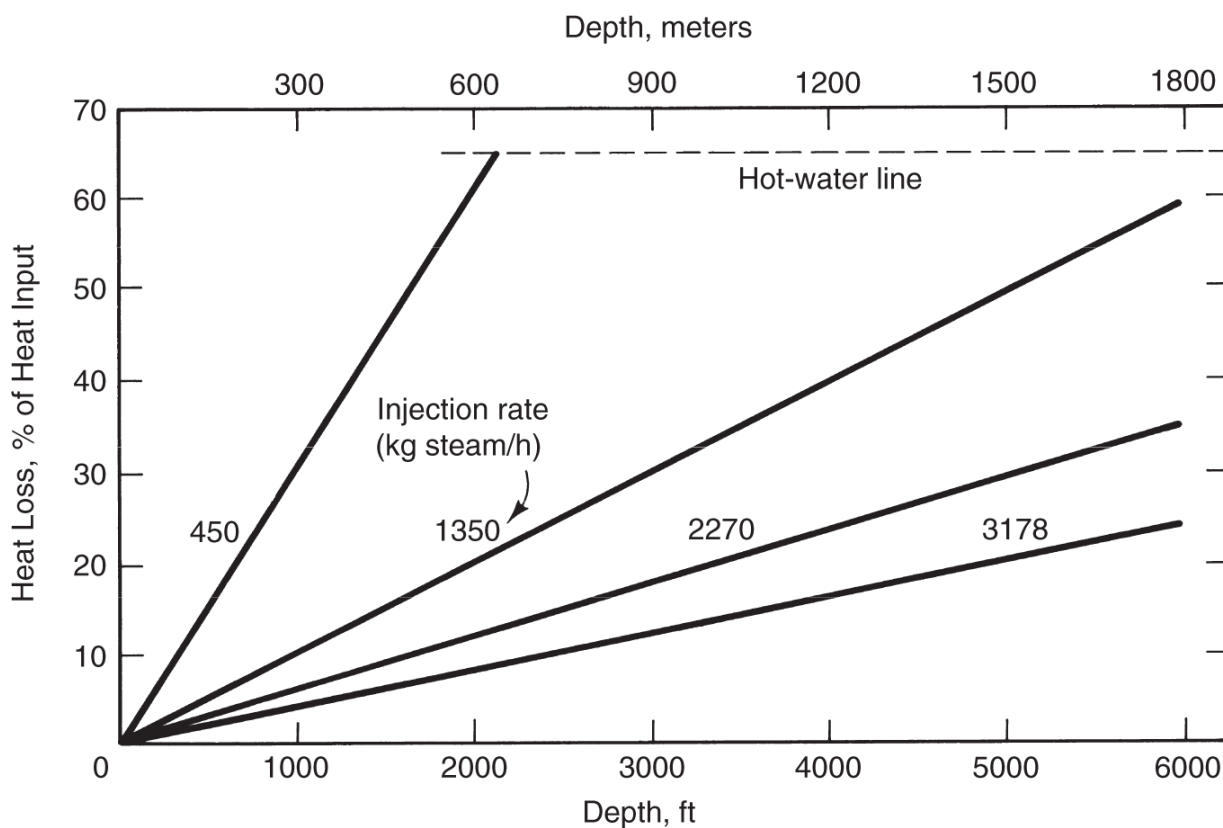


Fig. 11.15—Effect of injection rate on heat loss (Satter 1965).

Two types of downhole steam generators produce steam at the sandface. In the direct-fired generator, water and fuel are mixed in a combustion chamber, burned, and the entire mixture (steam, unburned fuel, and combustion products) is then injected. The CO₂ in the combustion products is an EOR agent in its own right, but the

device has proven difficult to operate and maintain. The indirect-fired generator returns the combustion mixture to the surface and, although a little easier to maintain, is clearly more complex. The combustion products for both can represent an environmental hazard.

11.5 Heat Losses to Overburden and Underburden

The fourth source of heat loss in thermal methods is loss to adjacent strata or to the overburden and underburden. As in Section 11.4, analysis of this loss involves a combination of local and overall heat-transfer techniques that leads to a highly practical result. We give here an exposition of the Marx- Langenheim (ML) (1959) theory as expounded by Farouq Ali (1966).

The objective of the ML theory is to calculate the heated area as a function of time and reservoir properties. The heated area leads then to expressions for oil rate, oil/steam ratio, and energy efficiency (see Exercise 11.7). The procedure is most appropriate for steamdrives, but the expression for heated area applies for all thermal processes.

[Fig. 11.16](#) shows a schematic illustration of heating. The figure is a top view of a single vertical heat-injection well. We assume that the heated zone in an areally infinite reservoir contains a single phase with negligible horizontal heat conduction. These assumptions result in an ideally sharp temperature profile. We further assume that the over- and underburden extend to infinity along both the positive and negative z-axis (out of the page).

11.5.1 The Local Problem. The objective of this section is to derive an expression for the rate of heat loss \dot{Q} to the over- and underburden and the area $A(t)$ of the heated zone as a function of time.

If the over- and underburden are impermeable, heat transfer is entirely through conduction. All fluid velocities and convective fluxes now being zero, the energy balance (Eq. 2.36) reduces to the 1D form,

$$\frac{M_{Ts}}{k_{Ts}} \frac{\partial T}{\partial t} = \frac{1}{K_{Ts}} \frac{\partial T}{\partial t} = \frac{\partial^2 T}{\partial z^2}. \dots \dots \dots \quad (11.50)$$

K_{Ts} is the thermal diffusion coefficient of the over- and underburden, and M_{Ts} is the total volumetric heat capacity of the same. Eq. 11.50 assumes that all thermal properties are independent of temperature.

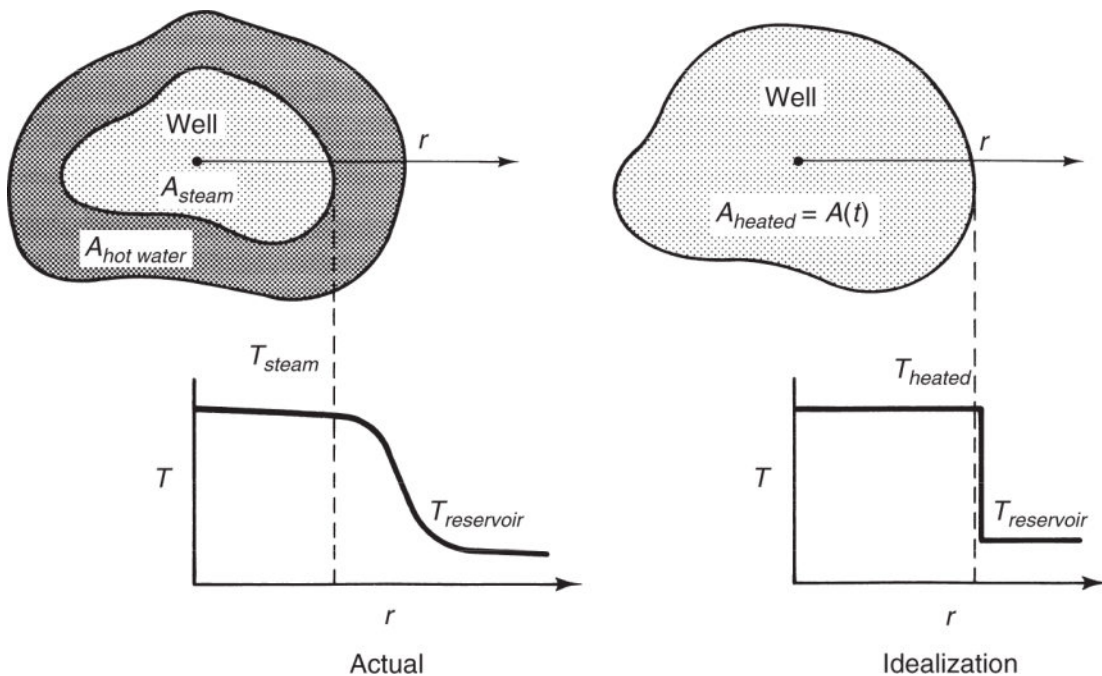


Fig. 11.16—Idealization of heated area for ML theory.

Eq. 11.50 applies to a vertical segment of the over- and underburden with cross-sectional area ΔA_k for which the face at $z = 0$ (the top of the reservoir) is at the original temperature T_i , until time t_k , when it is raised to T_j . The boundary conditions for Eq. 11.50 are now

$$T(z, 0) = T_i = T(\infty, t); \quad T(0, t > t_k) = T_j. \dots \dots \dots \quad (11.51a)$$

Eq. 11.51a neglects the geothermal gradient outside the reservoir, an assumption that implies, because the problem is symmetric, that we need not treat the over- and underburden separately. The time scale of the problem may be offset by t_k , so that the last boundary condition in Eq. 11.51a becomes

where $T = T(z, \tau)$, $\tau = t - t_k$, and $\tau > 0$.

Eqs. 11.50 and 11.51 are now of precisely the same form and boundary conditions as Eqs. 5.51 and 5.53, and their solutions can be abstracted directly as

where τ has replaced the time variable. The rate of heat transferred into ΔA_k from the reservoir is

With the solution in hand, we can differentiate the erfc solution (recalling its definition), evaluate it at $z = 0$, and substitute the result into Eq. 11.53 to give

where $\Delta T = T_J - T_i$. Eq. 11.54 expresses the rate of heat loss to any vertical segment when $t > t_k$. When we sum all similar segments so that the largest of these t_K is just smaller than t , we have

which, in the limit of the largest ΔA_k approaching zero, becomes

The factor two in these equations is to account for heat loss to both the over- and underburden. This procedure is the application of a

special case of Duhumel's theorem, which is a form of superposition for continuously changing boundary conditions (Carslaw and Jaeger 1959). For later operations, it is convenient to convert the integration variable in Eq. 11.55b to a time variable,

$$\dot{Q} = 2 \int_{\xi=0}^{\xi=t} \frac{k_{Ts} \Delta T}{\sqrt{\pi K_{Ts} (t - \xi)}} \frac{dA}{d\xi} d\xi. \dots \quad (11.55c)$$

Eq. 11.55c expresses the rate of heat loss at time t as a function of the rate of growth of the heated area. The integrand is finite because of the square root in the denominator, but it is of no use without some independent way of relating heat-loss rate to time.

11.5.2 Overall Heat Balances. The link between \dot{Q} and time comes from an overall energy balance. To simplify matters, we assume T_r to be the reference temperature for the enthalpy, which means that Eq. 2.91 applied to the reservoir now becomes

$$\dot{H}_J - \dot{Q} = \frac{d}{dt} (AH_r \rho_s U), \dots \quad (11.56)$$

there being no “out” term except for the heat loss. We have neglected the work (the PV) term, and $\rho_s U$ is the volumetric internal energy of the over- and underburden. Because the temperature reference is the original reservoir temperature, all energy terms involving the unheated or cold reservoir vanish. This simplification and the neglect of conduction imply that the time derivative in Eq. 11.56 merely expresses the change in heated-zone volume. If the reservoir thickness is constant, Eq. 11.56 becomes

$$\dot{H}_J = 2 \int_{\xi=0}^{\xi=t} \frac{k_{Ts} \Delta T}{\sqrt{\pi K_{Ts} (t - \xi)}} \frac{dA}{d\xi} d\xi + H_r M_{Tr} \Delta T \frac{dA}{dt}, \dots \quad (11.57)$$

where Eq. 11.55c has been inserted into Eq. 11.56.

Eq. 11.57 is an integral-differential equation for $A(t)$, which we solve using the initial condition $A(0) = 0$. The most direct solution

method is through Laplace transforms (Farouq Ali 1966). The inverted solution with \dot{H}_J constant (Roberts and Kaufmann 1966) is

$$A(t_D) = \frac{\dot{H}_J H_t}{4k_{Ts} \Delta T} \left[e^{t_D} \operatorname{erfc}(t_D^{1/2}) + \frac{2t_D^{1/2}}{\sqrt{\pi}} - 1 \right], \quad \dots \dots \dots \quad (11.58a)$$

where t_D is a dimensionless time, defined as

$$t_D = \frac{4K_{Ts} t}{H_t^2} = \frac{4k_{Ts} t}{M_n H_t^2}. \quad \dots \dots \dots \quad (11.58b)$$

The H_t^2 in Eq. 11.58b means that all heat-loss expressions will be especially sensitive to reservoir thickness H_t .

One important feature of the ML theory is that the final result is largely independent of the shape of the heated zone. To some extent, this observation is true even if there is gravity overlay, for here the larger heat loss to the overburden is very nearly balanced by a smaller loss to the underburden. To a lesser approximation, the heated area given by Eq. 11.58 applies after steam reaches a producing well in steamdrives if the *net* enthalpy rate (Injected – Produced) replaces \dot{H}_J .

Several immediate results follow from Eq. 11.59 or its time derivatives:

$$\frac{dA}{dt_D} = \frac{\dot{H}_J H_t}{4k_{Ts} \Delta T} e^{t_D} \operatorname{erfc}(t_D^{1/2}) = \frac{\dot{H}_J H_t}{4K_{Ts} M_n \Delta T} e^{t_D} \operatorname{erfc}(t_D^{1/2}). \quad \dots \dots \dots \quad (11.59)$$

All the equations stated above can be combined to give the heat-loss rate as

$$\dot{Q} = \dot{H}_J \left(1 - e^{t_D} \operatorname{erfc}(t_D^{1/2}) \right). \quad \dots \dots \dots \quad (11.60)$$

11.5.3 Applications. Eqs. 11.56 and 11.59 define an expression for the average heating efficiency E_{hs} ,

$$\bar{E}_{hs} \equiv 1 - \frac{\dot{Q}}{\dot{H}_J} = e^{t_D} \operatorname{erfc}(t_D^{1/2}). \quad \dots \dots \dots \quad (11.61)$$

\bar{E}_{hs} is the fraction of heat in the reservoir at time t_D expressed as a fraction of the heat entering the sandface at the injector.

[Fig. 11.17](#), which shows $\bar{E}_{hs}(t_D)$ graphically for a steamdrive, uses Eq.11.61 as a starting point. The figure contains the dimensionless latent heat first introduced in Eq. 11.16, which does not appear in Eq. 11.61 because it is based on more complex physics. In the limit $h_D \rightarrow 0$, the results revert to a hot waterdrive. This phenomenon underlines, once again, the benefit of using steam over hot water. Perhaps the most singular result from [Fig. 11.17](#) is the time dependency; the thermal efficiency of steamdrives inevitably declines with time.

If we assume that the displacement of a unit volume of oil from the heated zone causes the production of a unit volume of oil, the oil production rate in reservoir volumes is

$$\dot{N}_{p2} = \phi \Delta S_2 H_{NET} \frac{dA}{dt} \dots \dots \dots \quad (11.62a)$$

from applying Eq. 2.51 to the oil. Using Eq.11.61 this becomes

$$\dot{N}_{p2} = \dot{H}_J \left(\frac{\phi \Delta S_2}{M_t \Delta T} \right) \left(\frac{H_{NET}}{H_t} \right) \left(e^{t_D} \operatorname{erfc} t_D^{1/2} \right), \dots \dots \dots \quad (11.62b)$$

where $\Delta S_2 = S_2 - S_2'$ is the oil-saturation change caused by heating. The net thickness H_{NET} is the proportion of the reservoir contributing to flow; the gross thickness is the entire reservoir. The equation has been slightly rearranged to include explicitly the net-to-gross thickness ratio. Correlations for the oil saturation in the steam zone S_2' are available in the literature (see Section 11.6).

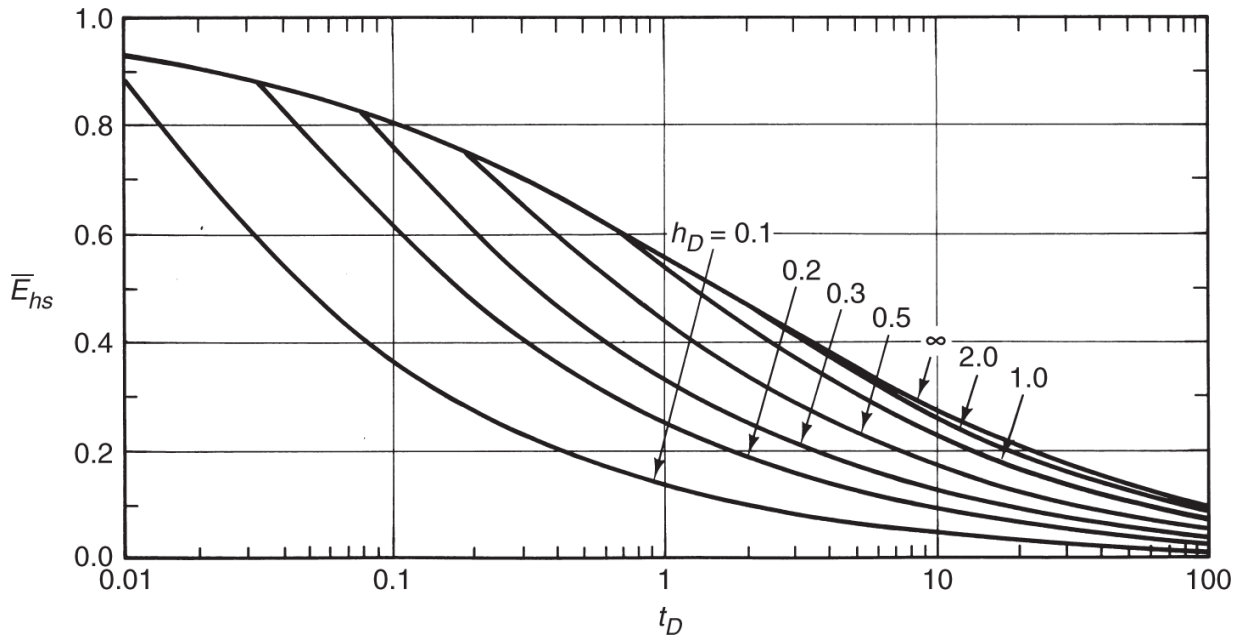


**Fig. 11.17—Steam-zone thermal efficiency (Myhill and Stegemeier 1978).
Dimensionless latent heat given in Eq. 11.16.**

Eq. 11.62b invariably overestimates the oil rate, especially after steam breakthrough in a steamdrive (after breakthrough, the equation predicts a more accurate oil rate if net enthalpy is used for the \dot{H}_J term), but it directly highlights two important parameters in thermal flooding. If the net-to-gross thickness ratio $\left(\frac{H_{\text{NET}}}{H_t}\right)$ is small, the oil rate will also be proportionally small. Physically, this means that a substantial amount of heat is being expended to warm up rock that does not contribute to production (nonpay). The second parameter exhibiting a direct proportionality to the oil rate is the combination $\phi\Delta S_2$, the “delsophi,” which has long been used as an indicator of thermal-flooding success. Delsophi should be as large as possible for steamdrive candidates. Occasionally, the $\phi\Delta S_2 H_{\text{NET}}$ from Eq. 11.62b is used as a screening parameter; a reservoir with $\phi\Delta S_2 H_{\text{NET}}$ greater than 2 m is a good candidate.

Finally, the cumulative volume of oil displaced up to time t is

$$N_{p2} = H_{\text{NET}} \phi \Delta S_2 A, \dots \dots \dots \quad (11.63a)$$

and the total heat injected to time t is

$$H_J = \frac{M_{Tt} H_t A \Delta T}{E_{hs}} \dots \dots \dots \quad (11.63b)$$

The amount of heat per unit mass of water is $(C_{p1}\Delta T + yL_V)$. The volume of *cold* water required to generate \dot{H}_J is

$$V_1 = \frac{H_J}{(C_{p1}\Delta T + yL_V)\rho_1} \dots \dots \dots \quad (11.63c)$$

Eqs. 11.63a through 11.63c lead to the cumulative oil/steam ratio F_{23} :

$$F_{23} = \frac{N_{p2}}{V_1} = \frac{M_{T1}}{M_{Tt}} (1 + h_D) \bar{E}_{hs} \left(\frac{\phi \Delta S_2 H_{NET}}{H_t} \right) \dots \dots \dots \quad (11.63d)$$

The oil/steam ratio is a measure of economic efficiency in steam processes. The steam is expressed as cold-water equivalents in Eq. 11.63d. [Fig. 11.18](#) shows a plot of the dimensionless oil/steam ratio,

$$\left(\frac{F_{23} H_t}{\phi \Delta S_2 H_{NET}} \right),$$

based on Eq. 11.63d. This figure assumes a constant value for the ratio (M_{T1}/M_{Tt}) . It also assumes that the oil saturation will be reduced wherever heat goes. The oil/steam ratio is another of the important economic indicators of steamflooding success.

11.5.4 Modifications. The ML theory has undergone several improvements. Each has yielded important insights into various facets of thermal flooding.

Prats (1982) showed that the ML theory could accommodate different heat capacities in the over- and underburden M_{Tu} and in the reservoir M_{To} . The heated area now becomes

$$A(t_D) = \frac{\dot{H}_J H_t M_{To}}{4k_{Ts} M_{Tu} \Delta T} \left[e^{t_D} \operatorname{erfc}(t_D^{1/2}) + \frac{2t_D^{1/2}}{\sqrt{\pi}} - 1 \right], \quad \dots \dots \dots \quad (11.64a)$$

and the dimensionless time definition is

$$t_D = \frac{4k_{Ts} M_{Tu} t}{H_t^2 M_{To}^2}. \quad \dots \dots \dots \quad (11.64b)$$

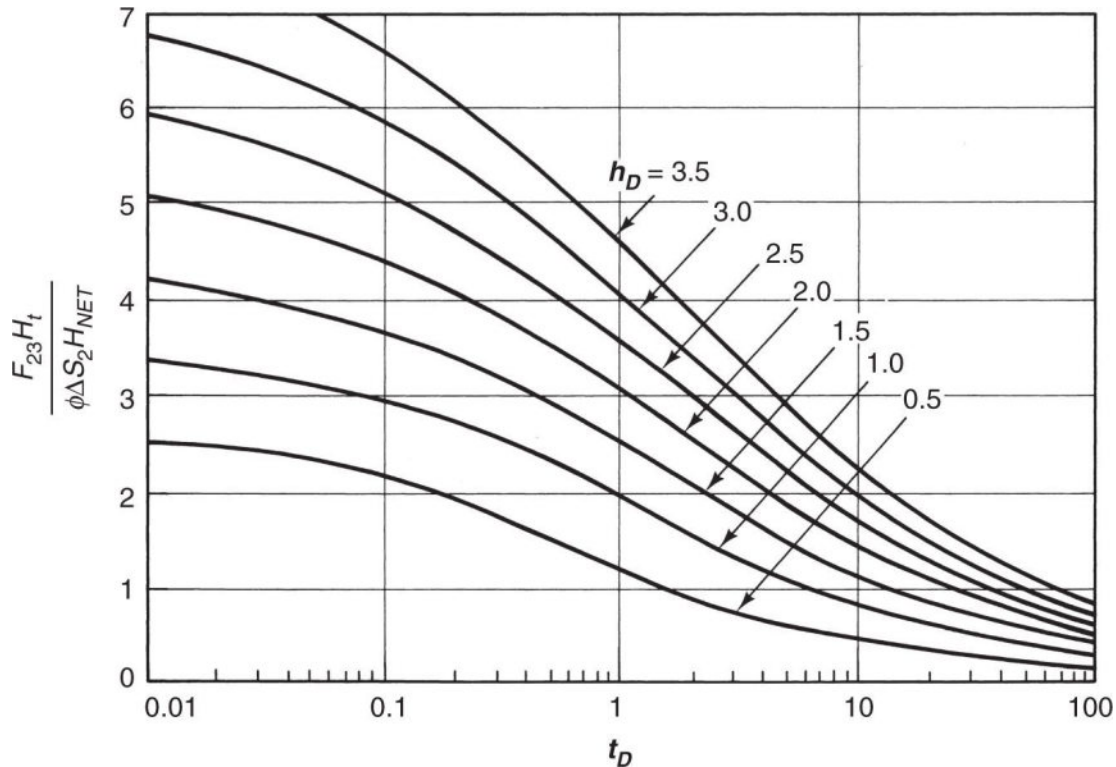


Fig. 11.18—Dimensionless cumulative oil/steam ratio (Myhill and Stegemeier 1978).

The quantities in Eqs. 11.60 through 11.63 still apply with this change as long as the new definitions are used.

One important point here is that the dimensionless time in Eq. 11.64b is very different from the dimensionless times in the remainder of this text. There, the normalizing factor for time was the rate of convective mass transfer for isothermal processes, or

$$t_D = \frac{ut}{\phi L} = \frac{qt}{V_p}.$$

In Eq. 11.64b, time is normalized by the rate of conductive heat transfer. Both time scales are present in actual steamfloods, but the widespread use of Eq. 11.64b implies that heat transfer is what governs production.

One of the most significant improvements to the ML theory was proposed by Mandl and Volek (1969), who noticed that the velocity of a saturated steam front declines with time until it can actually propagate at a slower rate than a hot-water front. After this time, the displacement forms a hot-water or condensate bank that propagates ahead of the steam front from then on. The time at which this happens is called the *critical time* (see [Fig. 11.19](#)).

We can derive an expression for the critical time on the basis of previous equations. Let us consider a medium with a constant cross-sectional area WH_t . For this case, the steam-front velocity is simply the rate of growth of the heated area dA/dt divided by the width W of the medium. The velocity of a hot-water front v_{HW} has already been given in Eq. 11.11. When these two velocities are equated and the area derivative eliminated by Eq. 11.61 the critical dimensionless time t_{Dc} is the solution to

$$e^{t_{Dc}} \operatorname{erfc} t_{Dc}^{1/2} = \frac{u_1 WH_t M_{Tt} \Delta T}{\phi(1 + D_{HW}) \dot{H}_J}. \quad \dots \dots \dots \quad (11.65)$$

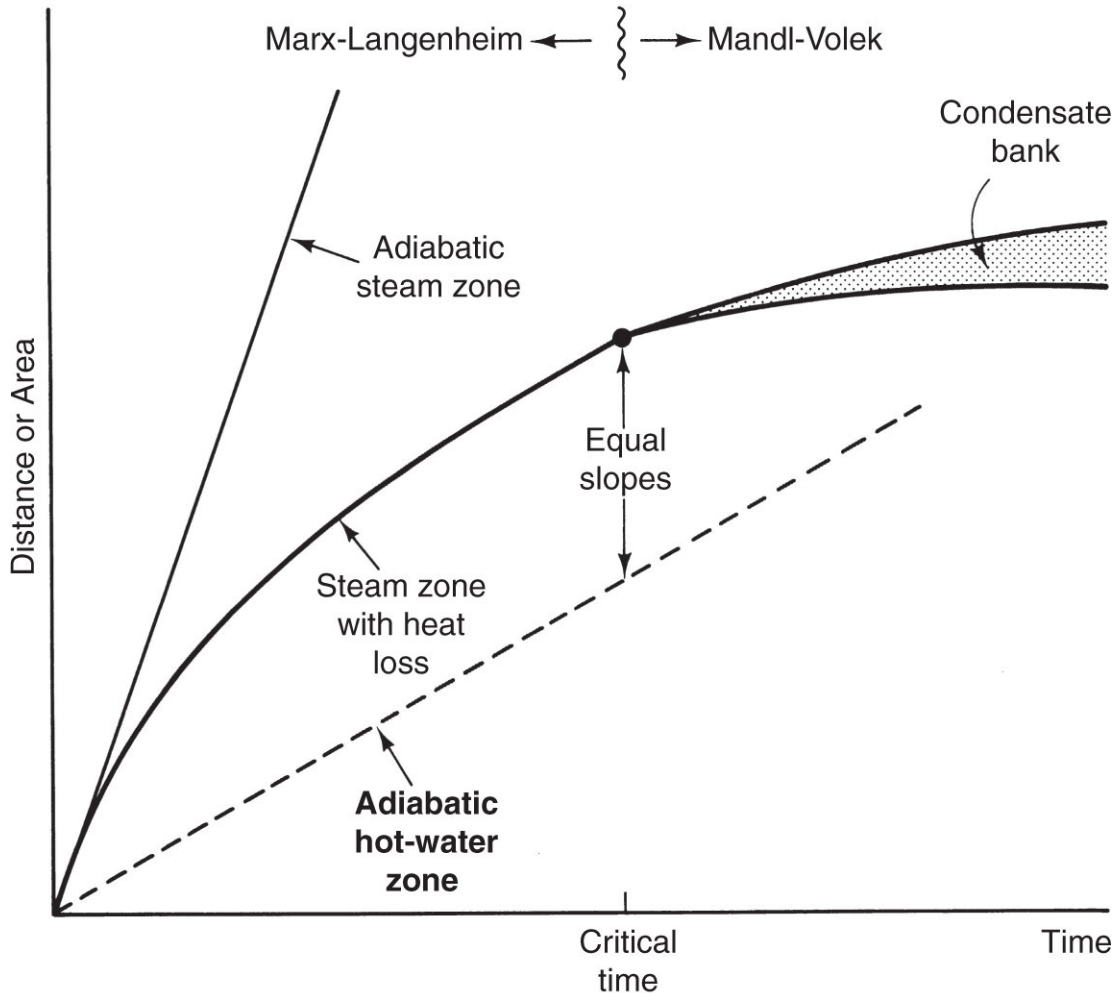


Fig. 11.19—Schematic of critical time.

Fig. 11.19 shows the velocities of the waves involved in this determination. *Adiabatic* means that there is no lateral heat loss.

Example 11.4. How Long Are Critical Times? The length of the critical time is illuminated by example calculation. Start with Eq. 11.65, which we evaluate at the following properties: $u_1/\phi = 1 \text{ ft/d}$,

$$M_n = 1.78 \frac{\text{MJ}}{\text{m}^3 \cdot \text{K}}, H_t = 30 \text{ ft}, D_{SF} = \Delta T = 298^\circ\text{F}, \dot{H}_J = 4 \times 10^8 \frac{\text{Btu}}{\text{day}}, W = 220 \text{ ft}, \text{ and } h_D = 1.28.$$

$$e^{t_{Dc}} \operatorname{erfc} t_{Dc}^{1/2} = \frac{u_i W H_t M_{Tl} \Delta T}{\phi(1 + D_{SF}) \dot{H}_J} = \left(1 \frac{\text{ft}}{\text{d}} \right) \left[\frac{(220 \text{ ft})(30 \text{ ft}) \left(1.78 \frac{\text{MJ}}{\text{m}^3 \cdot \text{K}} \right) (298^\circ \text{F})}{(1 + 1.28) \left(4 \times 10^8 \frac{\text{Btu}}{\text{day}} \right)} \right] \\ \times \left[\frac{(0.305 \text{ m})^3}{1 \text{ ft}^3} \frac{10^3 \text{ Btu}}{1 \text{ MJ}} \frac{1 \text{ K}}{1.8F} \right] = 0.0605$$

This is a transcendental expression for the dimensionless time to be evaluated by trial and error, a procedure which gives $t_{Dc} = 86$, which from Eq. 11.59 gives

$$t_c = \frac{t_{Dc} H_t^2}{4 K_{Ts}} = \frac{(86)(30 \text{ ft})^2}{4 \left(1.15 \frac{\text{mm}^2}{\text{s}} \right)} \left[\left(\frac{0.305 \text{ m}}{1 \text{ ft}} \right)^3 \frac{(10^3 \text{ mm})^2}{1 \text{ m}^2} \frac{1 \text{ days}}{(24)(3,600) \text{s}} \right] = 5,525 \text{ days.}$$

Evidently, more than ten years of injection are required for a condensate bank to form.

Strictly speaking, the ML theory applies only to times less than the critical time. After this point, the more sophisticated Mandl-Volek theory or the approximate Myhill-Stegemeier (1978) theory applies. Myhill and Stegemeier included the heat of vaporization in a condensing steamdrive in the ML theory by redefining the heated-zone growth rate in the manner of Eq. 11.14. [Figs. 11.14](#) and [11.15](#) both include this effect through the dimensionless latent heat h_D first defined in Eq. 11.16. The original ML theory is the case of h_D approaching infinity. Myhill and Stegemeier successfully correlated the cumulative oil/steam ratio of 18 steamdrive projects in [Fig. 11.15](#).

Finally, Ramey (1959) showed that the ML theory would apply to an arbitrary number of step changes in enthalpy at the injector. Applying superposition to Eq. 11.57, which despite everything we have done to it is still linear, yields

$$A(t_D) = \frac{H_t}{4 k_{Ts} \Delta T} \sum_{i=1}^n \dot{H}_{Ji} [\phi(t_{Di}) - \phi(t_{Di-1})], \dots \dots \dots \quad (11.66a)$$

where

$$\phi(t_{Di}) = e^{t_{Di}} \operatorname{erfc}(t_{Di}^{1/2}) + 2\sqrt{\frac{t_{Di}}{\pi}} - 1, \dots \quad (11.66b)$$

and t_{Di} in Eqs. 11.66 has the same form as in Eq. 11.64a but with $(t - t_i)$ replacing t . The enthalpy injection rate changes from $\dot{H}_{J(i-1)}$ to \dot{H}_{Ji} at t_i . Each change must maintain the same absolute value of ΔT and $t_D \geq t_{Dn}$.

[Fig. 11.20](#) shows the results of Eq. 11.66 applied to a slug injection of steam. During steam injection, the heated area grows at a steadily decreasing rate because of heat losses (this effect was present in [Fig. 11.19](#) also). In fact, the difference between the indicated curve and a straight line tangent to it at the origin is the diminution of the heated area because of heat loss. At $t = 10^3$ hours, cold water at the original reservoir temperature is injected, resulting now in heat transfer from the previously heated over- and underburden into the water and a very rapid decrease in the heated zone. The diverging nature of the flow in the vicinity of the injector causes a rapid decrease in which the rate of area cooling is much higher than the rate of area heating at the steam front. Calculations like those in [Fig. 11.20](#) probably account for why thermal processes are only infrequently conducted as slugs.

With the foregoing discussion as background, we can now address specific processes in a little more detail.

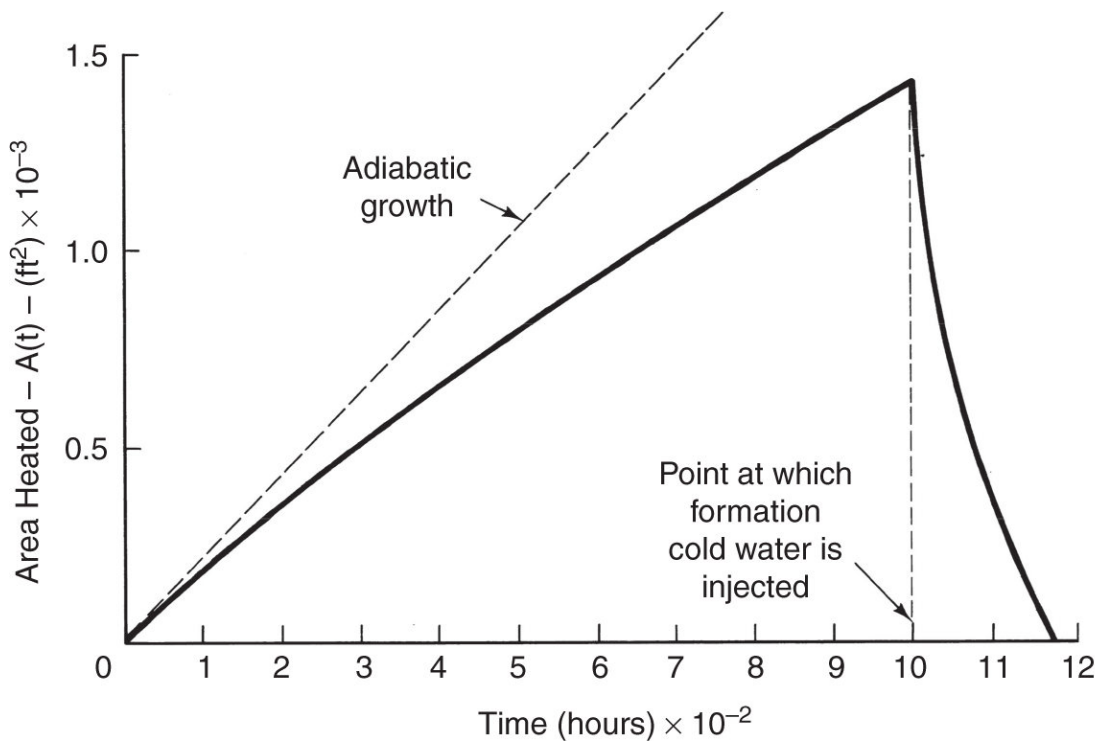


Fig. 11.20—Calculated area heated from superimposed ML theory (from David Goggin, personal communication).

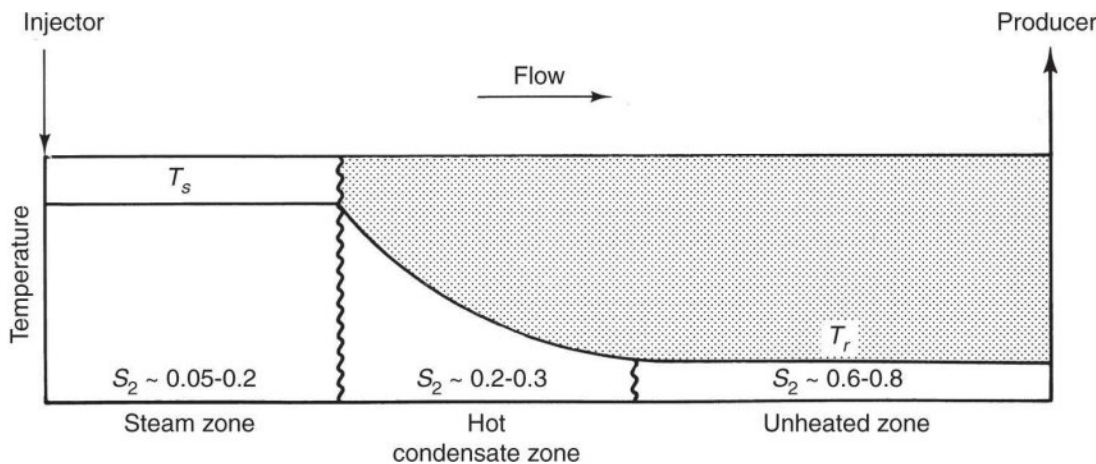


Fig. 11.21—Schematic zones in a steamdrive cross section.

11.6 Steamdrives

A steamdrive process beyond the Mandl-Volek critical time consists of an unheated zone, a condensate zone, and a steam zone ([Fig. 11.21](#)). The steam zone contains a two-phase mixture of steam and water flowing with a very small amount of oil. Because steam

viscosity is low, this zone is essentially at a constant pressure, which requires that it also be at a constant temperature. Most flow in this zone is steam, but the steam quality is very low because of the presence of a residual water phase. The enthalpy of the steam in this zone is often neglected. The zone contains oil at a very low saturation because that remaining behind the condensate zone has been at least partially distilled. Oil saturation is also low because the wetting state of the crude is frequently altered as the steam seeks to assume the position of the most nonwetting fluid in the pores. [Fig. 11.22](#) shows a correlation of steam-zone oil saturation.

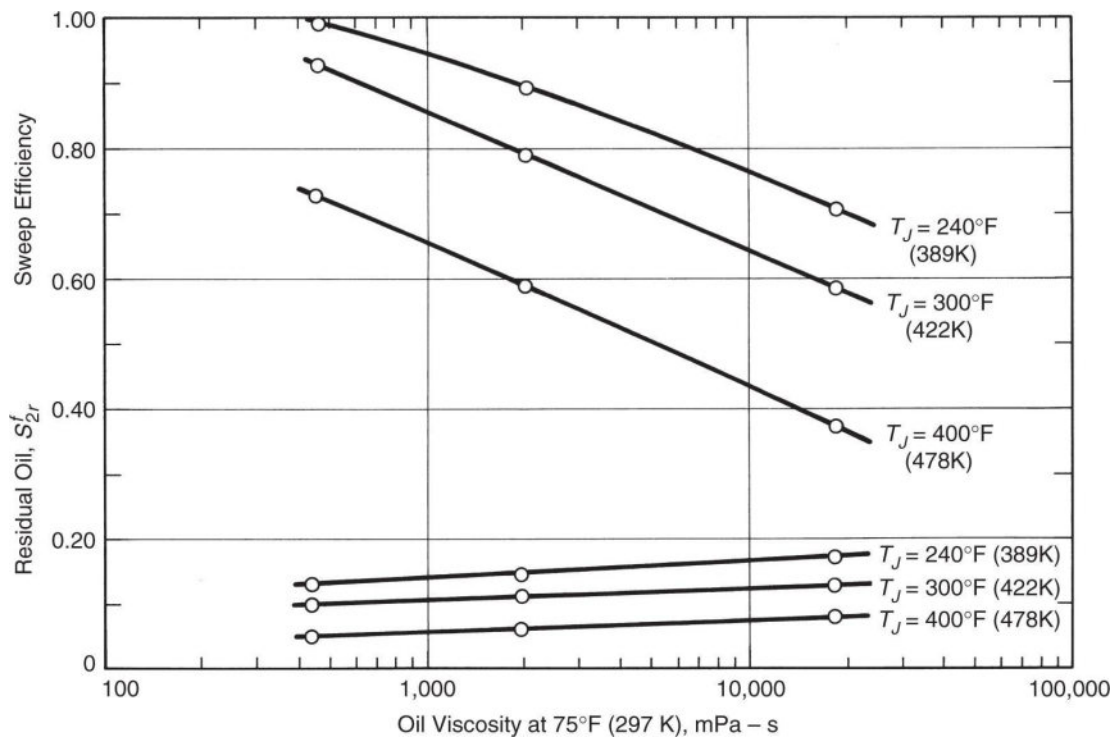


Fig. 11.22—Steam-zone sweep efficiency and residual-oil saturation from model experiment (Bursell and Pittman 1975).

It is easy to see where the incremental oil comes from in such a process. If the initial oil saturation is 0.7 and the oil saturation in the steam zone is 0.1, the oil displaced is 86% of that initially in place.

We can represent the profile in [Fig. 11.21](#) on the enthalpy/pressure plot in [Fig. 11.4](#). The unheated zone is a point in the liquid region on a low-temperature isotherm. The condensate

zone is a horizontal line segment from this isotherm to the bubblepoint curve, and the steam zone is a horizontal line from the bubblepoint curve to some low steam quality.

At a typical thermal-flooding condition of 1 MPa (147 psia), the densities of saturated liquid and of water vapor (steam) are 885 and 5.31 kg/m³ (55.3 and 0.33 lb_m/ft³), respectively. This pronounced difference between liquid and vapor properties is present in nearly all physical properties and contributes to several important effects in steamdrives, including in-situ quality, viscous stability, and override.

The quality of flowing steam in the reservoir is always quite low. Suppose that steam is flowing in a permeable medium in the presence of a residual water saturation. For two phases to be present, both the steam and water must be saturated. At a typical residual water saturation of 0.3 at 1 MPa and using the aforementioned densities, the in-situ quality is 1.3%. This low quality means that the fluids in the pore space of the medium are just barely inside the saturated liquid line in [Fig. 11.4](#), even though the *flowing* steam quality is nearly 100%.

A second consequence of the low steam density is related to viscous stability. Section 6.8 said that displacing with a fluid less viscous than the resident fluid in a horizontal medium inevitably leads to viscous fingering and reduced volumetric sweep efficiency. However, steam displacements are quite stable for the following reasons:

1. Steam is readily converted to water. If a perturbation of the steam front were to form, it would finger into the cold zone ahead of it and immediately condense. The condensation leads to a self-stabilizing effect that suppresses fingers.
2. In a steamdrive, the *kinematic* mobility ratio is usually favorable. It is more accurate for the mobility ratio to be based on kinematic viscosities for compressible flows. Mobility ratio is the ratio of pressure gradients ahead of and behind a piston-like front in a 1D displacement,

$$M_v = \frac{\left(\frac{dP}{dx}\right)_{\text{ahead}}}{\left(\frac{dP}{dx}\right)_{\text{behind}}} = \frac{\left(\frac{u\mu}{k}\right)_{\text{ahead}}}{\left(\frac{u\mu}{k}\right)_{\text{behind}}}. \dots \quad (11.67)$$

- If the flux u is not a function of position (fluids are incompressible), Eq. 11.67 reduces to that given in Section 5.2.
- If the mass flux ρu is not a function of position, Eq. 11.67 reduces to a definition of mobility ratio based on the *kinematic* viscosity (dynamic viscosity divided by density). See Exercise 5.10.

In a steamdrive, neither condition is true, but the mass flux is more nearly constant. [For a more sophisticated discussion of the stability of thermal fronts, see Krueger (1982).]

The kinematic viscosity of steam, in fact, is usually greater than that of hot water at the same temperature and pressure. [Fig. 11.23](#) shows the reciprocal kinematic mobility ratio of a steam displacement plotted against pressure. Hot waterfloods are unstable over the entire range, which partly accounts for their inferior performance compared to steam, but steamfloods are stable at all pressures less than approximately 1.5 MPa (220 psia). Furthermore, superheated steam is even more stable than saturated steam, a paradoxical result from an isothermal-displacement point of view given that superheated steam has a very low viscosity. The increase in kinematic mobility ratio with pressure is the consequence of approaching the critical point of water. It further reinforces low-pressure restrictions on steamdrives.

The last consequence of small steam density deals with gravity segregation, or what [Chapter 5](#) called buoyancy effects. Because of the density difference between poorly mobile crude and highly mobile steam, the latter has a tendency to rise to the top of the reservoir, causing override and reduced volumetric-sweep efficiency. The gravity number N_g^0 scales the severity of the override. [Fig. 11.24](#) plots the effect of the inverse gravity number (note the altered

definition from Eq. 5.5d to account for compressible fluids and radial flow) on overrunning. If we review what causes N_g^0 to be large, we see that many steam floods occur under conditions that make override almost inevitable—clean sands with high horizontal and vertical permeability, low aspect ratios caused by close well spacing, and large density differences caused by heavy oils.

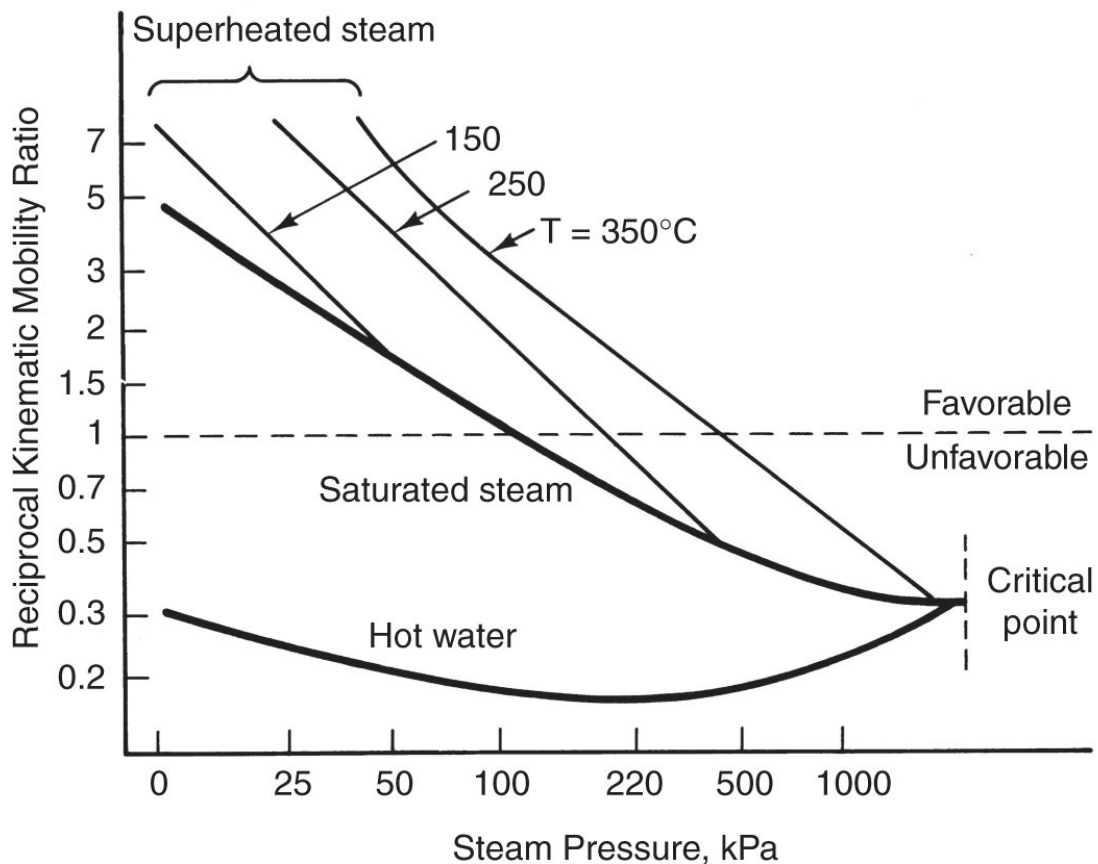


Fig. 11.23—Effective mobility ratio for steam displacements (Burger et al. 1985).

Two of the methods used in solvent flooding to prevent viscous fingering will mitigate override. If the reservoir has substantial dip, steam injected at the top of the reservoir will result in an interface that is more perpendicular to the reservoir trend. In addition, the interface can be made more vertical by adding foaming agents to the injected fluids (see [Chapter 10](#)). Another commonly used method is to inject steam near the bottom of the formation and produce from the top.

Gravity override has an important positive consequence. Once steam has broken through in the producing wells of a steamdrive, the injection rate is usually reduced to keep heat in the reservoir. At the reduced rate, heat transfer to the cold oil remains efficient because of the large area of the (now nearly horizontal) interface. Oil thus heated migrates to the top of the reservoir, because its density is now less than that of hot water, and subsequently flows to the producers through the steam zone. This is often called *drag flow*. If override is particularly severe, most of the oil is produced with steam through drag flow.

Override and drag flow lead to an alternative way to visualize steamdrives on the basis of the idea of the existence of a steam chest. [Fig. 11.25](#) illustrates this concept. According to Vogel (1984), the following simplifications are possible. First, the amount of time required for the steam to break through to the producing well is short compared to the life of the flood. Therefore, $(t - u) \approx t$ in Eq. 11.55, which renders the area constant, and, therefore, the energy injection rate is

$$\dot{H} = 2 \frac{k_T \Delta T A}{\sqrt{\pi K_T t}} + M_T A \Delta T v_z, \dots \quad (11.68a)$$

where the first two terms are heat losses to strata above and below the heated zones (the factor 2 in the equation), and the last term is the downward movement of the now-horizontal front. The downward velocity must be approximated by separate means. The oil production rate would be

$$\dot{q}_2 = A v_z. \dots \quad (11.68b)$$

Despite the fact that the frontal advance and drag mechanisms are conceptually very different, Vogel shows that the two approaches give similar results for heated areas. For example, the thermal efficiency illustrated in [Fig. 11.19](#) can be well approximated by

Frontal advance and drag mechanisms tend to be quite different with respect to their oil-recovery characteristics. Frontal-advance methods show large oil recovery early in the life of a field. Drag mechanisms tend to show prolonged periods in which the oil rate is constant after steam breakthrough.

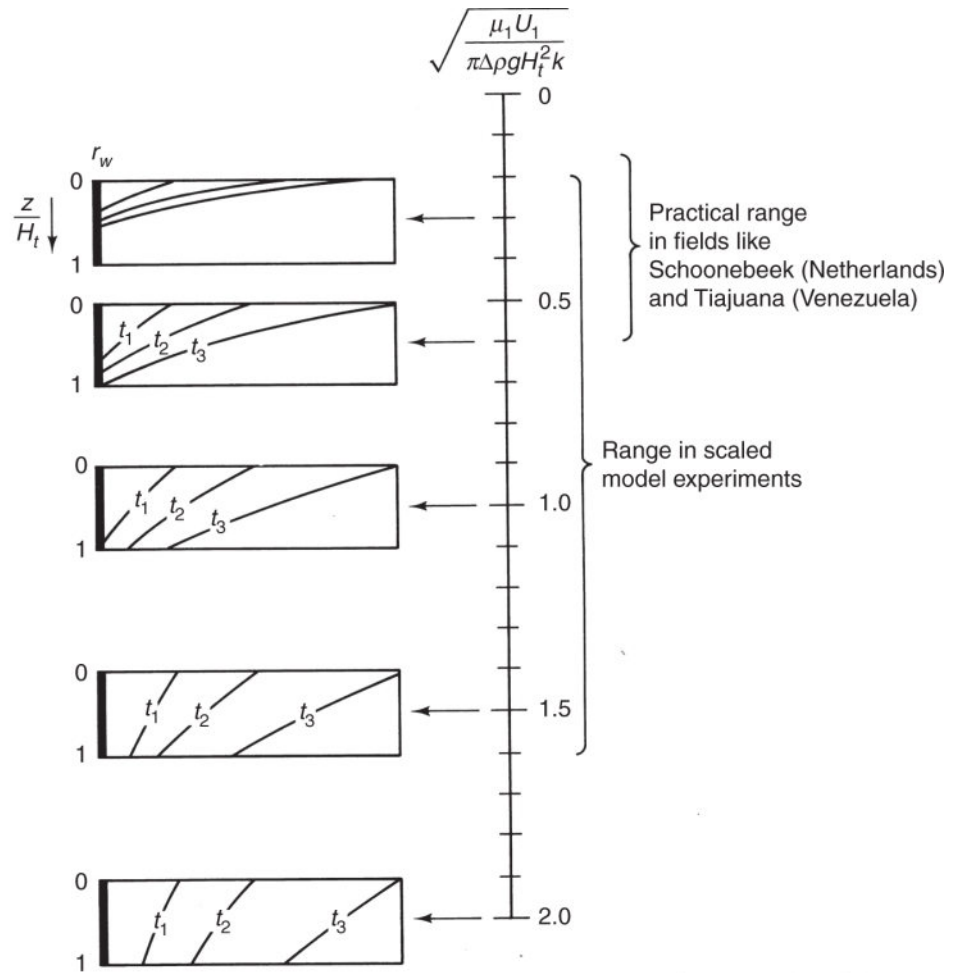


Fig. 11.24—Gravity override and gravity number for steamdrives (van Lookeren 1983).

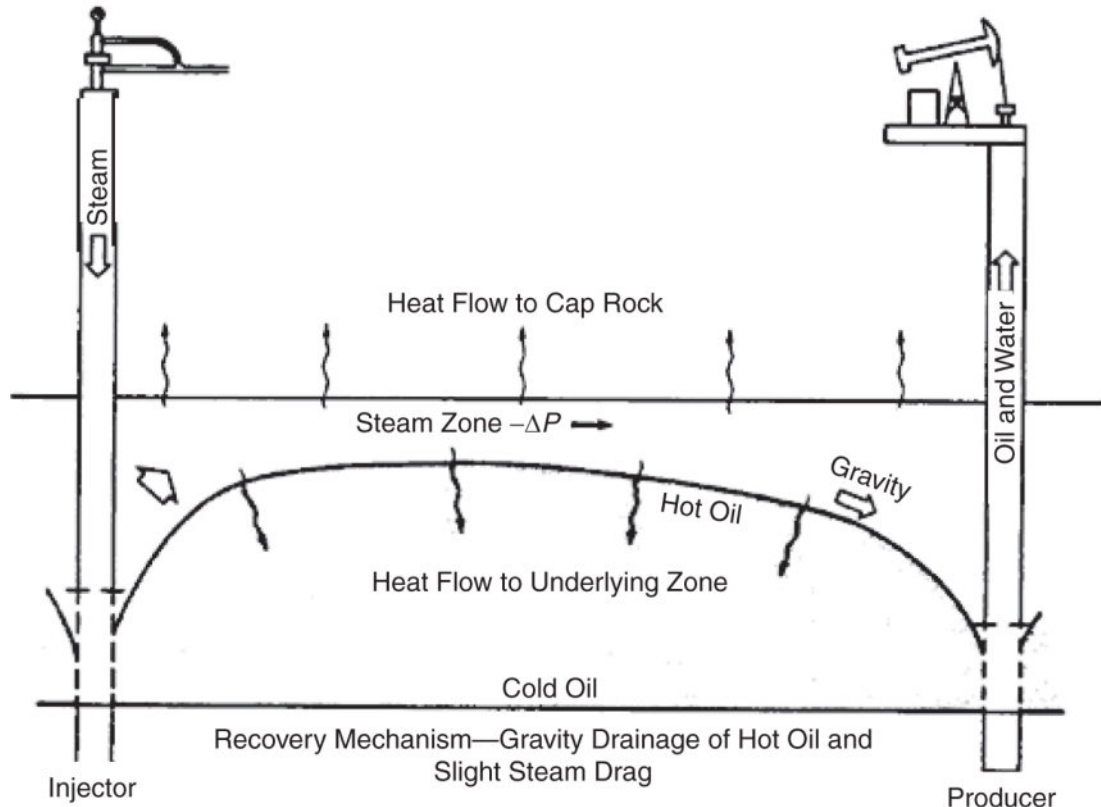


Fig. 11.25—Steamdrive with gravity override (Vogel 1984).

11.6.1 Case Histories. To illustrate a steamdrive, we discuss an early phase of a highly successful project in the Kern River Field, California. This large field has properties eminently typical of successful steamdrives: the field is shallow, the original reservoir pressure low, the sand fairly thick, and the permeability and porosity high ([Table 11.4](#)). As we discussed previously, each of these items will result in small heat losses to the over/underburden. The cold-oil viscosity is high, but not extremely so.

One of the projects at Kern River is the *Ten-Pattern Steamflood* with a well arrangement consisting of ten seven-spots (six injectors each surrounding an injector). The high density of wells in this area is made economically possible by the shallow depths.

Pattern size is correspondingly small. Because the productivity of the cold and heated oil is usually much less than the injectivity of steam, having more producers than injectors will better maintain fluid balance.

[**Fig. 11.26**](#) shows the response of the Ten-Pattern project. Steam injection began in early 1968. Oil-rate response was immediate and very strong. The prompt response was probably caused in part by the steam soaks that preceded the drive, but nearly all the later response is a result of the drive. Oil rate peaked in late 1970 and has sustained a surprisingly gentle decline thereafter, the decline being a consequence of override. Throughout the entire history shown, the oil rate was much greater than the estimated primary oil rate, meaning that incremental oil recovery was high. The cumulative steam/oil ratio reached a minimum in early 1972 and increased thereafter as steam broke through to more and more producers.

Some of the steam breakthrough came from gravity override. [**Fig. 11.27**](#) shows a temperature survey in a nearby well compared to the injection interval in the nearest injector well. Even though these two wells are quite near each other, the steam zone (indicated by the region of constant temperature) has migrated to the top of the zone. Upward migration of the steam zone confirms the oil-rate behavior shown in [**Fig. 11.24**](#). Injecting low in the interval like this is a common way to minimize gravity segregation. The hot-water zone below the steam zone shows a gradual temperature decrease that is uninterrupted at the bottom of the zone. The temperature gradients here and at the top of the zone are manifestations of heat losses to the adjacent strata.

TABLE 11.4—SUMMARY OF RESERVOIR DATA AS OF 1968, KERN RIVER FIELD STEAMFLOOD INTERVAL (BLEVINS AND BILLINGSLEY 1975)

Depth	700–770 ft	213–235 m
Estimated original reservoir pressure	225 psig	1.53 mPa
Current reservoir pressure	60 psig	0.41 mPa
Average net sand thickness	70 ft	21 m
Reservoir temperature	80°F	300 K
Oil viscosity at 85°F	2,710 cp	2710 mPa·s
Oil viscosity at 350°F	4 cp	4710 mPa·s
Average permeability to air	7,600 md	7.6 μm^2
Average porosity	35%	35%
Average oil content	1,437 bbl/ac-ft	0.185 m^3/m^3
Average oil saturation	52%	52%

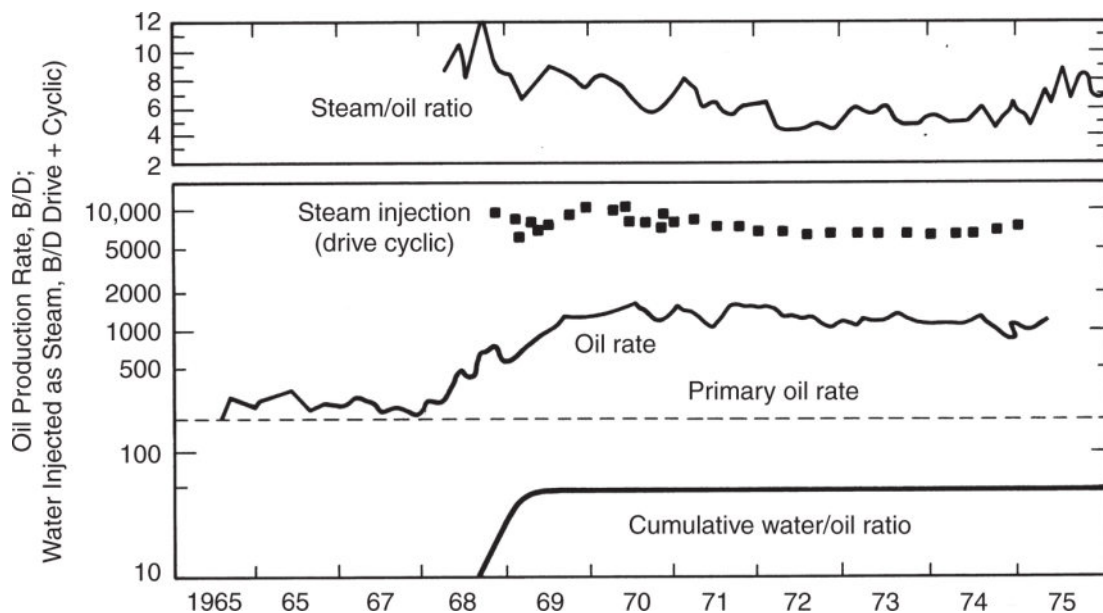


Fig. 11.26—Ten-pattern performance, Kern River field (Blevins and Billingsley 1975).

A more recent steamflood and one that illustrates many of the points made in the preceding theoretical sections is the Cruise E steamflood in the island nation of Trinidad and Tobago. As [Fig. 11.28](#) shows, the project injected steam for a little less than two years, followed by an equivalent period during which there was no steam injection. Injection then recommenced and continued from this time on. The major ideas learned from this field response are:

- In the first injection period, the oil production rate was essentially proportional to the steam injection rate. This observation is consistent with the growth of the steam zone being proportional to the heat injected and its being in turn proportional to the oil rate.
- The rapid collapse of the oil rate when steam injection ceased is consistent with [Fig. 11.19](#) and the discussion on this topic.
- The substantial increase in oil rate when steam injection recommenced suggests that the gravity override, which was discussed in connection with [Fig. 11.26](#), was quickly re-established and that oil production continued through downward movement of an already established interface.

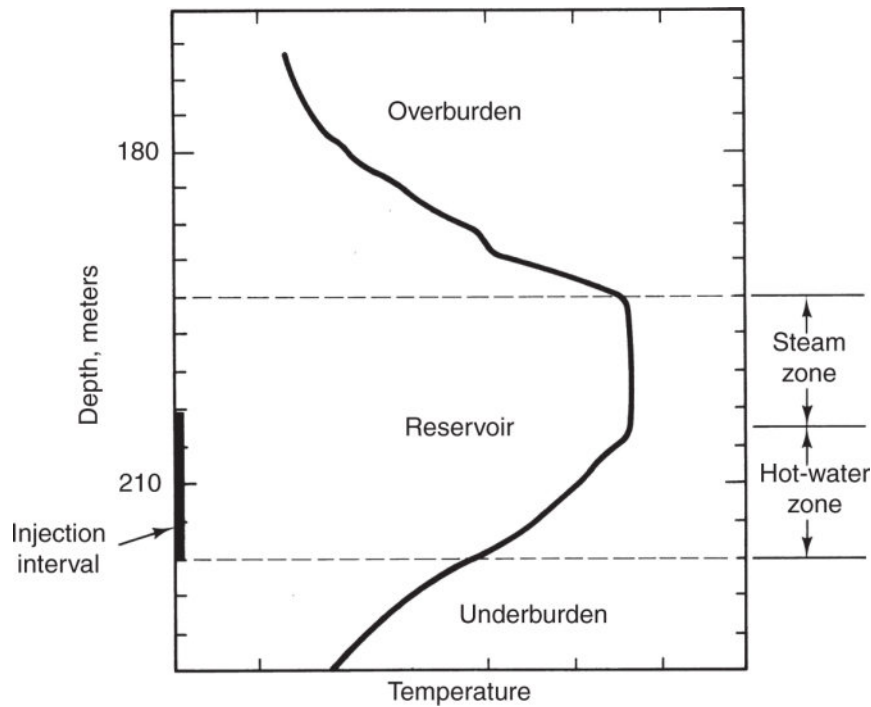


Fig. 11.27—Illustration of gravity override, Kern River field (Blevins and Billingsley 1975).

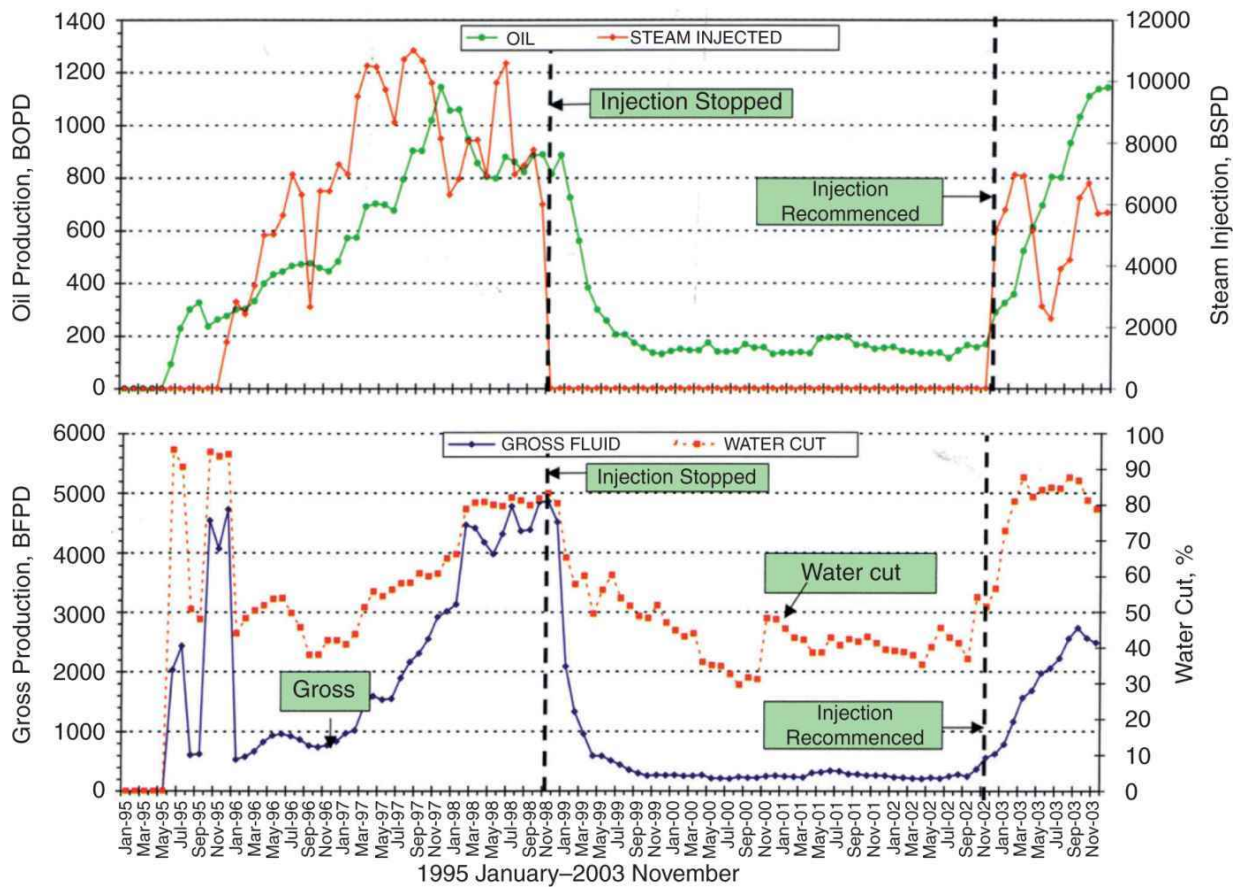


Fig. 11.28—Performance of the Cruise E (IADB) steamflood (Ramilal 2004).

In summary, we can say that the more steam injected, the more oil will be produced, a statement that could apply to many EOR processes.

11.7 Steam Soak

How a steam soak works is counterintuitive. Evidently, the steam displaces relatively little of the oil close to the well as it is injected. Instead, it channels or overrides through the oil to provide good thermal coverage for subsequent lateral conduction to take place. The process produces heated oil through several mechanisms: elevated pressure, solution gasdrive, thermal expansion, and gravity drainage. Even if the oil is heated inefficiently, increased production can result because of removal of skin damage and cleansing of the tubing string. Enough of the oil is removed near the wellbore so that subsequent injectivity improves. Therefore, steam soaks are

frequently used as precursors to steamdrives. See the discussion above in connection with [Fig. 11.2a](#).

Example 11.5. Estimating the Heated Radius. The productivity of a well undergoing cyclic steam injection is determined by the heated radius and the extent of viscosity reduction; see Exercise 11.1. The heated radius follows from energy-balance considerations, as illustrated in this example. The example also illustrates short cuts in the energy balance to make the results eminently practical.

Soak cycles are usually so short that heat losses to the adjacent strata are negligible. Eq. 11.51 consequently becomes

$$\dot{H}_J = \frac{d}{dt} (A H_t \rho_s U),$$

which integrates to yield

$$H_J = A H_t \rho_s H.$$

We use the integrated form of the energy balance because we are asking for a value at a point in time rather than a rate. The preceding equation has replaced the internal energy U on the right with the enthalpy H . Over a short time interval, the steam injection rate \dot{m} is constant, so that Eq. 11.6-4 becomes

$$\dot{m} \hat{H}_J = A H_t \rho_s H = A H_t \left[\phi (S_1 M_{T1} + S_2 M_{T2}) + (1 - \phi) M_{Ts} \right] \Delta T,$$

where \hat{H}_J is the specific injected enthalpy per unit mass and where the right side has been replaced with volumetric heat capacities under the assumption that all injected steam has been condensed. The only steam contribution to the balance remains in the \hat{H}_J term. Assuming the heated area A to be cylindrical enables solution of the preceding equation for the heated radius as

$$R_h = \sqrt{\frac{\dot{m} \hat{H}_J t_{inj}}{\pi H_t \left[\phi (S_1 M_{T1} + S_2 M_{T2}) + (1 - \phi) M_{Ts} \right] \Delta T}}.$$

As in many thermal calculations, the preceding equation contains many parameters; however, several of these can be evaluated through correlation or through generic properties. For example, we can assume the volumetric heat capacities to be

$$M_{T_1} = 62.5 \frac{\text{Btu}}{\text{ft}^3 - {}^\circ\text{F}}; M_{T_2} = 10 \frac{\text{Btu}}{\text{ft}^3 - {}^\circ\text{F}}; M_{T_s} = 41.8 \frac{\text{Btu}}{\text{ft}^3 - {}^\circ\text{F}},$$

The exercise will be worked in English units. The reservoir-specific parameters are $S_1 = 0.5 = S_2$; $\phi = 0.3$; $H_t = 50$ ft; $T_f = 100^\circ\text{F}$. The process values are $P_s = 200$ psia; $y = 0.6$; $\dot{m} = 3.5 \times 10^5 \frac{\text{lb}_m}{\text{day}}$. This rate is approximately 1,000 bbl of cold water/day. The injection period is $t_{\text{inj}} = 5$ days.

The correlations in [Table 11.1](#) give $T_f = 395^\circ\text{F}$, so that $\Delta T = 295^\circ\text{F}$ and $\hat{H}_{11} = 390 \frac{\text{Btu}}{\text{lb}_m}$; $\hat{H}_{13} = 1,218 \frac{\text{Btu}}{\text{lb}_m}$; $L_v = 828 \frac{\text{Btu}}{\text{lb}_m}$, which yields

$$\hat{H}_J = (1-y)\hat{H}_{11} + y\hat{H}_{13} = (0.4) \left(390 \frac{\text{Btu}}{\text{lb}_m} \right) + (0.6) \left(1,218 \frac{\text{Btu}}{\text{lb}_m} \right) = 887 \frac{\text{Btu}}{\text{lb}_m}.$$

The final result is

$$R_h = \sqrt{\frac{\left(3.5 \times 10^5 \frac{\text{lb}_m}{\text{day}} \right) \left(887 \frac{\text{Btu}}{\text{lb}_m} \right) (5 \text{ days})}{\pi (50 \text{ ft}) \left\{ (0.3) [(0.5)(62.5) + (0.5)(10)] + (1 - 0.3) \right\} \frac{\text{Btu}}{\text{ft}^3 - {}^\circ\text{F}} (279^\circ\text{F})}}$$

$$R_h = 29.8 \text{ ft.}$$

11.7.1 Case History. [Fig. 11.29](#) shows the response of a well in the Paris Valley field to seven steam-soak cycles. The oil response is in the upper part of the figure and the heat injection rate in the lower part. There were roughly two soaks per year from 1975 through 1978, each less than a month long. The cumulative oil produced after each cycle was roughly proportional to the amount of heat injected in each preceding soak. Within each cycle, the oil rate

rapidly peaked and then fell in a near-exponential decline. Because a similar decline was not as evident in the oil cut (not shown), the performance suggested that the total fluid rate was also declining within each cycle. The decline suggested that the reservoir pressure was falling, and for this reason, the operators mixed some air with the steam in the last cycle. For a given amount of heat injected, the peak rate in each cycle should decline because the heated zone will contain successively smaller amounts of oil. However, it is striking that substantial oil production occurred even after the seventh cycle.

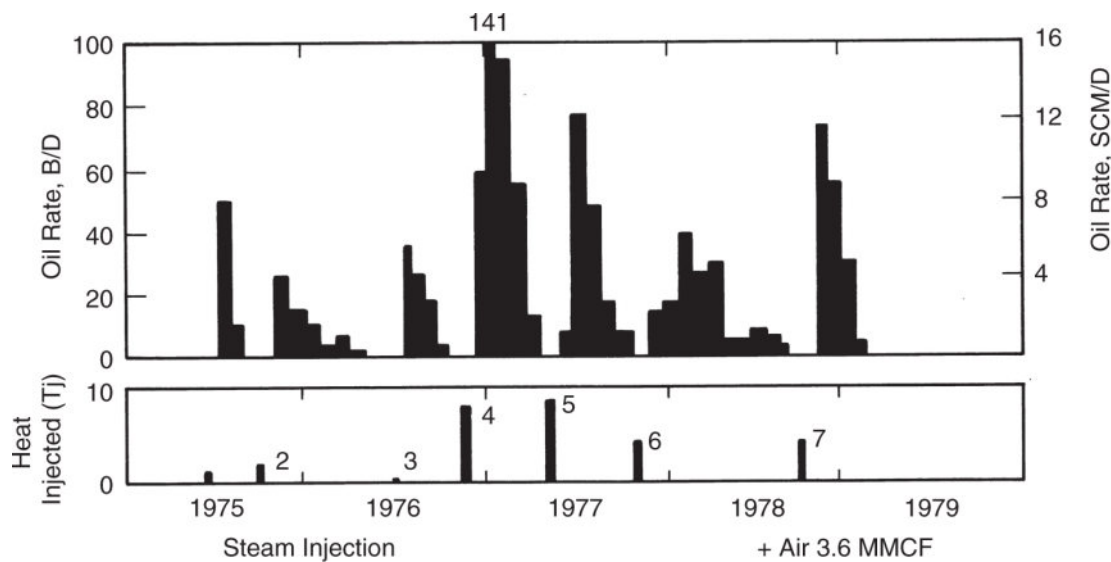


Fig. 11.29—Steam-soak response, Paris Valley field (Meldau et al. 1981).

11.8 In-Situ Combustion

If reservoir pressure, depth, and oil viscosity are too large for steam methods to work, in-situ combustion might be a good alternative. In this method, burning a portion of the crude in the formation generates thermal energy. Theoretically, the portion being burned is the coke or asphaltene portion of the crude, but the issue is far less clear-cut in practice. This complex process—the most complex of the EOR processes—involves heat and mass transfer along with kinetic phenomena.

[Fig. 11.30](#) and [Fig. 11.2c](#) show a schematic of an in-situ combustion process in cross section. In this process, usually some

form of oxidant (air or pure oxygen) is introduced into the formation, and the mixture is ignited (spontaneously or externally). Subsequent injection propagates the burning front through the reservoir. The burn front is very small (approximately one meter), but the combustion generates very high temperatures. These temperatures vaporize connate water and a portion of the crude. Both are responsible for oil displacement. The vaporized connate water forms a steam zone ahead of the burn front that operates very much like a steamdrive. The vaporized oil consists mainly of light components that form a miscible displacement. The reaction products of a high-temperature combustion can also form an in-situ CO₂ flood.

[Fig. 11.30](#) shows many variations of this process. Besides injection of oxidant, there can be coinjection of water in ratios to be determined by design. The water serves to improve the sweep efficiency of the process (you should note the parallel between this and WAG injection in [Chapter 7](#)) and to transport (scavenge) heat left behind in the burned zone. Too much water injection can quench the burn, as shown in [Fig. 11.30d](#). There is also a variation, not shown in [Fig. 11.30](#), in which water and oxidant are injected in opposite directions.

Another process variable is the temperature at which combustion occurs. [Fig. 11.31](#) is a plot from a laboratory experiment involving differential thermal analysis (DTA) of a crude. DTA consists of heating the crude in a preprogrammed fashion, usually linear over time, and measuring the rate of reactant consumption and the contents of the reaction products. Two general points can be made from this figure. First, oxygen is consumed in two peaks: a low-temperature oxidation at approximately 572 K (570°F) and a high-temperature oxidation at approximately 672 K (750°F). In the low-temperature oxidation, the crude is converted to alcohols, ketones, and aldehydes. Then, in the high-temperature oxidation, combustion proceeds completely to CO₂ and carbon monoxide. [Fig. 11.31](#) shows this progression and illustrates that the production of these two components is larger at high temperature. Furthermore, high temperatures oxidize many of the minerals in the permeable media,

particularly the clays (these may also exert a catalytic effect) and pyrite. High-temperature oxidation is better because it heats the oil more efficiently.

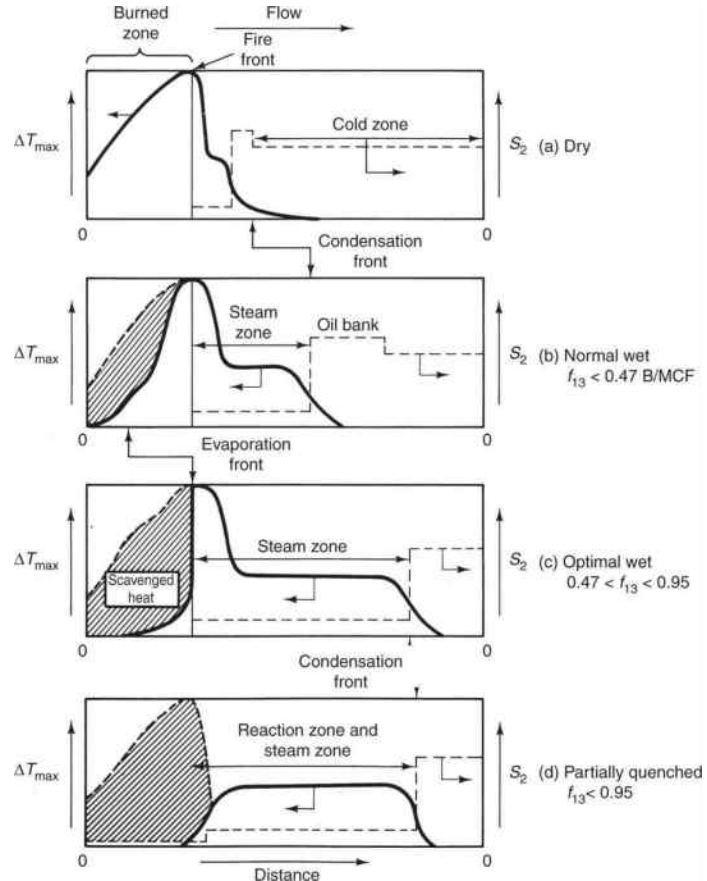


Fig. 11.30—In-situ combustion schematic (Prats 1982).

11.8.1 Case History. The Suplacu de Barcau Field in central Romania is one of the largest and longest-running EOR projects in existence.

This field is the site of an in-situ combustion project because of its very high oil viscosity and because it is very shallow. [Table 11.5](#) summarizes its properties. Other properties, most especially high porosity, permeability and oil saturation, have contributed to the success of the project.

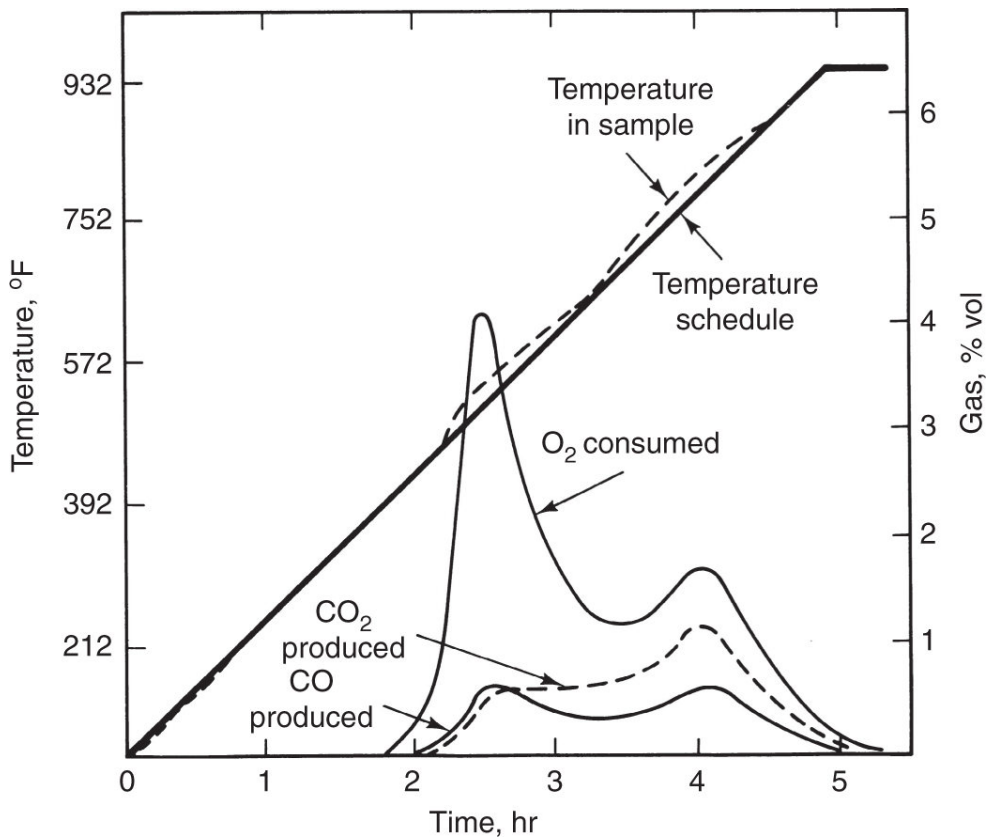


Fig. 11.31—Differential thermal analysis of a crude oil (Burger and Sahuquer 1972).

[**Fig. 11.32**](#) shows that the project has been going on from 1961 to 2005, or more than 40 years, without a significant decrease in oil rate. The ultimate recovery factor is likely to exceed 60%. Other in-situ projects are reviewed in Turta et al. (2007). See also Kumar et al. (2008) for an example of high-pressure air injection.

11.9 SAGD

We now return to SAGD, first discussed in Section 11.1 and [**Fig. 11.2d**](#). This is a technology that uses gravity with horizontal wells to produce extra-heavy crude and bitumen. [**Fig. 11.33**](#) shows a schematic of the SAGD process.

The schematics are on-end projections of a steam injector (upper well as a black dot) and a producer (lower well). After a short period of cycling, the injected steam rises (away from the producer) to the top of the formation to form a cavern or cavity. The cavity grows until the steam reaches the formation top, at which point heat begins to

be lost to the overburden and the cavity expands laterally. The rising steam heats the oil, which falls (again by gravity) to the bottom of the cavity to be collected by the producer. The rise of the steam and the fall of the oil occur in countercurrent flow.

[Fig. 11.33](#) also shows that, just as in in-situ combustion, there are several process variations that use combinations of injectants. Solvent injection with steam serves to improve the efficiency of displacements as well as to reduce the viscosity of the product. Injecting an inert gas with the steam serves the same purpose, but can also increase the pressure in the cavity. Many of these ideas have been tried in association with other forms of steam injection; most SAGD production is currently by the unaided SAGD process.

TABLE 11.5—PROPERTIES OF THE SUPLACU DE BARCAU FIELD (PANAIT-PATICA ET AL. 2006)

Lithology	Pliocene sandstone
Depth	50–200 m
Net pay	20 m
Porosity	0.32
Average permeability	1.7–2 μm^2
Reservoir oil viscosity	2 Pa·s
Initial oil saturation	0.85
Project area	1700 ha

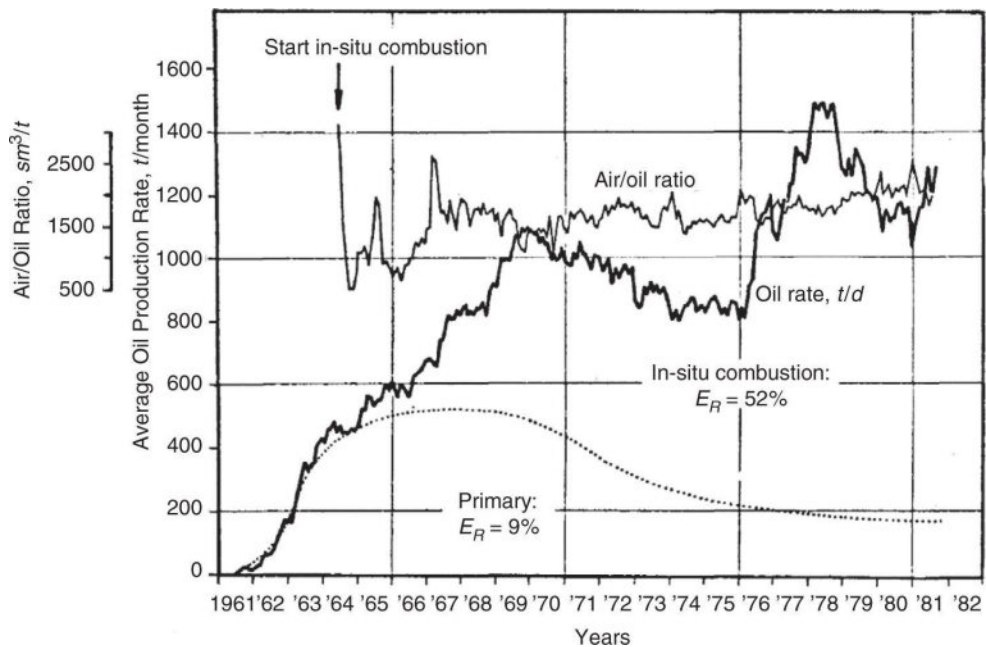


Fig. 11.32—Case history of in-situ combustion project in Suplacu de Barcau Field (Carcoana 1982).

These comments belie one of the principle difficulties with SAGD: the product, when cooled as it is produced to the surface, reverts nearly to its original state. The very high-viscosity product is difficult to transport at surface conditions, and therefore the process requires more surface facilities than other EOR processes, including:

- Provisions for constant heating of surface lines.
- Dilution by diluents. Mixing a low-molecular-weight hydrocarbon (e.g., kerosene at approximately 35%) with the cool bitumen makes it flowable and easy to transport. The diluent is stripped from the product at the processing point and returned to the wellsite for reuse.
- Bitumens are hydrocarbons that are deficient in hydrogen compared to their light-crude cousins. (Coal, which is even more viscous than bitumen, has a carbon/hydrogen molecular ratio of less than one. Natural gas has a ratio of 0.25.) The solution to this is to hydrogenate or upgrade the product. Many processes exist for doing this, but all require significant capital

expense. Often a combination of diluent and upgrading is called for.

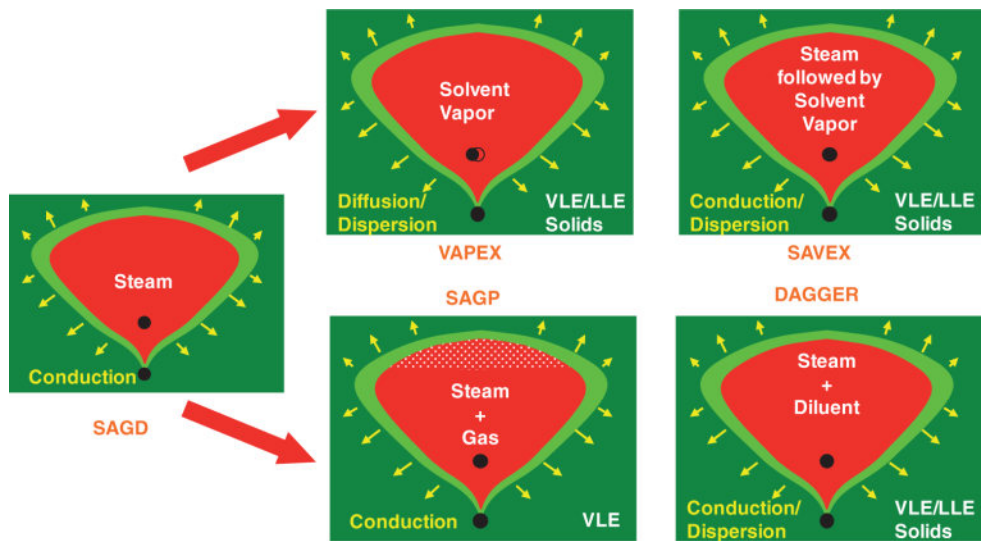


Fig. 11.33—Schematics of the SAGD process and variations.

Butler (1997) gives the basic equations for describing the rates in a SAGD process. See also Bonfantir and Gonzalez (1996).

11.9.1 Field Cases. SAGD is less mature than cyclic steam and steamdrives. The following is a summary from Jimenez (2008).

[**Fig. 11.34**](#) shows how the well pairs are arranged in a large field project. Each group of pairs extends from a central location or pad. The wells are approximately 10,000 ft long. The spacing of the wells is designed for maximum recovery efficiency: the pairs should be far enough apart so that their cavities do not overlap, but not so far as to leave unrecovered bitumen between them. The injector/producer distance is approximately 10 m, and in practice, wells are angled upward from the heel location to facilitate drainage.

As in [**Fig. 11.30**](#), there are several variations in implementation. For example, it is possible to use wells in groups of three (triads) to ensure interpair recovery. It seems possible also to use single horizontal wells in which injection is at the toe of the well and production from the heel.

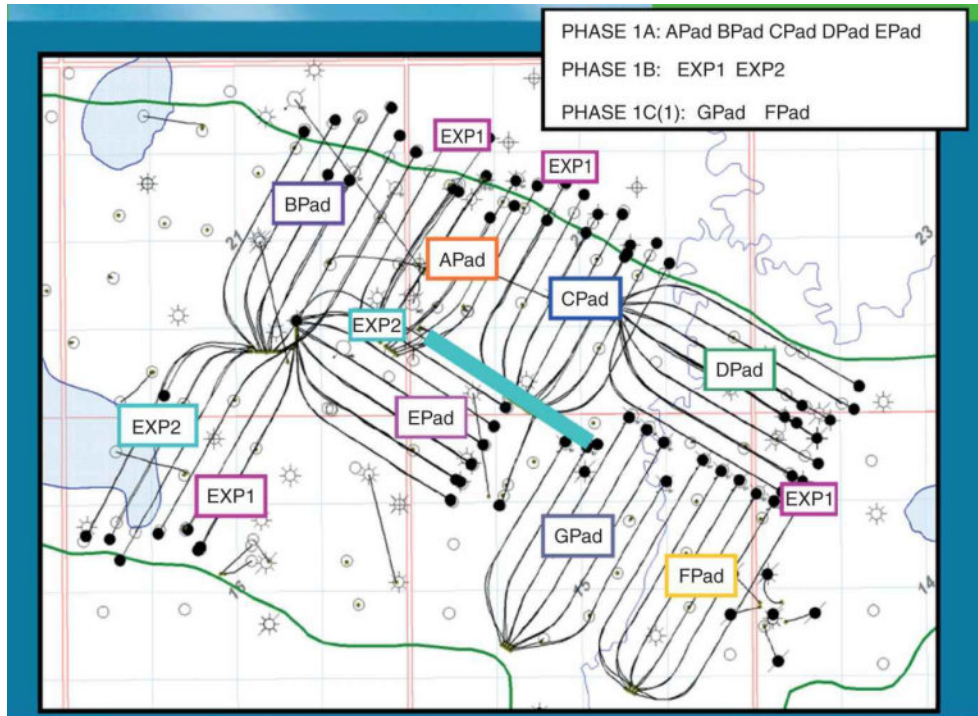


Fig. 11.34—Arrangement of well pairs at the Foster Creek project in Alberta, Canada.
Each trajectory is an injector/producer pair.

The performance of several pads in the McKay River field is shown in [Fig. 11.35](#). On first impression, this plot is unlike any that we have encountered so far. The horizontal axis shows the recovery efficiency, and the vertical axis represents the cumulative steam injected (as cold water) normalized by the original oil in place (not the pore volume). The plot is such that volumetric production (injecting a barrel of cold water in would result in a barrel of oil produced) would be a line of unit slope.

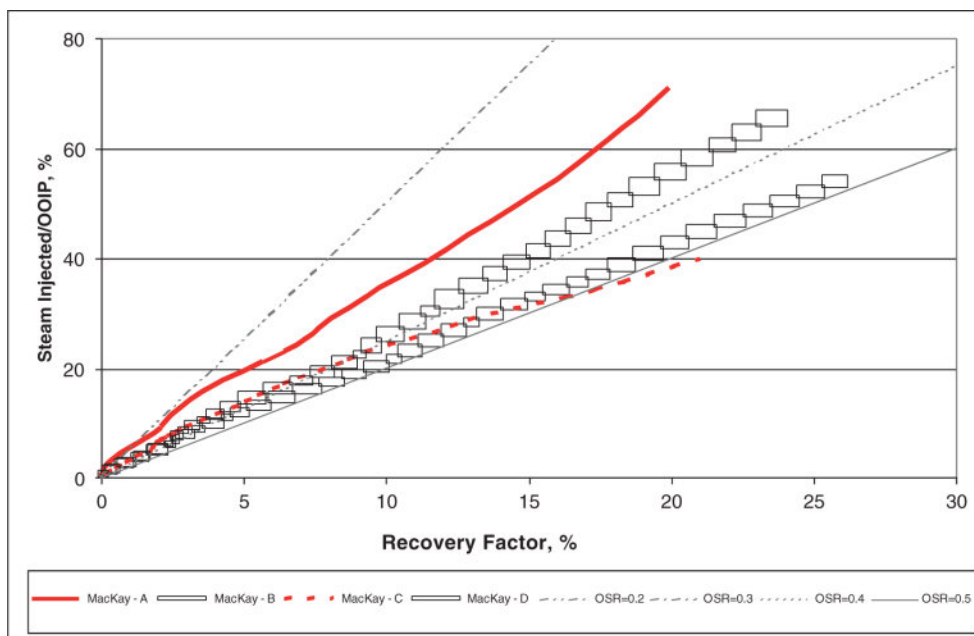


Fig. 11.35—Performance of seven well pads in the McKay River field (Jimenez 2008).

The recovery lines all have slopes less than one, suggesting either that there was mobile water initially present, or some bypassing between injectors and producers is occurring. Nevertheless, several of the recovery efficiencies are approaching 30%, and there is no evidence of their leveling out (which would be an upward curvature in this plot). The chances are excellent that ultimate recoveries will equal and exceed those for steamdrives.

11.10 Concluding Remarks

Our discussion here, and indeed throughout the text, has been from a reservoir-engineering viewpoint. For thermal methods, in particular, much of the success is a result of advancements in mechanical, completions, and production technology.

Surface steam generation, a simple concept in principle, is not easy under field conditions. For most cases, the waters available are brines of highly variable salinity. Such water cannot be used to generate 100% quality steam because of scaling. In fact, most boilers generate approximately 80% quality steam for this reason.

The evolution of the fuel used to generate steam is an example of the progress of these technologies. In the early days of steam

injection, the fuel used in surface generators was the produced crude. Because this usually heavy crude tends to be especially rich in components that cause air pollution when burned, surface steam generation can represent an environmental hazard. The expense of cleaning the boiler waste gases must be borne by the entire project. Environmental issues have been partially ameliorated by switching to natural gas as fuel. Nevertheless, water usage and air pollution continue to be issues for these technologies.

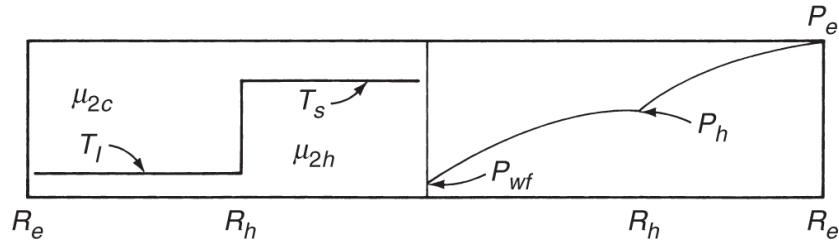
Difficulties in completing the wells plagued early steam operations, particularly the injectors. Thermal expansion of downhole equipment exacerbated the failures of the existing cementing techniques. Many of these difficulties have been remedied by using prestressed tubular goods in the wells. Current cement-bonding techniques and the development of thermal packers have dramatically reduced failure rates.

Undoubtedly, the future of thermal recovery rests on these and other technological advancements. These advancements include the cogeneration of electric power from steam boilers and the use of downhole steam generators, foams for mobility control, diluents in steam injection, and oxygen for in-situ combustion. Each of these extends the range of thermal methods to heavier or lighter crudes, deeper formations, or higher-pressure reservoirs. When this extension becomes a reality, thermal methods, already proven worldwide, will directly contend with other techniques for EOR of target oil.

Exercises

11.1 Effect of Temperature on Productivity Improvement. Steam soak is far from incompressible steady-state flow. However, rough estimates of productivity may be obtained by assuming both. The formula for the volumetric production rate q of a well that drains two concentric cylindrical volumes is

$$q = \frac{2\pi k H_{NET} (P_e - P_{wf})}{\mu_{2h} \ln\left(\frac{R_h}{R_w}\right) + \mu_{2c} \ln\left(\frac{R_e}{R_h}\right)}.$$



Assume that the inner cylinder is the heated volume after a steam soak.

- Derive an expression for the productivity index (*PI* or *J*) for this case in which

$$J \equiv \frac{q}{P_e - P_{wf}}.$$

Also derive an expression for the *PI* improvement,

$$(J)_{\text{improvement}} = \frac{(J)_{\text{stimulated}}}{(J)_{\text{unstimulated}}}.$$

- Estimate the *PI* improvement for a single steam cycle with the following data:

Reservoir temperature = 320 K

Heated-zone temperature = 480 K

Cold-oil density = 0.9 g/cm³

Hot-oil density = 0.8 g/cm³

Drainage radius = 116 m

Heated radius = 20 m

Well radius = 7 cm

API = 20°.

Use the viscosity data in [Fig. 11.1](#) for the hot (μ_{2h}) and cold (μ_{2c}) oil viscosities. Note that 1 cs = 1 mm²/s.

- c. Make subjective judgments about the effects of the following quantities on PI improvement: number of cycles, steam volume injected, cold-oil viscosity, permeability, and skin factor.

11.2 Estimating Generator Performance. Water at an initial temperature of 294 K (70°F) is being pumped through a steam generator at a rate of 15.9 m³/d (1,000 bbl/D) into an injection well. The wellhead temperature is 533 K (500°F). What is the wellhead steam quality? The generator burns 10,000 std m³/d of natural gas that has a heating value of 300 kJ/std m³. The generator efficiency is 80%.

11.3 Losses to Rock and Water for Steam. Rework Example 11.3 when steam is present. Use the same properties, except assume the medium to be filled with saturated steam of 50% quality.

11.4 Alternate Derivation of Thermal Velocity in Hot Waterflood. Eq. 11.22 can be derived in a fashion reminiscent of the composition-path constructions of Section 7.7. The coherence constraint for Eqs. 11.19a and 11.19c is

$$\frac{d(\rho_1 f_1 H_1 + \rho_2 f_2 H_2)}{d\left[\rho_1 S_1 H_1 + \rho_2 f_2 H_2 + \frac{(1-\phi)}{\phi} \rho_s H_s\right]} = \frac{\rho_1 H_1 d f_1}{\rho_1 H_1 d S_1}.$$

The density-enthalpy product has been added to the numerator and denominator of the right side to ensure units consistency below.

- a. By expansion of the numerator and denominator on the left side of the preceding equation, show that the lines of constant temperature satisfy the coherence condition. These

will represent the saturation change at the leading edge of the cold-oil bank.

- b. We know that the preceding equation will be satisfied if the numerators and denominators are identically equal. Show that equating the denominators yields an ordinary differential equation for which the solution is

$$T = I_1 \left\{ S_1 (M_{T_1} - M_{T_2}) + \left[M_{T_2} + \frac{(1-\phi)}{\phi} M_{T_s} \right] \right\}^{M_{T_2}/(M_{T_1}-M_{T_2})},$$

where I_1 is an integration constant. Recall that $\rho_j dH_j = M_{Tj} dT$. The preceding equation along with the $T = \text{constant}$ lines form the composition path grid in S_1-T space. Sketch a few lines in this grid.

- c. Equate the numerators of the first equation in the exercise and perform the analogous operation to give

$$T = I_2 \left[f_1 (M_{T_1} - M_{T_2}) + M_{T_2} \right]^{M_{T_2}/(M_{T_1}-M_{T_2})},$$

where I_2 is a second integration constant. The preceding equation and the $T = \text{constant}$ lines are the composition path grid in f_1-T space.

- d. Eliminate temperature between the second and third equations to show that the temperature-varying paths in composition space follow

$$f_1 + \frac{M_{T_2}}{M_{T_1} - M_{T_2}} = I_3 \left[S_1 + \frac{M_{T_2} + \frac{(1-\phi)}{\phi} M_{T_s}}{M_{T_1} - M_{T_2}} \right],$$

where I_3 is another integration constant.

- e. The preceding equation suggests that $df_1 = I_3 dS_1$. Use the similar differential forms of the third and fourth equations for dT to show that the first equation will yield $I_3 = df_1/dS_1$. Substituting this back into the fourth equation gives Eq. 11.22.

11.5 Fractional Flow for Hot Waterfloods. The following problem is intended to reinforce the fractional-flow construction in [Fig. 11.7](#) and to provide practice in estimating thermal properties.

- We are to perform a hot waterflood consisting of saturated liquid water at 1 MPa pressure. Estimate the hot-water temperature, the hot-oil viscosity, and the volumetric heat capacities for water, oil, and the solid phase. Additional data are as follows:

	Initial (cold)	Injected (hot)
Temperature, K	300	—
Water viscosity, mPa·s	1.0	0.5
Water density, g/cm ³	1.0	1.0
Oil viscosity, mPa·s	700	—
Oil density, g/cm ³	0.9	0.9

Use the data or correlations in [Tables 11.2](#) and [11.3](#) (the properties of water-saturated sandstone most nearly approximate the present case), Eq. 11.2, and [Fig. 11.7](#). The porosity is 0.2.

- The exponential relative-permeability curves apply to this horizontal reservoir with the following parameters:

$$S_{1r} = 0.2 \quad k_{r1}^0 = 0.3 \quad n_1 = 2$$

$$S_{2r} = 0.2 \quad k_{r1}^0 = 0.8 \quad n_2 = 2$$

You may assume that these functions are independent of temperature. Using these data and those of Part (a), calculate and plot the hot- and cold-water fractional-flow curves.

- Calculate and plot the 1D effluent history of oil and temperature based on the information given above. The initial water cut is 0.1.

11.6 Dimensional Analysis of Heat Transfer From Tubing. In this exercise, we develop the dimensional argument for Eq. 11.33, the heat-transfer coefficient correlation for heat flow from the tubing. [Fig.11.11](#) shows the approximate velocity and temperature profiles. If the fluid flow is steady-state, laminar, Newtonian, and incompressible, the velocity profile in the tubing becomes

$$v = v_{\max} \left[1 - \left(\frac{r}{R_{ti}} \right)^2 \right].$$

- a. The energy balance of Eq. 2.39 applies to the flowing fluid if the porosity is set to one. If the energy balance retains only radial conduction and axial convection, show that when applied to the fluid in the tubing, it reduces to

$$\rho_f C_{pf} v_{\max} \left[1 - \left(\frac{r}{R_{ti}} \right)^2 \right] \frac{\partial T}{\partial z} = k_{Tf} \frac{1}{r} \frac{\partial}{\partial r} \left(r \frac{\partial T}{\partial r} \right).$$

The preceding equation assumes constant thermal conductivity k_{Tf} and viscosity μ_f of the flowing fluid. The boundary conditions on this equation are

$$\left(\frac{\partial T}{\partial r} \right)_{r=0} = 0, \quad T(R_{ti}, z) = T_{ti}, \quad T(r, 0) = T_f,$$

where T_{ti} is constant.

- b. Introduce the following dimensionless variables:

$$r_D = \frac{r}{R_{ti}}, \quad z_D = \frac{K_{Tf} z}{v_{\max} R_{ti}^2}, \quad T_D = \frac{T - T_{ti}}{T_f - T_{ti}}$$

into the second and third equations, and show that they reduce to

$$(1 - r_D^2) \frac{\partial T_D}{\partial z_D} = \frac{1}{r_D} \frac{\partial}{\partial r_D} \left(r_D \frac{\partial T_D}{\partial r_D} \right) \left(\frac{\partial T_D}{\partial r_D} \right)_{r_D=0} = 0, \quad T_D(1, z_D) = 0, \quad T_D(r_D, 0) = 1.$$

The dimensionless temperature must therefore be a function only of r_D and z_D .

- c. The heat-transfer rate $\dot{Q} \rightarrow$ from the tubing is

$$\dot{Q} = -2\pi \int_{\xi=0}^{\xi=L} \left(rk_{Tf} \frac{\partial T}{\partial r} \right)_{r=R_i} d\xi.$$

Show that the dimensionless form of this equation is

$$\frac{\dot{Q}}{2\pi L k_{Tf} r_D (T_f - T_{ti})} = -\frac{2\pi}{Z_{DL}} \int_0^{Z_{DL}} \left(r_D \frac{\partial T}{\partial r_D} \right)_{r_D=1} d\xi,$$

where the additional term in sixth equation is

$$Z_{DL} = \frac{K_{Tf} L}{v_{\max} R_{ti}^2}$$

and L is the length of the heated tubing. Because of the evaluation at $r_D = 1$ and the integration between known limits, the integral is a function of Z_{DL} only.

- d. Define an average heat-transfer coefficient h_{Tf} as

$$\dot{Q} \equiv \pi R_{ti} L (T_f - T_{ti}) h_{Tf}.$$

Eliminate \dot{Q} between the equation in part c and the preceding equation to show that, after rearranging,

$$\frac{R_{ti} h_{Tf}}{k_{Tf}} = N_{Nu} = f(Z_{DL}).$$

Eq. 11.33 follows from this because Z_{DL} decomposes into

$$\begin{aligned}\frac{K_{If}L}{v_{\max}R_{ti}^2} &= \frac{k_{If}L}{\rho_f C_{pf} v_{\max} R_{ti}^2} = \frac{k_{If}}{\mu C_{pf}} \cdot \frac{\mu}{\rho_f v_{\max} R_{ti}} \cdot \frac{L}{R_{ti}} \\ &= \frac{1}{N_{Pr}} \cdot \frac{1}{N_{Re}} \cdot \frac{1}{R_{ti}}\end{aligned}$$

The Brinkman number is absent from the last equation because the original equation did not include viscous heating.

11.7 Calculating Heat Losses. For steamdrives, the rate of heat loss to the over- and underburden is frequently so significant that it alone can furnish a good measure of success. In this exercise, you will use theoretical relations to estimate measures of the success of a steamdrive. Use the following quantities in this exercise:

$$\begin{array}{ll} T_i = 317 \text{ K} & k_{Ts} = 2.1 \text{ J/s-m-K} \\ H_i = H_{NET} = 11 \text{ m} & M_{To} = 2.3 \text{ MJ/m}^3\text{-K} \\ \phi = 0.3 & M_{Tu} = 2.8 \text{ MJ/m}^3\text{-K} \\ \Delta S_2 = 0.31 & t = 4.5 \text{ yr} \\ H_3 = 44.4 \text{ MJ/kg} & \end{array}$$

- Estimate the steam-zone temperature. P_i , the initial reservoir pressure, is 2.72 MPa.
- Calculate the dimensionless time and dimensionless latent heat from Eq. 11.16. The steam quality y is 0.7.
- From the Myhill-Stegemeier charts ([Figs. 11.15](#) and [11.16](#)), estimate the useful heat fraction \bar{E}_{hs} and the dimensionless oil/steam ratio.
- From the results of Part c, calculate the oil/steam ratio F_{23} and the energy efficiency. The latter is defined as

$$\eta_E = \frac{\text{Oil heating value}}{\text{Heat requirement to produce steam}}$$

and is given by

$$\eta_E = \frac{F_{23}\gamma_2\eta_B H_3}{C_{p1}\Delta T(1+h_D)},$$

where η_B is the boiler efficiency and γ_2 is the specific gravity of the oil. Assume that $\gamma_2 = 0.94$ and $\eta_B = 0.8$.